

A unified harmonic framework for dark siren cosmology

April Qiu Cheng^{1,2,*} and Jonathan Gair²

¹*Department of Astrophysical Sciences, Princeton University, Princeton, New Jersey 08544, USA*

²*Max Planck Institute for Gravitational Physics (Albert Einstein Institute), Am Mühlenberg 1, 14476 Potsdam, Germany*

(Dated: March 16, 2026)

The galaxy catalog dark siren method aims to infer cosmological parameters from gravitational waves (GWs) without an electromagnetic counterpart by statistically marginalizing over possible host galaxies. The cross-correlation of GW sources and galaxies is a promising avenue for cosmological inference without requiring observed host galaxies, by leveraging 2-point statistics. We provide a detailed guide to the cross-correlation method, clarifying its relationship to standard dark siren techniques as well as the assumptions necessary to be able to use this formalism on GW data. We show that the cross-correlation method is an extension of the angular part of the galaxy catalog method in which we effectively marginalize over all possible realizations of the unknown galaxy field, jointly adding information from galaxy–galaxy clustering. Combined with the spectral sirens method, which encodes information from the GW rate evolution, mass distribution, and selection effects, one can perform an inference that leverages the joint constraining power of all dark siren methods. We also present a strategy to rigorously fold GW measurement errors into the likelihood. Using this method, we show that with a 2 Einstein Telescope (ET) + 1 Cosmic Explorer (CE) setup, the GW–galaxy cross-correlation part alone can jointly measure H_0 and $\Omega_{m,0}$ to 1% and 5% precision with just 2 years of data, demonstrating its potential as a precise and scalable inference technique in the next generation of GW and galaxy surveys. This is in contrast with canonical population inference techniques, which are known to scale poorly with the precision and catalog size expected of next-generation GW experiments. Contrary to some previous projections, we remain pessimistic about the cross-correlation method until these next generation detectors are online, due to its implicit requirement of large-number statistics.

I. INTRODUCTION

The present-day expansion rate of the universe H_0 is a key observable of Λ CDM cosmology. There is currently a large ($\gtrsim 4\sigma$) tension between early-universe and late-universe measurements of H_0 with electromagnetic probes [1–5], motivating alternate avenues of cosmological inference. The observation of GWs sourced from merging compact objects is one such independent avenue, as one can directly measure their luminosity distance from the waveform amplitude and phase evolution without any need for a distance ladder [6–8]. Hence, GW sources are often dubbed *standard sirens*.

The goal of GW cosmology can be cast as an inference problem on the redshifts of the GW sources, which allows one to probe the $d_L - z$ relation. The source redshift can be measured directly with the observation of an electromagnetic counterpart and subsequent host galaxy identification [9, 10]. However, the vast majority of GW sources have no electromagnetic counterpart, and a variety of methods have been developed and applied in the literature to use these *dark sirens* for cosmological inference.

A core method of this inference is known as the *spectral sirens method*, which leverages features in the GW mass distribution to infer the redshifts of the GW sources [11–

20]. One can also use a galaxy catalog to statistically marginalize over possible host galaxies on an event-by-event basis, accounting for the catalog completeness [21–34]. This *galaxy catalog method* is now understood to be an extension of the spectral sirens method, in which the spatial population prior is upgraded to one informed by the observed galaxy field. Both of these methods fall within the standard hierarchical Bayesian formalism for inferring population properties of GWs, in which one infers the hyperparameters of an assumed population model by marginalizing over the possible source parameters of the observed strain data of each event [35–37].

One of the primary limitations of the galaxy catalog method is the incompleteness of galaxy catalogs at moderate to high redshifts [20, 26, 38, 39]. Because the galaxy catalog method typically assumes a uniform distribution for the unobserved galaxies, little to no information is gained on the redshift of the GW source at these distances. This ignores the clustering of galaxies, as in principle the observed galaxy field can be used to inform the field of missing galaxies. On the other hand, techniques which directly infer cosmology from the cross-correlation statistics of GWs and galaxies have been proposed as a complementary method to dark siren techniques. These *cross-correlation methods* generally aim to constrain cosmology by cross-correlating GWs in luminosity distance space with galaxies in redshift space, most straightforwardly via the 3x2pt analysis of the GW–GW, GW–galaxy, and galaxy–galaxy power spectra [40, 41]. Alternate methods have also been proposed, including a

* aqcheng@princeton.edu

6x2pt extension that includes weak gravitational lensing [42], inference with the GW–galaxy power spectra conditioned on the observed galaxy overdensity field [43–45], and using 2-point correlations to predict local galaxy overdensities near observed GWs [46]. There is also significant interest in the GW clustering itself, both to inform the large-scale structure (LSS) of the universe as well as to infer the GW tracer bias, which could provide insights on the host environments and formation origins of GW sources [47–52].

Because the cross-correlation method uses the estimated cross-correlation of the GW field as the observable, they bypass the standard hierarchical Bayesian formalism for GW population analysis, obscuring the question of how selection effects and individual event localizations should be rigorously treated. In particular, it is not clear how to construct the GW overdensity field in the first place when the GW sky localizations are not directly measured, but rather are a Bayesian posterior obtained from the measured strain data. Most forecasts of the cross-correlation method use a Fisher matrix formalism [40–42, 53, 54], bypassing any explicit form of a hierarchical likelihood on the strain data. Cross-correlation analyses that do perform Bayesian inference on real or mock GW catalog typically use the GW posterior localization ellipses themselves to construct the overdensity field [44, 45, 55]. This localization uncertainty is either ignored by assuming the cross-correlation signal is unaffected at the scales probed [40, 42, 45], or more commonly by modeling it as a convolution of the map of the true GW positions with a single circular Gaussian kernel, which can be neatly folded into the theoretical prediction analytically [41, 44]. Given that GWs have a wide range of localization uncertainties that are often neither isotropic nor Gaussian, there is reason to scrutinize the robustness of these assumptions. Furthermore, a convolution of the true source position with a Gaussian kernel is an ellipse centered at the true source position, which is a suitable model for the point spread function of a telescope, but not necessarily the posterior measurement of GW strain data.

This motivates us to cautiously examine some of the optimistic forecasts of the cross-correlation method in the literature. In at least one case, the cross-correlation method has been used to place tighter constraints on cosmological parameters than the standard galaxy catalog method with real GW data [32, 45]. A possible explanation is that the cross-correlation method gains information from 2-point statistics. Nonetheless, the cross-correlation method uses a compressed form of the GW data as its observable (i.e., the cross-correlation power spectra) and imposes weaker requirements, namely that GW sources need only to trace the same underlying LSS rather than necessarily being hosted in galaxies. Moreover, the cross-correlation method makes no use of the information from the source-frame mass distribution and rate evolution, which is used by the spectral sirens method. Further complicating the picture are various

techniques in the middle, which extend the galaxy catalog method to use some form of galaxy clustering to help inform the distribution of unobserved galaxies [56–59]. This motivates a clarification of the relationship between the galaxy catalog and cross-correlation methods. Given the same two datasets—a GW catalog and a galaxy catalog—how does one maximize the constraining power of the inference? What information is lost or gained by the galaxy catalog method with respect to the cross-correlation method, and vice versa?

With these questions in mind, we are motivated to provide a rigorous derivation of the cross-correlation method from first principles, with the simultaneous goal of acting as a pedagogical resource for those newer to 2-point statistical analyses, especially those from the GW population inference side. Moreover, we derive expressions for modeling GW localization errors within the machinery of cross-correlation analyses, making explicit our model of the GW measurement process and its underlying assumptions. Because this paper is written with the aim of bridging cross-correlation and dark siren population analyses, we limit the scope of this paper to Gaussian 2-point statistics in the linear regime. In particular, we ignore peculiar velocities and relativistic effects in this work, including lensing, magnification, redshift space distortions (RSDs) and luminosity-distance space distortions (LSDs). We refer the reader to references [60–65] and references therein for the theoretical treatment of these effects.

This paper is thus organized as follows. In Section II, we summarize for the reader’s reference the notation used in this work. In Section III, we review the formalisms for dark siren population analyses, Gaussian Random Fields (GRFs), and multi-tracer cross-correlations in both Cartesian and spherical coordinates. In Section IV, we describe the relationship between the standard dark siren and cross-correlation methods by outlining a continuous perturbation in the population prior from the former to the latter. In Section V, we describe how to treat GW and galaxy measurement noise, with an emphasis on GW angular localizations. We summarize our theoretical results by presenting a unified hierarchical Bayesian posterior in Section VI; a reader interested in the main theoretical results but not in the details can jump ahead here. Finally, we demonstrate our cross-correlation formalism on simulated catalogs of galaxies and binary black holes (BBHs), outlining our methodology in Section VII and presenting the inference results in Section VIII. We conclude and summarize in Section IX.

II. NOTATION

In this section, we define for the reader’s reference the basic notation used throughout this manuscript; these quantities will be defined in detail in Sections III and V. Table I summarizes the symbols used to describe various quantities. In general, superscripts will be used to denote

	Symbol	Definition
population inference	p, \mathcal{L}	probability distribution, likelihood
	Π	prior distribution
	\mathcal{P}	posterior distribution
	\mathbf{d}	data vector
	$\boldsymbol{\lambda}$	event-level parameters
	$\mathbf{\Lambda}$	population parameters
spatial quantities	\mathbf{r}, \mathbf{k}	3D position vector, wave-vector
	r	arbitrary radial distance measure
	d_L	luminosity distance
	z	redshift
	χ	radial comoving distance
	$\boldsymbol{\Omega}$	2D sky position vector
	θ	Angular distance, $\cos \theta = \boldsymbol{\Omega} \cdot \boldsymbol{\Omega}'$
GRFs	$P(k)$	3D power spectrum
	C_ℓ	2D angular power spectrum
	\tilde{C}_ℓ	2D angular power spectrum estimator
	n^X	number density field of tracer X
	$\bar{\rho}^X$	probability density field of tracer X
	ρ	matter density field
	δ	3D overdensity field
	Δ	2D overdensity field
	$s_{\{\ell, k\}}$	(angular, 3D) power spectrum shot noise

TABLE I: Summary of key symbols and notation used throughout this work.

the tracer, while subscripts will denote the position vector or wavenumber in real or Fourier space. For example, $\delta_{\mathbf{k}}^g$ denotes the galaxy overdensity field in Fourier space. This is not to be confused with $\delta^{(D)}$ and $\delta^{(K)}$, the Dirac and Kronecker delta functions.

Power spectra with two superscripts (e.g., C_ℓ^{XY}) indicates a cross-power spectrum between fields X and Y . In this text, we will often use X or Y to denote arbitrary tracers, and substitute in G (gravitational wave source) or g (galaxy) as needed. We use greek letters α, β to index bins of any tracer. For brevity and consistency with the notation of GW population analyses, individual event-level parameters such as d_L, z , etc. refer to GW event parameters, unless otherwise specified by a superscript to belong to a different tracer (e.g., z^g for galaxies). We will do the same for probability distributions, using $p(\boldsymbol{\lambda}|\mathbf{\Lambda})$ to refer to by default the GW population prior. We will also use GW, GW source, and BBH somewhat interchangeably to refer to GW sources as tracers of LSS, as BBHs make up the vast majority of GW sources and their population modeling is currently more robust.

As we will describe in Section III, GW sources can be modeled as a Poisson realization of the galaxies, which in turn are a Poisson realization of the underlying dark matter field. Thus, to distinguish between probability density fields and Poisson-realized density fields, and between the presence and absence of measurement noise, we introduce the following notation:

- An overline denotes the *probability* density field. For example, $\bar{\rho}^X(k)$ denotes the probability density field of tracer X , which is proportional to the dark

matter density field.

- A plain symbol, such as $a_{\ell m}^X$ or $P^X(k)$, indicates the *realized* tracer overdensity field and its angular power spectrum without measurement noise. For the power spectrum $P^X(k)$, this is $\bar{P}^X(k)$ plus a Poisson shot noise term.
- A hat ($\hat{\cdot}$) indicates a measured quantity. For example, the measured GW map $\hat{a}_{\ell m}^G$ can differ from the true GW map $a_{\ell m}^G$ of the observations due to localization errors. All tracer overdensity fields (both of the true positions $a_{\ell m}^X$ and the observed positions $\hat{a}_{\ell m}^X$) are constructed from finite observations, i.e. with selection effects implicitly folded in.
- A tilde ($\tilde{\cdot}$) denotes an *estimator*. Because we only observe one realization of the universe, it is impossible to access the true power spectrum. We estimate the power spectrum with observations by computing an estimator \tilde{C}_ℓ , with $\langle \tilde{C}_\ell \rangle = C_\ell$ for an unbiased estimator.

Because some quantities such as $C_\ell^{\alpha\beta}$ are symmetric in $\alpha \leftrightarrow \beta$ by construction, we will denote all unique pairings with $[\alpha, \beta]$, which enforces $\alpha \geq \beta$. $\{C_\ell^{[\alpha\beta]}\}$ thus refers to the set of all unique cross-correlation power spectra.

In this work, we will refer to the galaxy catalog method with a heuristic (e.g., uniform) completion of missing galaxies as the “standard galaxy catalog method”, and the full 3x2pt analysis of the power spectra of GWs and galaxies in radial tomographic bins as the “cross-correlation method”. Although these are the methods

we focus on bridging, we will make some references to alternate flavors of galaxy catalog and cross-correlation methods throughout this work.

III. THEORY

A. The canonical dark siren formalism

In this section, we will review the standard methods for population inference with GW observations without electromagnetic counterparts. For more in-depth reviews, see, e.g., [25, 66, 67].

Given a set of N GW observations $\{\mathbf{d}\}$, the Bayesian posterior on a set of parameters $\mathbf{\Lambda}$ is

$$\mathcal{P}(\mathbf{\Lambda}|\{\mathbf{d}\}, N) \propto \Pi(\mathbf{\Lambda})\mathcal{L}(\{\mathbf{d}\}, N|\mathbf{\Lambda}) \quad (1)$$

Under the presence of selection effects, these probabilities become implicitly conditioned on the fact that the data are detected. If we denote the detection of each observation as D , then the posterior can be given in terms of an inhomogeneous Poisson likelihood [16, 35–37, 68]

$$\begin{aligned} \mathcal{P}(\mathbf{\Lambda}|\{\mathbf{d}\}, \{D\}, N^G) &\propto \Pi(\mathbf{\Lambda})\mathcal{L}(\{\mathbf{d}\}|N^G, \{D\}, \mathbf{\Lambda})p(N^G|\mathbf{\Lambda}) \\ &\propto \Pi(\mathbf{\Lambda})\frac{\mathcal{L}(\{\mathbf{d}\}|\mathbf{\Lambda})}{\xi(\mathbf{\Lambda})^{N^G}}e^{-N_{\text{exp}}(\mathbf{\Lambda})}[N_{\text{exp}}(\mathbf{\Lambda})]^{N^G} \end{aligned} \quad (2)$$

where the fact that the likelihood conditioned on detection $\mathcal{L}(\{\mathbf{d}\}|N^G, \{D\}, \mathbf{\Lambda})$ is equal to the unconditioned likelihood up to a renormalization $\mathcal{L}(\mathbf{d}_i|\mathbf{\Lambda})/\xi(\mathbf{\Lambda})$ follows from the fact that detection is a property of the observed data only, $P(D_i|\mathbf{d}_i) = 1$. Here, $\xi(\mathbf{\Lambda})$ is the fraction of detectable events, and $N_{\text{exp}}(\mathbf{\Lambda}) = N_{\text{tot}}(\mathbf{\Lambda})\xi(\mathbf{\Lambda})$ is the expected number of observed events in the space-time 4-volume, given the rate of events in the Universe is $N_{\text{tot}}(\mathbf{\Lambda})$. Therefore, the Bayesian posterior under selection effects is

$$\mathcal{P}(\mathbf{\Lambda}|\{\mathbf{d}\}, \{D\}) \propto \Pi(\mathbf{\Lambda})e^{-N_{\text{exp}}(\mathbf{\Lambda})}N_{\text{tot}}^N\mathcal{L}(\{\mathbf{d}\}|\mathbf{\Lambda}). \quad (3)$$

If the parameters of interest $\mathbf{\Lambda}$ are population-level parameters that govern a probability distribution p on the individual event-level parameters $\{\boldsymbol{\lambda}\}$, the likelihood on the data is expressed as a marginalization over $\{\boldsymbol{\lambda}\}$

$$\mathcal{L}(\{\mathbf{d}\}|\mathbf{\Lambda}) = \prod_{i=1}^{N^G} \int d\boldsymbol{\lambda}_i p(\boldsymbol{\lambda}_i|\mathbf{\Lambda}) \mathcal{L}(\mathbf{d}_i|\boldsymbol{\lambda}_i, \mathbf{\Lambda}). \quad (4)$$

Because of this, the population parameters $\mathbf{\Lambda}$ are often referred to as “hyperparameters”, as opposed to the (event-level) parameters $\boldsymbol{\lambda}$.

The goal of GW cosmology is to infer cosmological parameters $\mathbf{\Lambda}_c$ such as the Hubble parameter H_0 and the present-day matter density parameter $\Omega_{m,0}$ as our population parameters of interest. Unlike electromagnetic standard candles, the luminosity distance to the

GW source can be inferred directly from the amplitude and phase evolution of the waveform, bypassing any sort of calibrated distance ladder. On the other hand, the redshift is degenerate with the source-frame mass in the waveform, and therefore constraining the astrophysical source-frame mass distribution will also constrain the $d_L - z$ relation, and therefore the cosmology [6, 7]. Thus, the relevant event-level parameters are $\boldsymbol{\lambda} = \{m_1, m_2, d_L\}$, and the population prior can be most generally written as

$$p(\boldsymbol{\lambda}|\mathbf{\Lambda}) = p(m_1, m_2|d_L, \mathbf{\Lambda}_m)p(d_L|\mathbf{\Lambda}_c, \mathbf{\Lambda}_r) \quad (5)$$

where $p(d_L|\mathbf{\Lambda}) = \frac{dz}{dd_L}(\mathbf{\Lambda}_c)p(z|\mathbf{\Lambda}_c, \mathbf{\Lambda}_r)$ is usually parameterized in terms of the redshift z as a source-frame rate $\mathcal{R}(z)$ per comoving volume

$$p(z, \boldsymbol{\Omega}|\mathbf{\Lambda}) \propto \frac{\mathcal{R}(z|\mathbf{\Lambda}_r)}{1+z} \frac{1}{4\pi} \frac{dV_c}{dz}(z|\mathbf{\Lambda}_c). \quad (6)$$

The factor of $1+z$ comes from the conversion of the source-frame rate to detector-frame rate. In Equations (5) and (6), we have used $\mathbf{\Lambda}_m$ and $\mathbf{\Lambda}_r$ to refer to hyperparameters which govern the source-frame mass distribution and rate evolution, respectively. Assuming Equation (6) in Equation (5) is known as the spectral sirens method, and uses no supplementary electromagnetic data in the inference. All methods in dark siren cosmology can be understood as generalizations of this method with the inclusion of additional information.

Assuming that GWs are hosted in galaxies, the spatially uniform redshift prior $\frac{dV_c}{dz}$ in Equation (6) can be upgraded to a 3D spatial prior for galaxies $p^{g,\text{tot}}(z, \boldsymbol{\Omega})$,

$$p(z, \boldsymbol{\Omega}|\mathbf{\Lambda}, \{\mathbf{d}^g\}) \propto \frac{\mathcal{R}(z|\mathbf{\Lambda}_r)}{1+z} p^{g,\text{tot}}(z, \boldsymbol{\Omega}|\mathbf{\Lambda}_c, \{\mathbf{d}^g\}) \quad (7)$$

in which case Equation (6) is the statement that the redshift prior for galaxies is uniform in comoving volume in the absence of galaxy data. The galaxy catalog method improves the constraining power of Equation (6) by using a galaxy catalog $\{\mathbf{d}^g\}$ to inform $p^{g,\text{tot}}(z, \boldsymbol{\Omega})$.

If we knew the positions of all the galaxies of the universe, then the redshift prior would be a sum¹ of Dirac-delta functions at the galaxy positions

$$p^{g,\text{tot}}(z, \boldsymbol{\Omega} | \mathbf{\Lambda}_c, \{\mathbf{d}^g\}) = \frac{1}{N^{g,\text{tot}}} \sum_{i=1}^{N^{g,\text{tot}}} \delta^{(D)}(z-z_i)\delta^{(D)}(\boldsymbol{\Omega}-\boldsymbol{\Omega}_i) \quad (8)$$

¹ A more general model modifies Equation (8) to a weighted sum, rather than assuming that GWs are drawn uniformly from the galaxies. In practice, this replaces our galaxy field with an effective weighted galaxy field, with an accordingly modified detection probability (since the weight may be a function of e.g., the galaxy luminosity). Therefore, without loss of generality, we will proceed in the rest of the paper with the uniform weights in Equation (8).

or equivalently,

$$\frac{dN^G}{dzd\Omega} \propto \frac{\mathcal{R}(z)}{1+z} \frac{dN^{g,\text{tot}}}{dzd\Omega}. \quad (9)$$

Therefore, the general goal is to infer $\frac{dN^{g,\text{tot}}}{dzd\Omega}$, from which we can infer the GW field $\frac{dN^G}{dzd\Omega}$ from which the observed GWs are drawn.

In practice, galaxy surveys are flux-limited, and therefore the underlying galaxy density field $\frac{dN^{g,\text{tot}}}{dzd\Omega}$ usually cannot be recovered. We can rewrite the total underlying galaxy field in Equation (8) as a weighted sum of the observed and unobserved galaxy fields:

$$\begin{aligned} \frac{1}{N^{g,\text{tot}}} \frac{dN^{g,\text{tot}}}{dzd\Omega} &= \frac{1}{N^{g,\text{tot}}} \left[\sum_{i=1}^{N^{g,\text{obs}}} \delta^{(D)}(z - z_i) \delta^{(D)}(\Omega - \Omega_i) \right. \\ &\quad \left. + \sum_{i=1}^{N^{g,\text{miss}}} \delta^{(D)}(z - z_i) \delta^{(D)}(\Omega - \Omega_i) \right] \\ &= f^{g,\text{obs}} \frac{1}{N^{g,\text{obs}}} \frac{dN^{g,\text{obs}}}{dzd\Omega} + (1 - f^{g,\text{obs}}) \frac{1}{N^{g,\text{miss}}} \frac{dN^{g,\text{miss}}}{dzd\Omega} \end{aligned} \quad (10)$$

where $f^{g,\text{obs}} = \frac{N^{g,\text{obs}}}{N^{g,\text{tot}}}$ is the detectable fraction of galaxies over the integration volume. In Bayesian language, this is a marginalization of whether (D^g) or not (\underline{D}^g) the host galaxy of a GW is detected in the catalog [23, 24, 34]:

$$p^{g,\text{tot}}(z, \Omega | \Lambda_c, \{\mathbf{d}^g\}) = p(D^g | \Lambda_c) p^g(z, \Omega | \Lambda_c, \{\mathbf{d}^g\}, D^g) + [1 - p(D^g | \Lambda_c)] p^g(z, \Omega | \Lambda_c, \{\mathbf{d}^g\}, \underline{D}^g) \quad (11)$$

where $p(D^g | \Lambda_c) = f_{\text{obs}}^g$ is the host galaxy detection probability and the in-catalog term $P(z, \Omega | \Lambda_c, \{\mathbf{d}^g\}, D^g)$ is the observed galaxy field Equation (8). The out-of-catalog term $P(z, \Omega | \Lambda_c, \{\mathbf{d}^g\}, \underline{D}^g)$ is typically taken to be completely uninformative

$$p(z, \Omega | \Lambda_c, \{\mathbf{d}^g\}, \underline{D}^g) \propto [1 - p(D^g | z, \Lambda_c)] \frac{dV_c}{dz}(z | \Lambda_c). \quad (12)$$

where the redshift-dependent prefactor reflects the fact that the galaxy completeness is not uniform over the survey volume. Alternatively, one may assume that the missing galaxies trace the observed galaxies, such that

$$p(z, \Omega | \Lambda_c, \{\mathbf{d}^g\}, \underline{D}^g) \propto \frac{1 - p(D^g | z, \Lambda_c)}{p(D^g | z, \Lambda_c)} \times p(z, \Omega | \Lambda_c, \{\mathbf{d}^g\}, D^g) \quad (13)$$

These two methods, dubbed the ‘‘homogeneous completion’’ and ‘‘multiplicative completion’’ methods [34] represent two extremes of modeling the distribution of the missing galaxies. In either case, the low completeness of galaxy catalogs compared to the sensitivity depth of GW observations is a primary bottleneck of the standard galaxy catalog method. This method also requires

modeling electromagnetic selection effects for the galaxy detection probability $p(D^g | \Lambda_c)$, which is dependent on the assumed galaxy luminosity function.

B. Gaussian Random Fields

In this section, we will review the basic formalism of modeling the underlying matter field and its Poisson tracers as a GRF, beginning with the 3D power spectrum in Section III B 1 and changing to spherical coordinates in Section III B 2. For simplicity we will assume perfect localizations and complete sky coverage, and leave treating noise for Section V. Much of the information in this section can be found in standard cosmology texts [69, 70]

1. The 3D power spectrum

It is well-known that the primordial dark matter field which formed the initial seeds of LSS is a GRF. That is, the random realization of initial dark matter fluctuations can be modeled as a draw from its characteristic power spectrum. In linear perturbation theory, the matter density field at late times can still be considered to be Gaussian on sufficiently large scales, allowing one to write down the probability distribution of an observed field given a power spectrum.

For a homogeneous and isotropic survey volume V with periodic boundary conditions, the power spectrum of a GRF $\delta(\mathbf{r})$ is defined as

$$\langle \delta_{\mathbf{k}}^* \delta_{\mathbf{k}'} \rangle \equiv \frac{1}{V} P(k) \delta^{(D)}(\mathbf{k} - \mathbf{k}'), \quad (14)$$

describing the power concentrated across comoving scales $k \equiv |\mathbf{k}|$. Here, $\delta_{\mathbf{r}}$ denotes the field in real space whereas $\delta_{\mathbf{k}}$ denotes its Fourier transform; $\delta^{(D)}$ is the Dirac-delta function.

In perturbation theory, the field of interest is the matter overdensity field

$$\delta^m(\mathbf{r}) \equiv \frac{\rho^m(\mathbf{r}) - \langle \rho^m \rangle}{\langle \rho^m \rangle}. \quad (15)$$

where $\rho^m(\mathbf{r})$ is the matter density field and $\langle \rho^m \rangle$ is its expectation value. The underlying matter fields ρ^m and δ^m are not directly observable; however, bright astrophysical objects such as galaxies, galaxy clusters, and even GW sources trace the underlying matter field. These tracers are generally modeled as a biased Poisson realization of the matter field:

$$\bar{\delta}^X(\mathbf{r}) \equiv \frac{\bar{\rho}^X(\mathbf{r}) - \langle \bar{\rho}^X \rangle}{\langle \bar{\rho}^X \rangle} = b^X \delta^m(\mathbf{r}). \quad (16)$$

where $\bar{\rho}^X(\mathbf{r})$ is now the Poisson probability density field of tracer X , and b^X is its bias parameter. Here, we use

the overline $\bar{\delta}$ to indicate that this is the overdensity field of the tracer probability (i.e. Poisson rate), whereas a plain δ denotes the Poisson-realized overdensity field, as we describe below.

The relevant observable for tracers is not the Poisson probability, but rather the realized number counts field $n^X(\mathbf{r})$ and corresponding overdensity field

$$\delta^X(\mathbf{r}) \equiv \frac{n^X(\mathbf{r}) - \langle n^X \rangle}{\langle n^X \rangle}. \quad (17)$$

We can write the shot noise as an additive component s

$$\begin{aligned} \delta^X(\mathbf{r}) &= \bar{\delta}^X(\mathbf{r}) + s^X(\mathbf{r}) \\ \delta^X(\mathbf{k}) &= \bar{\delta}^X(\mathbf{k}) + s^X(\mathbf{k}). \end{aligned} \quad (18)$$

Substituting the Poisson variance $\langle s^X(\mathbf{r})s^X(\mathbf{r}') \rangle = \frac{\delta^{(D)}(\mathbf{r}-\mathbf{r}')}{\langle n^X(\mathbf{r}) \rangle}$ and the definition of the power spectrum in Equation (14) yields

$$P^X(k) = \bar{P}^X(k) + \frac{1}{\langle n^X \rangle} = (b^X)^2 P^m(k) + \frac{1}{\langle n^X \rangle}, \quad (19)$$

i.e., the power spectrum of the number counts field is the power spectrum of the probability field plus a scale-independent shot noise. Applying the central limit theorem ($n^X V \gg 1$), the observed number overdensity field δ^X also approximately follows a Gaussian, with an effective power spectrum of $P^X(k)$.

Writing down the probability distribution for a GRF is simple, especially in Fourier space. The Fourier modes are discrete for a finite rectangular survey volume, and homogeneity and isotropy imply that they are independent:

$$p(\{\delta_{\mathbf{k}}^X\}) = \prod_{\mathbf{k} \geq 0} \frac{1}{\sqrt{2\pi \langle |\delta_{\mathbf{k}}^X|^2 \rangle}} \exp\left(-\frac{1}{2} \frac{|\delta_{\mathbf{k}}^X|^2}{\langle |\delta_{\mathbf{k}}^X|^2 \rangle}\right). \quad (20)$$

We take the product for modes $k_{\{x,y,z\}} \geq 0$ because the reality condition implies that $\delta_{\mathbf{k}} = \delta_{-\mathbf{k}}^*$, reducing the number of independent modes. The elements of the diagonal covariance matrix, $\langle |\delta_{\mathbf{k}}^X|^2 \rangle$, are given by the 3D power spectrum (up to a volumetric constant dependent on the Fourier convention), as in Equation (14). Note that $\langle \delta^X \rangle = 0$ by the definition of the overdensity field. The power spectrum characterizes the clustering patterns of a tracer.

Equation (20) is straightforwardly generalized to multiple tracers. The joint Gaussian distribution on the overdensity fields of two tracers X and Y is

$$p(\{\delta_{\mathbf{k}}^X\}, \{\delta_{\mathbf{k}}^Y\}) = \prod_{\mathbf{k} \geq 0} \mathcal{N}[\delta_{\mathbf{k}}; 0, \mathbf{C}_{\mathbf{k}}] \quad (21)$$

where

$$\mathcal{N}[\delta_{\mathbf{k}}; 0, \mathbf{C}_{\mathbf{k}}] \equiv \frac{1}{\sqrt{(2\pi)^2 \det \mathbf{C}_{\mathbf{k}}}} \exp\left(-\frac{1}{2} \delta_{\mathbf{k}}^\dagger \mathbf{C}_{\mathbf{k}}^{-1} \delta_{\mathbf{k}}\right) \quad (22)$$

is a complex multivariate Gaussian on the field vector

$$\delta_{\mathbf{k}} \equiv \begin{pmatrix} \delta_{\mathbf{k}}^X \\ \delta_{\mathbf{k}}^Y \end{pmatrix}. \quad (23)$$

with mean 0 and covariance matrix

$$\mathbf{C}_{\mathbf{k}} \equiv \begin{pmatrix} \langle |\delta_{\mathbf{k}}^X|^2 \rangle & \langle \delta_{\mathbf{k}}^X \delta_{\mathbf{k}}^{Y*} \rangle \\ \langle \delta_{\mathbf{k}}^X \delta_{\mathbf{k}}^{Y*} \rangle & \langle |\delta_{\mathbf{k}}^Y|^2 \rangle \end{pmatrix} = V \begin{pmatrix} P^X(k) & P^{XY}(k) \\ P^{XY}(k) & P^Y(k) \end{pmatrix}. \quad (24)$$

This defines the cross-correlation power spectrum $P^{XY}(k)$.

One can similarly derive an expression for the cross shot noise

$$\langle s^X(\mathbf{r})s^Y(\mathbf{r}) \rangle = \frac{\langle n^X n^Y \rangle}{\langle n^X \rangle \langle n^Y \rangle} \quad (25)$$

where $\langle n^X n^Y \rangle$ is equal to the number density of coincident tracers. Thus,

$$P^{XY}(k) = b^X b^Y P^m(k) + \frac{\langle n^X n^Y \rangle}{\langle n^X \rangle \langle n^Y \rangle} \quad (26)$$

The shot noise of the cross-power spectrum is typically taken to be 0, since for two distinct fields the coincident number density is 0. Nonetheless, the cross shot noise plays an important role in relation to the standard galaxy catalog method because it encodes the GW–galaxy coincident number density, i.e., how often one expects a GW host galaxy to be in the catalog. In the limit of galaxy catalog completeness, the cross shot noise is the same as the galaxy shot noise, $1/\langle n^g \rangle$.

Generally, both the power spectrum and bias parameters are functions of z , characterizing the growth of LSS throughout cosmic history. Additionally, the simple constant linear bias in Equation (16) only works on linear scales where $|\delta| \ll 1$. On non-linear scales (~ 10 Mpc), the matter density field is highly non-linear with steep overdensities in the form of clusters and halos. In the quasi-linear regime, one can continue the perturbation theory series expansion and fit a polynomial bias (e.g., [71])

$$b(k) = b + \sum_{n=1} a_n \left(\frac{k}{k_*}\right)^n. \quad (27)$$

for some suitable pivot scale k_* . In the fully non-linear regime, one would need a halo model to describe the 2-point (and higher order) statistics of the matter field [72–74]. We do not consider this further in this work.

2. The angular power spectrum

The 3D Fourier prescription is usually insufficient for modern surveys, which are deep enough to probe the evolution of the power spectrum as a function of redshift and wide enough such that the survey area can no longer

be approximated as a Cartesian box. Many galaxy surveys have turned to a spherical harmonic approach to the problem [75–79], analyzing the data in tomographic radial slices. This approach has the added benefit of allowing the separate characterization of angular and radial sources of error, which we will discuss in Section V. Moreover, it allows us to analyze maps of tracers with different radial distance measures, such as galaxies in redshift space and GWs in luminosity distance space, without assuming a cosmology *a priori*.

Let us bin tracer X into M radial bins using radial window functions $w^{X_\alpha}(r)$ for $\alpha = 1, 2, \dots, M$. The projected angular number counts density field of each bin is

$$n^{X_\alpha}(\mathbf{\Omega}) = \int dr w^{X_\alpha}(r) \frac{dN_{\text{obs}}^X}{dr d\mathbf{\Omega}} \quad (28)$$

where

$$\frac{dN_{\text{obs}}^X}{dr d\mathbf{\Omega}} = p_{\text{obs}}^X(r) \frac{dN_{\text{obs}}^X}{d\mathbf{\Omega}} \Big|_r \quad (29)$$

is the *observed* distribution of tracer X , i.e., with selection effects folded in. The 3D overdensity field at an infinitesimal slice at distance r is²

$$\begin{aligned} \delta^X(\mathbf{r} = (r, \mathbf{\Omega})) &= \frac{n_{3\text{D}}^X(\mathbf{r})}{\langle n_{3\text{D}}^X(\mathbf{r}) \rangle} - 1 \\ &= \frac{\frac{1}{\chi(r)^2} \frac{dN_{\text{obs}}^X}{d\chi d\mathbf{\Omega}} \Big|_{\chi(r)}}{\left\langle \frac{1}{\chi(r)^2} \frac{dN_{\text{obs}}^X}{d\chi d\mathbf{\Omega}} \Big|_{\chi(r)} \right\rangle} - 1 \\ &= \frac{n^X(\mathbf{\Omega}|r)}{\langle n^X(\mathbf{\Omega}|r) \rangle} - 1. \end{aligned} \quad (30)$$

where χ is the radial comoving distance. Thus, if we define the effective window function

$$\phi^{X_\alpha}(r) \equiv \frac{w^{X_\alpha}(r) p_{\text{obs}}^X(r)}{\int dr w^{X_\alpha}(r) p_{\text{obs}}^X(r)}, \quad (31)$$

the 2D-projected overdensity field $\Delta^X(\mathbf{\Omega})$ can be expressed as a weighted integral of the 3D overdensity field

$$\Delta^{X_\alpha}(\mathbf{\Omega}) \equiv \frac{n^{X_\alpha}(\mathbf{\Omega}) - \langle n^{X_\alpha} \rangle}{\langle n^{X_\alpha} \rangle} = \int dr \phi^{X_\alpha}(r) \delta^X(\mathbf{r}). \quad (32)$$

Because linear operations preserve Gaussianity, the radially projected 2D density field can also be described by a GRF. Many of the results for the 3D power spectrum have analogous angular counterparts, with the spherical harmonic transform (SHT) as the spherical analog of the

Fourier transform. Let $a_{\ell m}^{X_\alpha}$ be the SHT of $\Delta^{X_\alpha}(\mathbf{\Omega})$:

$$\Delta^{X_\alpha}(\mathbf{\Omega}) = \sum_{\ell=0}^{\infty} \sum_{m=-\ell}^{\ell} a_{\ell m}^{X_\alpha} Y_{\ell m}(\mathbf{\Omega}) \quad (33)$$

$$a_{\ell m}^{X_\alpha} = \int d\mathbf{\Omega} \Delta^{X_\alpha}(\mathbf{\Omega}) Y_{\ell m}^*(\mathbf{\Omega}). \quad (34)$$

Analogously to the 3D power spectrum, the M overdensity fields of tracer X are characterized by their angular power spectra

$$C_\ell^{X_\alpha X_\beta} \delta_{\ell\ell'}^{(K)} \delta_{mm'}^{(K)} \equiv \left\langle \left(a_{\ell m}^{X_\alpha} \right)^* a_{\ell' m'}^{X_\beta} \right\rangle, \quad (35)$$

which is diagonal in ℓ and m due to the spherical symmetry of the fields; $\delta^{(K)}$ denotes the Kronecker delta function. Note that radial Fourier modes couple different angular shells together. Similarly, the angular cross-power spectrum describes the coupling between the binned density fields of two tracers X and Y :

$$C_\ell^{X_\alpha Y_\beta} \delta_{\ell\ell'}^{(K)} \delta_{mm'}^{(K)} \equiv \left\langle \left(a_{\ell m}^{X_\alpha} \right)^* a_{\ell' m'}^{Y_\beta} \right\rangle. \quad (36)$$

Equation (32) expresses the projected angular density field as a weighted integral of the 3D density field over the bin's effective window function. Using this and the definition of the angular power spectrum in Equation (36), one can show that the angular power spectrum is itself an integral of the 3D power spectrum over the window functions. Specifically, given tracers X, Y with probability density fields characterized by a 3D power spectrum \bar{P}^{XY} , the cross-correlation of the angular probability overdensity fields $\bar{C}_\ell^{\alpha\beta}$ between bin α of tracer X and bin β of tracer Y is

$$\begin{aligned} \bar{C}_\ell^{\alpha\beta} &= \int_0^\infty \frac{d\chi}{\chi^2} \left(\frac{dr}{d\chi} \right) \left(\frac{dr'}{d\chi} \right) \phi_i^\alpha(r(\chi)) \phi_j^\beta(r'(\chi)) \\ &\quad \times b^X(k, z) b^Y(k, z) P^m \left(k = \frac{\ell + 1/2}{\chi}, z(\chi) \right) \end{aligned} \quad (37)$$

where r is the radial coordinate for tracer X and r' is the radial coordinate for tracer Y , which are not necessarily the same (as is the case for GWs and galaxies). Recall that the 3D power spectrum of the probability density fields is given by $\bar{P}^{XY}(k, z) = b^X(k, z) b^Y(k, z) P^m(k, z)$ (where b are the bias parameters and P^m is the matter power spectrum); it has gained a z dependence because working in spherical slices allows us to probe the evolving LSS of the universe as we go back farther in z . Equation (37) is a first-order approximation in $(\ell + 1/2)^{-1}$ known as the Limber equation³ [80, 81]. The Limber approximation has its limitations; it breaks down at large

² Henceforth, 3D number densities will be referred to explicitly as $n_{3\text{D}}(\mathbf{r})$, and $n(\mathbf{\Omega})$ will refer to angular number densities.

³ The exact formula is a complicated integral of the unequal-time power spectrum $P(k, z(r), z(r'))$ over k , r , and r' . The *Limber approximation* assumes the power spectrum is slowly-varying with respect to the sharply peaked spherical Bessel function $j_\ell(k\chi)$ at $k\chi(r) = k\chi(r') \approx \ell + 1/2$, which greatly simplifies the expression.

angular scales ($\ell \lesssim 20$), and also if the relative bin width $\delta\chi/\chi$ is too small [82]. Furthermore, while clustering in the radial direction is encoded in the coupling between radial shells, it is a higher-order term that is ignored in the Limber approximation. Nonetheless, it is in principle possible to use the exact integral form, or include higher orders in the approximation [81].

At this point, we will drop the tracer label for brevity (as the tracer and bin label always appear together) and use labels $\alpha, \beta \in \{1, 2, \dots, M+M'\}$, such that $1 \leq \alpha, \beta \leq M$ corresponds to the M bins of tracer X and $M+1 \leq \alpha, \beta \leq M+M'$ corresponds to the M' bins of tracer Y .

Analogously to Equation (26), we can also derive the shot noise for the 2D number counts field. If we model each infinitesimal volume dV in space as a Poisson point process, then for any given radial bin the number count per pixel $d\Omega$ integrated over the bin is also Poisson. Thus, the power spectrum of the number counts field can again be written as a sum of the power spectrum of the probability field and a scale-independent shot noise

$$a_{\ell m}^\alpha = \bar{a}_{\ell m} + s_\ell \quad (38)$$

$$C_\ell^{\alpha\beta} = \bar{C}_\ell^{\alpha\beta} + \frac{\langle n^\alpha n^\beta \rangle}{\langle n^\alpha \rangle \langle n^\beta \rangle} \quad (39)$$

If the coincident number density is negligible (e.g. different tracers or non-overlapping bins), the shot noise is given by

$$C_\ell^{\alpha\beta} = \bar{C}_\ell^{\alpha\beta} + \frac{\delta_{\alpha\beta}^{(K)}}{\langle n^\alpha \rangle}, \quad (40)$$

which is its usual form in the literature. As before, modeling the shot noise term as Gaussian requires a sufficiently large number of objects expected per radial bin.

To write down the probability distribution for M and M' overdensity fields of tracers X and Y , respectively, we define for each ℓ, m the vector and corresponding covariance matrix

$$\mathbf{a}_{\ell m} = \left(a_{\ell m}^1, a_{\ell m}^2, \dots, a_{\ell m}^{M+M'} \right)^T \quad (41)$$

$$\Sigma_{\ell, \alpha\beta} = \langle \mathbf{a}_{\ell m}^*[\alpha] \mathbf{a}_{\ell m}[\beta] \rangle = C_\ell^{\alpha\beta}. \quad (42)$$

Thus, the probability of realizing these $M+M'$ overdensity fields given a power spectrum $C_\ell^{\alpha\beta}$ is then a complex multivariate Gaussian diagonal in ℓ and m :

$$p(\{a_{\ell m}^X\}, \{a_{\ell m}^Y\} | \{C_\ell^{\alpha\beta}\}) = \prod_{\ell=\ell_{\min}}^{\ell_{\max}} \prod_{m=0}^{\ell} \mathcal{N}[\mathbf{a}_{\ell m}; 0, \Sigma_\ell] \quad (43)$$

where the covariance matrix Σ_ℓ is given by Equation (42). Note that ℓ_{\min} and ℓ_{\max} are typically set by either the Limber approximation or the survey size and resolution, and that the product in Equation (43) runs from $m=0$ to $m=\ell$ because the reality condition requires $a_{\ell m} = a_{\ell-m}^*$.

C. An optimal data compression step

If we now let $X = G$ (GW sources, $r = d_L$) and $Y = g$ (galaxies, $r' = z$), then Equation (43) defines a joint probability distribution for the observed GW and galaxy overdensity fields given a theoretical power spectrum. Equation (43), however, is not the population prior used in the cross-correlation method. This is because Equation (43) is effectively a joint distribution of all voxels in the volume, which quickly becomes unwieldy with even modest resolutions; a map with a 1° resolution will have a $\mathcal{O}(10^4) \times (M+M')^2$ size covariance matrix *after* factoring in the decoupling of different harmonic modes!

The problem of how to compress the data stored in these maps without losing information on the cosmological parameters of interest was studied extensively for the efficient analysis of high-resolution Cosmic Microwave Background (CMB) maps. Much of the following discussion is taken from [83]; we review the core pieces here.

[83] defined the notion of a *lossless compression* as one in which “any set of cosmological parameters can be measured just as accurately from the compressed data set as from the original data set”. In particular, for some unknown parameters Λ , the Cramer-Rao inequality sets a lower bound on the error of any unbiased estimator constructed from the data \mathbf{d}

$$\Delta\Lambda_i(\mathbf{d}) \geq (\mathbf{F}^{-1})_{ii}^{1/2} \quad (44)$$

where \mathbf{F} is the Fisher information matrix. Therefore, if the variance of an unbiased estimator $\hat{\Lambda}(\tilde{\mathbf{d}})$ constructed from the compressed data $\tilde{\mathbf{d}}$ achieves the bound set by the Cramer-Rao inequality on the original dataset \mathbf{d} , then the compression $\tilde{\mathbf{d}}$ can be considered lossless.

In the problem at hand, our uncompressed data are the maps $\{\Delta^\alpha(\Omega)\}$, or equivalently, its SHT $\{a_{\ell m}^\alpha\}$; the parameters of interest Λ are the cosmological parameters Λ_c . Because all the cosmological information in the Gaussian distribution of the fields in Equation (43) is encoded in the elements of the covariance matrix (i.e., the angular power spectra $\{C_\ell^{\alpha\beta}\}$), it is sufficient to show that a compression is lossless on the power spectra to show that it is lossless on any cosmological parameters derived from the power spectrum. That is, for this exercise we can effectively take $\{C_\ell^{\alpha\beta}\}$ itself to be the parameters of interest Λ .

Using Equation (43), the inverse Fisher matrix for data $\{a_{\ell m}^\alpha\}$ and parameters $\{C_\ell^{\alpha\beta}\}$ is [84, 85]

$$\mathbf{F}^{-1} = \left\langle C_\ell^{\alpha\beta} C_{\ell'}^{\mu\nu} \right\rangle = \frac{\delta_{\ell\ell'}^{(K)}}{2\ell+1} \left[C_\ell^{\alpha\mu} C_\ell^{\beta\nu} + C_\ell^{\alpha\nu} C_\ell^{\beta\mu} \right]. \quad (45)$$

Next, we want to construct an unbiased estimator for the power spectrum that can saturate this bound. The most straightforward estimator, which can be shown to be minimum-variance with isotropic noise and sky coverage, is constructed by simply averaging over the modes

for each ℓ :

$$\tilde{C}_\ell^{\alpha\beta} = \frac{1}{2\ell + 1} \sum_{m=-\ell}^{\ell} a_{\ell m}^{\alpha*} a_{\ell m}^{\beta} \quad (46)$$

Under the assumption of Gaussianity of the field, the error of this estimator can be computed with Wick's theorem and also shown to be equal to Equation (45), thus saturating the Cramer-Rao bound on the uncompressed data, i.e., the fields themselves.

Therefore, we can take the power spectrum estimator of Equation (46) itself to be our compressed data; $\{\tilde{C}_\ell^{\alpha\beta}\}$ compresses $\{a_{\ell m}^{\alpha}\}$ from $\sim (M + M')\ell_{\max}^2$ numbers to $\sim (M + M')^2\ell_{\max}/2$ numbers without losing any information on the angular power spectra $\{C_\ell^{\alpha\beta}\}$ ⁴. This ought to make sense intuitively: due to isotropy, the astrophysically relevant information is encoded in the total power in different angular scales ℓ rather than the phase information in each m . In the case of GWs and galaxies, for example, the cross power spectrum of a given z -shell and d_L -shell is encoded in how similarly the galaxies and GWs cluster together averaged over the entire sphere, rather than in any specific direction. This is analogous to how in standard GW population analyses, the product of individual event likelihoods probes $p^g(z, \mathbf{\Omega})$ at event positions over the entire sky for each dz .

This motivates the use of the cross-correlation estimator $\{\tilde{C}_\ell^{\alpha\beta}\}$ as our observable, rather than the fields themselves. Because the cross-correlation estimators are symmetric in $\alpha \leftrightarrow \beta$ by construction, we use the notation $\{\tilde{C}_\ell^{[\alpha\beta]}\}$ to enforce $\alpha \geq \beta$, referring to the non-redundant set of cross-correlation power spectra. For α, β spanning two tracers X, Y , this is a “3x2pt” analysis, referring to the 2-point statistics of 3 sets of power spectra: C_ℓ^{XX} , C_ℓ^{XY} , and C_ℓ^{YY} .

Strictly speaking, $\{\tilde{C}_\ell^{[\alpha\beta]}\}$ is a complex Wishart distributed, since it is the sample covariance of a multivariate-Gaussian distributed variable. However, one can use the central limit theorem to approximate the distribution as Gaussian

$$p\left(\left\{\tilde{C}_\ell^{[\alpha\beta]}\right\} \mid \left\{C_\ell^{[\alpha\beta]}\right\}\right) = \prod_{\ell=\ell_{\min}}^{\ell_{\max}} \frac{1}{\sqrt{(2\pi)^r \det \mathbf{\Sigma}_\ell}} \exp\left[-\frac{1}{2} \sum_{\alpha \leq \beta} \sum_{\mu \leq \nu} \sum_{\ell} \Delta C_\ell^{\alpha\beta} (\mathbf{\Sigma}_\ell)_{\alpha\beta, \mu\nu}^{-1} \Delta C_\ell^{\mu\nu}\right], \quad (47)$$

where $r = \frac{(M+M')(M+M'+1)}{2}$ is the number of power spectra per ℓ for $1 \leq \beta \leq \alpha \leq M + M'$, the covariance matrix $\mathbf{\Sigma}_\ell$ was given in Equation (45), and

$$\Delta C_\ell^{\alpha\beta} \equiv \tilde{C}_\ell^{\alpha\beta} - C_\ell^{\alpha\beta} \quad (48)$$

⁴ Of course, this is only a compression if $\ell_{\max} > (M + M')/2$, which is to say that this compression becomes less efficient if we try to use a large number of bins while having poor resolution (low ℓ_{\max}).

is the difference between the power spectrum estimator and our model for the power spectrum. Note that the central limit theorem does not work for small ℓ [86]. Imposing $\ell \gtrsim 20$, for example, ensures at least ~ 40 independent modes. Another caveat is that Equation (46) is a cosmic variance estimator, which means it estimates the power spectrum by assuming the different m modes sample independent realizations of the power spectrum; the Gaussianity of Equation (47) also relies on the independence of the different modes via the central limit theorem. This requires the number of observations per bin $N \gg 2\ell + 1$, the number of degrees of freedom per ℓ ; if N is small, then the shot noise is highly non-Gaussian and the variance of the \tilde{C}_ℓ no longer satisfies Equation (45). Probing scales up to $\ell \sim 60$ ($\sim 1^\circ$ resolution), for example, would require at least hundreds of events per bin.

In summary, a probability distribution on GRFs $\{a_{\ell m}^{\alpha}\}$ can be compressed into a distribution on the cross-correlation estimator $\{\tilde{C}_\ell^{\alpha\beta}\}$; this compression is both optimal and lossless. The distribution is Gaussian if ℓ is not small and, for a Poisson-realized tracer field, $N \gg 2\ell + 1$.

IV. TOWARDS A UNIFIED POPULATION PRIOR

In order to construct a method that can leverage the combined information from the canonical galaxy catalog and cross-correlation methods, it is useful to first examine qualitatively where each method derives its cosmological constraining power.

The GW and galaxy data can be effectively considered as measurements $\{d_L, \mathbf{\Omega}, m_1, m_2, \dots\}$ and $\{z^g, \mathbf{\Omega}^g, \dots\}$, respectively, for N^G events and N^g galaxies. As described in Section III A, dark siren methods probe cosmology by directly measuring the luminosity distance and redshifted masses of the source merger, thus allowing one to probe the $d_L - z$ relation by modeling the source-frame mass and redshift distributions. The galaxy catalog method uses a 3D spatial prior informed by the positions of observed galaxies

$$p(z, \mathbf{\Omega} \mid \{\mathbf{d}^g\}, \mathbf{\Lambda}) = p(z \mid \mathbf{\Lambda}, \{\mathbf{d}^g\}) p(\mathbf{\Omega} \mid z, \{\mathbf{d}^g\}, \mathbf{\Lambda}) \propto \frac{\mathcal{R}(z \mid \mathbf{\Lambda}) dV_c}{1+z} (\mathbf{\Lambda}) p(\mathbf{\Omega} \mid z, \mathbf{\Lambda}, \{\mathbf{d}^g\}) \quad (49)$$

where in going from the first line to the second line, we have approximated the distribution of galaxies as uniform in comoving volume averaged over all sky directions. One can in more generality use a $p(z \mid \mathbf{\Lambda}, \{\mathbf{d}^g\})$ informed by the radial distribution of the observed galaxies, but given the incompleteness of galaxy surveys at typical GW luminosity distances, the information we get from galaxies after factoring out the angular dependence is negligible. Thus, Equation (49) splits the spatial distribution into a radial part, encoding information from the vanilla spectral sirens method (or in greater generality the radial part of the galaxy catalog method), and a conditional angular

part, which encodes the additional information on field overdensities from a galaxy catalog.

The cross-correlation method, on the other hand, models a population prior on the GW and galaxy *fields*, rather than individual events. The cosmological information in the cross-correlation method is contained entirely in the covariance matrix of the Gaussian fields and therefore the angular power spectrum $\overline{C}_\ell^{\alpha\beta}$. If we revisit Equation (37), we can see that there are three ways in which cosmological parameters can enter $\overline{C}_\ell^{\alpha\beta}$:

- The $d_L - z$ relation, as we integrate over radial window functions in two different coordinates $r = d_L$ and $r' = z$
- The comoving angular diameter distances χ to each shell, which leverages features of the power spectrum at scales $P^m(k \approx \ell/\chi)$ as standard rulers
- $P^m(k)$ itself, which is sensitive to the cosmology

Much of the cross-correlation literature focuses on the $d_L - z$ relation as the source of constraining power, as the cross-correlation matches shells of the GW angular density field in d_L space to shells of the galaxy angular density field in z -space [41, 55]. However, as noted in [41], the amplitude and scale of these correlations are coupled to the shape of the power spectrum and therefore also to galaxy (C_ℓ^{gg}) and GW (C_ℓ^{GG}) auto-correlations. The constraining power of these auto-power spectra are highly nontrivial, as they form the basis of experiments such as DESI [87–89], Euclid [90], SKA [87], and LSST [91, 92]. We will demonstrate an example of this later in Figure 7, where the combined 3x2pt analysis of power spectra $C_\ell^{GG}, C_\ell^{Gg}, C_\ell^{gg}$ sets significantly stronger constraints than an analysis of galaxy–galaxy or GW–galaxy cross-correlations alone.

Upon comparing the dark siren and cross-correlation methods, we can identify information that is used by one method but not the other. The cross-correlation method does not use any kind of information on the rate evolution of GWs in $p(z|\mathbf{A})$. It is also agnostic to the completeness of the galaxy catalog, which the galaxy catalog method makes use of to predict how often GWs and galaxies are coincident. In fact, the cross-correlation method does not even require GW and galaxies to be coincident at all, only that they trace (with possibly different biases) the same underlying matter field. On the other hand, canonical dark siren methods do not use any 2-point statistics, effectively assuming a flat power spectrum. Nonetheless, there are similarities: both methods derive information by coupling the luminosity distance of GWs to the redshift measurements of galaxies.

One can imagine a unified population prior that utilizes both the spectral sirens rate information and the full Gaussian 2-point statistics of the cross-correlation method, from both galaxies and GWs. The goal of this section is to describe such a method.

A. What is our model conditioned upon?

The most obvious difference between a standard GW population analysis and the cross-correlation method is that the former models the probability of the positions of individual GW events and galaxies, while the latter models the distribution of GW and galaxy density fields jointly at all points in space. A standard hierarchical GW population prior (i.e., Equation (4)) assumes that GWs are independent and identically distributed (IID) (implicit in the factorization of the event-level likelihoods), and thus does not allow for any 2-point correlations in the spatial field.

This assumption of independence is a subtle one. Physically, it must be true: whether or not a BBH merges in one galaxy must be independent of what is happening in another galaxy. Given the underlying galaxy field from which the GW sources are drawn, the location of GW sources are conditionally independent. However, if we only have a probabilistic description of the galaxy field, then the observed GWs are no longer independently distributed because one must marginalize over its possible realizations. In any realization of the universe, the positions of galaxies are correlated and its 2-point statistics are given by the matter power spectrum which sources the galaxy probability field. In other words, the GW tracer density field is a *doubly stochastic process*, because the underlying probability density field sourcing the Poisson process (the galaxy field) is itself random, and thus the tracers cannot be considered to be IID if the underlying probability density field is not known.

In the case of dark siren cosmology, we do not have information on the missing galaxies. Therefore, one must either condition upon the observed galaxy density field and marginalize over all possible realizations of the missing galaxies according to the power spectrum, or jointly model the observed GWs and galaxy fields. As we will describe below, the latter method lends itself to the cross-correlation method.

B. From dark sirens to cross-correlations

We begin by recasting the dark siren galaxy prior $p^g(z, \mathbf{\Omega})$ in terms of the overdensity field. Consider the angular overdensity field of some tracer X binned in an infinitesimal shell at radius r :

$$1 + \Delta^{X_r}(\mathbf{\Omega}) = \frac{n^{X_r}(\mathbf{\Omega})}{\langle n^{X_r} \rangle} = \frac{dN^X}{dr d\mathbf{\Omega}} \left[\frac{1}{4\pi} \frac{dN^X}{dr}(r) \right]^{-1} \quad (50)$$

The conditional angular distribution of some tracer $p^X(\mathbf{\Omega}|r)$ can be written via Bayes' theorem as

$$\begin{aligned} p^X(\mathbf{\Omega}|r) &= \frac{p(r, \mathbf{\Omega})}{p(r)} \\ &= \frac{dN^X}{dr d\mathbf{\Omega}} \left(\frac{dN^X}{dr} \right)^{-1} \end{aligned} \quad (51)$$

and hence the angular overdensity field is directly related to the angular distribution $P(\boldsymbol{\Omega}|r)$:

$$\frac{1}{4\pi} [1 + \Delta^X(\boldsymbol{\Omega}|r)] = p^X(\boldsymbol{\Omega}|r). \quad (52)$$

Equation (51) also implies from Equation (9)

$$p^G(\boldsymbol{\Omega}|z) = p^{g,\text{tot}}(\boldsymbol{\Omega}|r) \quad (53)$$

or equivalently

$$\bar{\Delta}^G(\boldsymbol{\Omega}|z) = \Delta^{g,\text{tot}}(\boldsymbol{\Omega}|z), \quad (54)$$

i.e., the GW rate evolution $\mathcal{R}(z)$ is normalized out. Note that $\bar{\Delta}^G$ indicates that the GW field is itself a stochastic realization of $\Delta^{g,\text{tot}}(\boldsymbol{\Omega}|z)$.

The angular distribution of galaxies at a given redshift z is the weighted sum of the distributions of observed and unobserved galaxies

$$p^{g,\text{tot}}(\boldsymbol{\Omega}|z, \{\mathbf{d}^g\}) = p(D^g|z, \mathbf{\Lambda}_c) p^{g,\text{obs}}(\boldsymbol{\Omega}|z, \{\mathbf{d}^g\}, \mathbf{\Lambda}) + (1 - p(D^g|z, \mathbf{\Lambda}_c)) p^{g,\text{miss}}(\boldsymbol{\Omega}|z, \{\mathbf{d}^g\}, \mathbf{\Lambda}). \quad (55)$$

where $\{\mathbf{d}^g\}$ is the galaxy data, and D^g (\bar{D}^g) indicates whether (or not) the galaxy is detected. This is equivalent to the galaxy catalog method population prior derived in Equation (11). The detection coefficient in Equation (55) is different than Equation (11) because the former conditions on the redshift.

Equation (55) can be written in terms of overdensity fields via Equation (52)

$$\Delta^{g,\text{tot}}(\boldsymbol{\Omega}|z) = p(D^g|z, \mathbf{\Lambda}_c) \Delta^{g,\text{obs}}(\boldsymbol{\Omega}|z) + (1 - p(D^g|z, \mathbf{\Lambda}_c)) \Delta^{g,\text{miss}}(\boldsymbol{\Omega}|z). \quad (56)$$

As we will show, the differences between the cross-correlation and standard galaxy catalog method lie in how the missing galaxies $\Delta^{g,\text{miss}}(\boldsymbol{\Omega}|z)$ are treated, as well

$$p(\boldsymbol{\Omega}|z, \mathbf{\Lambda}, \{\Delta^g\}) \propto p(D^g|\mathbf{\Lambda}_c) [1 + \Delta^g(\boldsymbol{\Omega}|z)] + (1 - p(D^g|\mathbf{\Lambda}_c)) \left[1 + \int d\{\Delta^{g,\text{miss}}\} \Delta^{g,\text{miss}}(\boldsymbol{\Omega}|z) p(\{\Delta^{g,\text{miss}}\} | \{\Delta^g\}, \{z^g\}, \mathbf{\Lambda}_b, \mathbf{\Lambda}_c) \right] \quad (58)$$

Here, the possible angular distributions of the missing galaxies $\{\Delta^{g,\text{miss}}\}$ can be taken to be a vector of values on a discretized set of voxels. The conditional distribution $p(\{\Delta^{g,\text{miss}}\} | \{\Delta^{g,\text{obs}}\}, \dots)$ is a conditional multivariate Gaussian, which can be evaluated from the full multivariate Gaussian in Equation (43) when transformed to harmonic space. The theoretical power spectrum can be computed from the cosmology, bias parameters $\mathbf{\Lambda}_b$, and shot noise.

An equivalent approach is to make a change of vari-

ables in Equation (56) and marginalize over the total galaxy field. This approach has been taken by recent works such as [34, 57, 58], and can be considered a hybrid approach that directly incorporates large-scale structure to inform the underlying $p^{g,\text{tot}}(z, \boldsymbol{\Omega})$ in the dark siren method. The downside of this method is that it can be quite computationally expensive; one must marginalize over all possible realizations of the entire galaxy field, and thus the dimensionality of the parameter space is proportional to the survey volume at fixed resolution.

as what data we are conditioning on. We will now put everything together and describe four different approaches to dealing with the missing galaxies, representing a continuous deformation from the standard galaxy catalog method to the cross-correlation method.

For the rest of this manuscript, we will abbreviate the superscript $g, \text{obs} \rightarrow g$, such that a lone g implicitly refers to the observed galaxies.

1. The canonical galaxy catalog method

The simplest way to deal with the missing galaxies is just to ignore their 2-point statistics altogether and take $\Delta^{g,\text{miss}} = 0$. It is easy to see from Equation (52) that this is equivalent to taking the distribution of the missing galaxies to be uniform, such that

$$p(\boldsymbol{\Omega}|z, \mathbf{\Lambda}, \{\mathbf{d}^g\}) = p(D^g|z, \mathbf{\Lambda}_c) p^g(\boldsymbol{\Omega}|z, \mathbf{\Lambda}, \{\mathbf{d}^g\}) + \frac{1 - p(D^g|z, \mathbf{\Lambda}_c)}{4\pi} \quad (57)$$

which, once we put back in $p^{g,\text{tot}}(z) \propto dV_c/dz$, is just the ‘‘homogeneous completion’’ of missing galaxies in the standard galaxy catalog method.

Alternatively, one can assume that the missing galaxies trace the observed galaxies $\Delta^{g,\text{miss}} = \Delta^g$, which is the ‘‘multiplicative completion’’ of missing galaxies in the standard galaxy catalog method. In either case, one conditions on a fixed distribution as the ground truth for the distribution of missing galaxies, which we by definition have no knowledge of.

2. Marginalizing over the missing galaxies

A correction would be to marginalize over all possible realizations of the missing galaxies, given the observed galaxies and a power spectrum:

3. From coordinates to fields

Gaussian 2-point statistics are much more easily expressed if we write the probability distribution in terms of the GW density field $n^G(\mathbf{r})$, rather than the individual event parameters $\{z, \mathbf{\Omega}\}$. Besides the voxel resolution, the only information that is lost in this change of variables is the distinguishability of the different objects, which is irrelevant for evaluating the population prior, as the ordering of the product in Equation (4) does not matter. Nonetheless, the labelling of different objects is generally important in GW population analyses because one must account for the different measurement errors of different events, which we will revisit in Section V.

For GWs, the desired change of variables for thin radial shells \bar{r} and pixels $\bar{\mathbf{\Omega}}$ is

$$\{r, \mathbf{\Omega}\} \rightarrow \{r\}, \Delta^G(\bar{\mathbf{\Omega}}|\bar{r}) \leftrightarrow \{r\}, \mathbf{a}_{\ell m}^G(\bar{r}) \quad (59)$$

which factors the information on the 3D distribution of the tracer into a radial distribution $\{r\} \rightarrow n^G(\bar{r})$ and a conditional angular distribution $\Delta^G(\bar{\mathbf{\Omega}}|\bar{r})$. This is sensible, since we showed earlier that the angular distribution $p(\mathbf{\Omega}|r)$ is equivalent to the overdensity field $\bar{\Delta}^G(\mathbf{\Omega}|r)$. Note that just as the pixel resolution sets a finite truncation of the field in real space, the pixel resolution also sets a $\ell_{\max} \sim 1/\delta\theta$, such that our data vector is finite.

Under this change of variables, the GW population prior $p(\mathbf{\Omega}|z)$ is replaced by a prior on the overdensity field $a_{\ell m}^G[\bar{z}]$ at each redshift shell \bar{z}

$$p(\{\mathbf{\Omega}\}|\{z\}, \{\mathbf{d}^g\}, \mathbf{\Lambda}) \rightarrow p(\{a_{\ell m}^G[\bar{d}_L]\}|\{a_{\ell m}^g[\bar{r}]\}, \{d_L\}, \{z^g\}, \mathbf{\Lambda}) \quad (60)$$

which is again a complex multivariate Gaussian given in Equation (43). Here, we have changed coordinates from z to d_L for GWs (binning the GWs in luminosity distance space); the conditional dependence on the $\{d_L\}$ and galaxy redshifts $\{z^g\}$ remains in order to compute the expected shot noise $1/\langle n^{\{G,g\}}[\bar{r}] \rangle$. As is standard in survey cosmology, we approximate $\langle n^\alpha \rangle$ with the sample mean for each bin α , which allows us to compute the overdensity field without a simultaneous inference of the overall rate. This is satisfied if the Poisson fluctuations per bin $1/\sqrt{N^\alpha} \ll 1$, requiring at least $N^\alpha \sim \mathcal{O}(10^2)$ events per bin for a 10% error.

In the infinitesimal limit, it can be shown that the standard galaxy catalog method can be recovered exactly from modeling GWs as a GRF, using Equation (56) to express the GW overdensity field as a noisy Poisson realization of the observed and missing galaxy fields. In particular, the probability distribution on the GW field conditioned on the GW redshifts and *total* galaxy field recovers $p(\mathbf{\Omega}|z, \mathbf{\Lambda})$ of the standard galaxy catalog method (i.e., Equation (55)), as the standard galaxy catalog assumes that the distribution of missing galaxies is known. We show this in detail in Appendix A.

In general, for any tracer X that directly traces another tracer Y , the probability distribution of the field

$a_{\ell m}^X$ conditioned on the field $a_{\ell m}^Y$ will have no 2-point correlations. This is as we discussed earlier in Section IV A: we can model the events as independently distributed if and only if the underlying probability distribution is known. This does not necessarily imply that the standard galaxy catalog method is incorrect, only that whatever is assumed for the distribution of missing galaxies constitutes an uninformative prior guess.

4. A joint GW – galaxy population prior

The galaxy data is both noisy (from spectroscopic or photometric redshift errors) and informative on the cosmology (from features in the matter power spectrum). A natural extension is therefore to jointly model the GWs and galaxies, which was also noted by [25] as the exactly correct approach to accounting for galaxy measurement errors.

Our angular conditional population prior now includes the observed galaxy field

$$p(\{a_{\ell m}^G[\bar{d}_L]\}, \{a_{\ell m}^g[\bar{z}]\} | \{d_L\}, \{z^g\}, \mathbf{\Lambda}) \quad (61)$$

which is now the full joint Gaussian probability distribution in Equation (43).

A population prior on the GW positions conditioned on the observed galaxy positions asks what cosmology best matches the GWs to the galaxies; a population prior on the observed galaxies asks what cosmology can best reproduce the observed galaxy clustering patterns, among all possible realizations of the matter density field. A joint GW–galaxy population model adds these two complementary pieces of information together.

5. The cross-correlation method

The final change of variables is the optimal compression described in Section III C. Let α, β again index the radial shells of both GWs and galaxies. We reduce the population prior on the full fields $\{a_{\ell m}^\alpha\}$ to a prior on the cross-correlation estimator $\{\tilde{C}_\ell^{\alpha\beta}\}$

$$p(\{\tilde{C}_\ell^{[\alpha\beta]}\} | \{d_L\}, \{z^g\}, \mathbf{\Lambda}) \quad (62)$$

which is just Equation (47).

6. The joint cross-correlation + spectral sirens method

A probability distribution on angular overdensity fields (or equivalently, their estimated power spectra) is an angular distribution conditioned on the radial distances. Adding back the radial dependence, as well as any other GW parameters we are modeling ($\{m_1, m_2, \dots\}$), yields

the full population prior

$$p(\{\tilde{C}_\ell^{[\alpha\beta]}\}, \{d_L, m_1, m_2, \dots\} | \{z^g\}, \Lambda) = \left[\prod_{i=1}^{N^G} p(d_{L,i}, m_{1,i}, m_{2,i}, \dots | \Lambda) \right] \times p(\tilde{C}_\ell^{[\alpha\beta]} | \{d_L\}, \{z^g\}, \Lambda) \quad (63)$$

where the middle line is just the spectral sirens population model⁵! Equation (63) is the unified joint population prior encoding the full joint information from the cross-correlation, galaxy catalog, and spectral siren analyses. The fact that it is neatly factorizable into a probability on the cross-correlation statistic and the spectral sirens population prior shows that they use exactly complementary information. This is because the cross-correlation is an analysis on the overdensity fields, which are normalized to the rate at each radial bin, whereas the spectral sirens method uses information on the overall rate evolution of GWs. As we discussed above, this decoupling is only possible if the number of events per bin is sufficiently large (at least $\mathcal{O}(10^2)$), in order for the expected shot noise to be well approximated by the sample mean for each bin. Otherwise, the expected cross-correlation would be coupled to an inference on the expected rate for each bin.

V. BUILDING NOISE INTO THE LIKELIHOOD

Thus far, we have only discussed the population model on the true positions of the GWs and galaxies. In canonical GW population analyses, one writes down the likelihood on the data by marginalizing over all possible values of the true source parameters. This is typically done via Monte-Carlo integration over the posterior $p_{\text{PE}}(\boldsymbol{\lambda} | \mathbf{d}^G)$ for each GW source \mathbf{d}^G , using samples generated from parameter estimation (PE), using a fixed prior $\pi_{\text{PE}}(\boldsymbol{\lambda})$. The i -th event-level likelihood in Equation (4) would be computed as

$$\begin{aligned} \mathcal{L}_i(\Lambda) &\equiv \int d\boldsymbol{\lambda} p(\boldsymbol{\lambda} | \Lambda) \mathcal{L}(\mathbf{d}_i^G | \boldsymbol{\lambda}) \\ &= \int d\boldsymbol{\lambda} p(\boldsymbol{\lambda} | \Lambda) \frac{p_{\text{PE}}(\boldsymbol{\lambda} | \mathbf{d}_i^G)}{\pi_{\text{PE}}(\boldsymbol{\lambda})} \mathcal{Z}_{\text{PE}}(\mathbf{d}_i^G) \\ &\propto \frac{1}{m} \sum_{k=1}^m \frac{p(\boldsymbol{\lambda}_i^k | \Lambda)}{\pi_{\text{PE}}(\boldsymbol{\lambda}_i^k)} \end{aligned} \quad (64)$$

for m PE samples per event. Here, $\mathcal{Z}_{\text{PE}}(\mathbf{d}_i^G) \equiv \int d\boldsymbol{\lambda} \mathcal{L}(\mathbf{d}_i^G | \boldsymbol{\lambda}) \pi_{\text{PE}}(\boldsymbol{\lambda})$ is the Bayesian evidence for the PE prior for each event.

⁵ Recall from discussion at the beginning of Section IV that we take the redshift distribution of galaxies marginalized over sky direction to be uniform in comoving volume even after conditioning upon the observed galaxies, which is a good enough approximation given galaxy completeness at typical GW distances.

In principle, one could do the same here and marginalize over all possible true maps $\{a_{\ell m}^G\}$ and therefore all possible $\{\tilde{C}_\ell^{\alpha\beta}\}$ by repeatedly drawing from PE samples. Direct Monte Carlo marginalization is impractical, however, for at least three compounding reasons:

1. **Exponential sample complexity.** The population prior on the $\{a_{\ell m}^G\}$ is effectively a joint prior on the positions of all N^G events. Thus, unlike standard population inference, one would have to generate joint samples across all N^G events, and covering this space at fixed resolution requires exponentially many samples with the number of events. In standard population inference, the product over individual event likelihoods

$$\mathcal{L} = \prod_{i=1}^{N^G} \mathcal{L}_i \sim \prod_{i=1}^{N^G} \sum_{k=1}^m \frac{p(\boldsymbol{\lambda}_i^k | \Lambda)}{\pi_{\text{PE}}(\boldsymbol{\lambda}_i^k)} \quad (65)$$

implicitly explores a grid of m^{N^G} samples in the joint parameter space $\{\boldsymbol{\lambda}_1, \boldsymbol{\lambda}_2, \dots, \boldsymbol{\lambda}_N\}$ for m samples per event. Attempting to keep this resolution would cause the per-likelihood computational cost to grow exponentially with the number of events.

2. **Nonlinearity.** The mapping from coordinates $\{\mathbf{r}\}$ to $\{\tilde{C}_\ell^{\alpha\beta}\}$ is highly non-linear, which means that PE samples do not yield an unbiased estimate of the power spectra. For GWs with noisy measured positions $\{\hat{\mathbf{r}}\}$ and true positions $\{\mathbf{r}\}$ satisfying $\mathbb{E}_{\text{noise}}[\hat{\mathbf{r}}_i] = \mathbf{r}_i$, the expectation value of the corresponding measured cross-correlation statistic $\mathbb{E}_{\text{noise}}[\hat{\tilde{C}}_\ell^{\alpha\beta}]$ is not equal to $\tilde{C}_\ell^{\alpha\beta}$, the cross-correlation computed from the true positions $\{\mathbf{r}\}$. As we will show in Section V A, angular localization errors act as a smoothing kernel that suppress power at angular scales on the order of the localization error. As a result, the fraction of PE posterior samples consistent with the true $\{\tilde{C}_\ell^{\alpha\beta}\}$ shrinks exponentially with the number of events with localizations worse than $\sim 1/\ell$.
3. **Per-sample computational cost.** Finally, each sample requires its own evaluation of $\{\tilde{C}_\ell^{\alpha\beta}\}$, a non-trivial computation that includes sorting the GWs into radial bins, computing the SHT of the field in each shell, and computing all auto- and cross-power spectra. Beyond computation time, memory constraints also limit the Monte Carlo sample size: for a combined total of ~ 30 GW and galaxy bins and ℓ up to $\sim 1^\circ$ resolution, a single realization of $\{\tilde{C}_\ell^{\alpha\beta}\}$ takes ~ 1 Mb of storage! This limits us to Monte Carlo integrals with at most $10^4 - 10^5$ samples over a parameter space that is, as argued above, extremely high dimensional.

Therefore, we take a different approach where we forward model the errors into the theory-level prediction,

which are the mean and covariance matrices of the likelihood on the cross-correlation power spectra $\tilde{C}_\ell^{[\alpha\beta]}$. To do so, we need to be able to model the GW posterior measurement in an analytically tractable way. This is possible in the high signal-to-noise ratio (SNR) limit ($\gtrsim 25$), where posteriors are expected to be Gaussian [93, 94].

Our approach will be as follows. We will take our GW sky location data to be the maximum a-posteriori (MAP) point of each event $\hat{\lambda} = \{\hat{d}_L, \hat{\Omega}\}$ and their associated measurement errors $\Delta\lambda = \{\Delta d_L, \Delta\Omega\}$. Assuming flat priors, the high SNR limit implies that the posterior and likelihood are Gaussian:

$$\begin{aligned} P(\lambda|\hat{\lambda}, \Delta\lambda) &= \mathcal{N}(\lambda; \hat{\lambda}, \Delta\lambda) \\ \mathcal{L}(\hat{\lambda}|\lambda, \Delta\lambda) &= \mathcal{N}(\hat{\lambda}; \lambda, \Delta\lambda) \end{aligned} \quad (66)$$

We will make the further assumption that the GW radial and angular localization errors can be considered to be independent (i.e., the off-diagonal components of the Fisher covariance matrix are small), allowing us to analyze them separately.

A. Angular localization errors

The effect of a localization error on the power spectrum of a 2D map is well known from studies of the CMB. In particular, if the observed map can be modeled by a convolution of the true map with a kernel that describes the point-spread function of the telescope, then the observed SHT coefficients are just a linear combination of the true coefficients from the convolution theorem. For a homogeneous and isotropic kernel, the relationship between the blurred map $d_{\ell m}$ and the true map $a_{\ell m}$ is simply multiplicative:

$$d_{\ell m} = B_\ell a_{\ell m}. \quad (67)$$

We will refer to B_ℓ as the angular beam window function. For a circular Gaussian kernel with root mean squared (RMS) width σ , one can show that

$$B_\ell(\sigma) = e^{-\frac{1}{2}\ell(\ell+1)\sigma^2} \quad (68)$$

and hence the convolution has the effect of suppressing the signal for $\ell \gtrsim 1/\sigma$. This result has been extrapolated to model GW localization errors in the literature, often by using the GW angular localization posteriors themselves as the observed density field. In doing so, one assumes that a) the posteriors are Gaussian, b) all events can be modeled as having the same localization error σ (say, the median localization error of the radial bin [41]), and crucially c) the MAP points are located at the true positions. To our knowledge, these assumptions have yet to be explicitly addressed in the GW cross-correlation literature. Ultimately, a GW posterior measurement is a result of a Bayesian inference on a noisy GW strain measurement, and cannot be naively modelled as blurred

image of the true position as one can for electromagnetic maps such as the CMB.

We discussed that the high-SNR limit can justify the Gaussianity of the GW measurement error. If the MAP points are Gaussian-distributed from the true positions, then the probability distribution under measurement noise of the measured sky position $\hat{\Omega}$ of each *individual* event is a convolution of the true position with a Gaussian kernel the size of its localization error. This allows us to apply Equation (68) on an individual event basis. A more rigorous derivation of this result is given in Appendix B.

The number counts overdensity field constructed from the true positions of N^α GWs in radial bin α is given by

$$\begin{aligned} \delta^\alpha(\Omega) &= \frac{1}{n^\alpha} \sum_{i=1}^{N^\alpha} \delta^{(D)}(\Omega - \Omega_i) \\ a_{\ell m}^\alpha &= \frac{1}{n^\alpha} \sum_{i=1}^{N^\alpha} Y_{\ell m}^*(\Omega_i) \equiv \frac{1}{n^\alpha} \sum_{i=1}^{N^\alpha} a_{\ell m}^{(i)} \end{aligned} \quad (69)$$

where $n^\alpha = \frac{N^\alpha}{4\pi}$ is the mean angular density of bin α , and $a_{\ell m}^{(i)} \equiv Y_{\ell m}^*(\Omega_i)$ is the SHT of a Dirac-delta localization at the i th event's true position Ω_i . For brevity, we omit the negative offset term that sets $\langle \delta^\alpha \rangle = 0$, since it only has the effect of setting $a_{00} = 0$.

The MAP position $\hat{\Omega}_i$ of each event is drawn from a Gaussian probability distribution $p^{(i)}(\Omega)$ centered on the true position Ω_i . Each $p^{(i)}$ is given by a convolution of the true position with the Gaussian kernel given in Equation (68) corresponding to its localization error σ_i , which in harmonic space is

$$d_{\ell m}^{(i)} = B_\ell(\sigma_i) a_{\ell m}^{(i)} \quad (70)$$

where $d_{\ell m}^{(i)}$ is the SHT of $p^{(i)}$. Note that if we were to take the posterior distributions themselves as the map, this would correspond to an *additional* Gaussian convolution, since the MAP measurements are offset from the true positions! This would have the effect of doubly suppressing the signal at small scales.

The total noise probability overdensity field is would therefore be

$$d_{\ell m}^\alpha = \frac{1}{n^\alpha} \sum_{i=1}^{N^\alpha} d_{\ell m}^{(i)} = \frac{1}{n^\alpha} \sum_{i=1}^{N^\alpha} B_\ell(\sigma_i) a_{\ell m}^{(i)}. \quad (71)$$

This is the expectation value over noise of the measured overdensity field $\hat{a}_{\ell m}^\alpha$, i.e.

$$\mathbb{E}_{\text{noise}} [\hat{a}_{\ell m}^\alpha] = d_{\ell m}^\alpha \quad (72)$$

$$\mathbb{E}_{\text{noise}} [\hat{a}_{\ell m}^{(i)}] = d_{\ell m}^{(i)}. \quad (73)$$

which we will use later in Equation (79). The measured density field is a sum of Dirac delta functions drawn from each $p^{(i)}(\Omega)$, and thus $\hat{a}_{\ell m}^{(i)}$ is the SHT of the delta function draw from event probability distribution $d_{\ell m}^{(i)}$. The

SHT of this measured overdensity field is therefore

$$\hat{a}_{\ell m}^\alpha = \frac{1}{n^\alpha} \sum_{i=1}^{N^\alpha} \hat{a}_{\ell m}^{(i)} = \frac{1}{n^\alpha} \sum_{i=1}^{N^\alpha} Y_{\ell m}^*(\hat{\Omega}_i). \quad (74)$$

We are interested in finding the auto- and cross-power spectra corresponding to these measured maps. The GW auto-power spectrum is given by

$$\langle \hat{a}_{\ell m}^{\alpha*} \hat{a}_{\ell' m'}^\alpha \rangle = \frac{1}{(n^\alpha)^2} \sum_{i,j}^{N^\alpha} \langle \hat{a}_{\ell m}^{(i)*} \hat{a}_{\ell' m'}^{(j)} \rangle \quad (75)$$

for some luminosity distance slice α . This expectation value now averages over both measurement noise realizations and realizations of the universe, i.e.,

$$\langle Z \rangle = \mathbb{E}_{\text{cosmo}} \left[\mathbb{E}_{\text{noise}} [Z] \right] \quad (76)$$

for any quantity Z . Since the $\hat{a}_{\ell m}^{(i)}$ are drawn from $d_{\ell m}^{(i)}$,

$$\mathbb{E}_{\text{noise}} \left[\hat{a}_{\ell m}^{(i)} \right] = d_{\ell m}^{(i)} = \int d\Omega p^{(i)}(\Omega) Y_{\ell m}^*(\Omega) \quad (77)$$

and therefore

$$\begin{aligned} \mathbb{E}_{\text{noise}} \left[\hat{a}_{\ell m}^{(i)*} \hat{a}_{\ell' m'}^{(j)} \right] &= \mathbb{E}_{\text{noise}} \left[Y_{\ell m}^*(\hat{\Omega}_i) Y_{\ell' m'}(\hat{\Omega}_j) \right] \\ &= \begin{cases} \int d\Omega p^{(i)}(\Omega) Y_{\ell m}^*(\Omega) Y_{\ell' m'}(\Omega) & (i = j) \\ \int d\Omega d\Omega' p^{(i)}(\Omega) p^{(j)}(\Omega') Y_{\ell m}^*(\Omega) Y_{\ell' m'}(\Omega') & (i \neq j) \end{cases} \end{aligned} \quad (78)$$

Now we need to take an expectation value over realizations of the universe. For the $i = j$ case, we have $\langle p^{(i)}(\Omega) \rangle = \frac{1}{4\pi}$ for a homogeneous and isotropic universe, and thus

$$\sum_i^{N^\alpha} \langle \hat{a}_{\ell m}^{(i)*} \hat{a}_{\ell' m'}^{(i)} \rangle = \frac{N^\alpha}{4\pi} \delta_{\ell\ell'}^{(K)} \delta_{mm'}^{(K)} \quad (79)$$

Because taking the expectation value over noise returns us to a map of probability distributions of the GW measurements (i.e., $\mathbb{E}_{\text{noise}} [\hat{a}_{\ell m}] = d_{\ell m}$), a further expectation value over realizations of the universe takes us to the power spectrum of the probability map $d_{\ell m}$. We can use this fact to deduce the sum of the $i \neq j$ terms in Equation (78). Using the definition of the SHT yields

$$\begin{aligned} \langle d_{\ell m}^\alpha d_{\ell' m'}^\alpha \rangle &= \frac{1}{(n^\alpha)^2} \sum_{i,j} \langle d_{\ell m}^{(i)*} d_{\ell' m'}^{(j)} \rangle \\ &= \frac{1}{(n^\alpha)^2} \sum_{i,j} \int d\Omega d\Omega' \langle p^{(i)}(\Omega) p^{(j)}(\Omega') \rangle \\ &\quad \times Y_{\ell m}^*(\Omega) Y_{\ell' m'}(\Omega') \end{aligned} \quad (80)$$

We can see that the $i \neq j$ terms are the same as those of Equation (78). To compute these terms, we can plug in

Equation (70):

$$\frac{1}{(n^\alpha)^2} \sum_{i,j} \langle d_{\ell m}^{(i)*} d_{\ell' m'}^{(j)} \rangle = \frac{\langle B_\ell(\sigma) \rangle \langle B_{\ell'}(\sigma) \rangle}{(n^\alpha)^2} \sum_{i,j} \langle a_{\ell m}^{(i)*} a_{\ell' m'}^{(j)} \rangle \quad (81)$$

The independent brackets indicate the independent draws of the localization error σ . The summand is simply the power spectrum of the true number counts overdensity field:

$$\begin{aligned} \frac{1}{(n^\alpha)^2} \sum_{i,j} \langle a_{\ell m}^{(i)*} a_{\ell' m'}^{(j)} \rangle &= \langle a_{\ell m}^{\alpha*} a_{\ell' m'}^\alpha \rangle \\ &= \delta_{\ell\ell'}^{(K)} \delta_{mm'}^{(K)} \left[\overline{C}_\ell^{\alpha\alpha} + \frac{1}{n^\alpha} \right]. \end{aligned} \quad (82)$$

One can show that the shot noise $1/n^\alpha$ can be identified with the $i = j$ terms, while the $i \neq j$ terms add up to $\overline{C}_\ell^{\alpha\alpha}$. Therefore, we obtain our $i \neq j$ terms

$$\begin{aligned} \frac{1}{(n^\alpha)^2} \sum_{i \neq j} \langle \hat{a}_{\ell m}^{(i)*} \hat{a}_{\ell' m'}^{(j)} \rangle &= \frac{1}{(n^\alpha)^2} \sum_{i \neq j} \langle d_{\ell m}^{(i)*} d_{\ell' m'}^{(j)} \rangle \\ &= \delta_{\ell\ell'}^{(K)} \delta_{mm'}^{(K)} \langle B_\ell(\sigma) \rangle^2 \overline{C}_\ell^{\alpha\alpha}. \end{aligned} \quad (83)$$

Finally, combined with Equation (79), we have the auto-power spectrum under independent event-level localization errors:

$$\langle \hat{a}_{\ell m}^{\alpha*} \hat{a}_{\ell' m'}^\alpha \rangle = \delta_{\ell\ell'}^{(K)} \delta_{mm'}^{(K)} \left[\langle B_\ell \rangle^2 \overline{C}_\ell^{\alpha\alpha} + \frac{1}{n^\alpha} \right]. \quad (84)$$

We can see that for the GW–GW auto-power spectrum, the signal component is suppressed by the localization beam, while the shot noise is not: each event has random localization errors, but the realized position of each event is still self-correlated.

Deriving the cross-power spectra is a straightforward generalization. For two non-overlapping shells of GWs, it is always the case that $i \neq j$, and hence there is no shot noise. The GW–GW angular cross-correlation is therefore

$$\hat{C}_\ell^{G_\alpha G_\beta} \equiv \langle \hat{a}_{\ell m}^{G_\alpha*} \hat{a}_{\ell m}^{G_\beta} \rangle = \langle B_\ell \rangle_\alpha \langle B_\ell \rangle_\beta \overline{C}_\ell^{G_\alpha G_\beta} + \frac{\delta_{\alpha\beta}^{(K)}}{n^{G_\alpha}}. \quad (85)$$

where $\langle B_\ell \rangle_\alpha$ is the expected GW angular beam window function in bin α .

The GW–galaxy cross-correlation is a bit trickier, since overlapping shells can have a coincident case corresponding to the GW host galaxy being in the galaxy catalog. Because galaxy and GW localizations are independent, we always have $\hat{\Omega}_i \neq \hat{\Omega}_j$ for GW i and galaxy j and therefore

$$\begin{aligned} \mathbb{E}_{\text{noise}} \left[\hat{a}_{\ell m}^{G,(i)*} \hat{a}_{\ell' m'}^{g,(j)} \right] &= \mathbb{E}_{\text{noise}} \left[Y_{\ell m}^*(\hat{\Omega}_i) Y_{\ell' m'}(\hat{\Omega}_j) \right] \\ &= \int d\Omega d\Omega' p^{G,(i)}(\Omega) p^{g,(j)}(\Omega') Y_{\ell m}^*(\Omega) Y_{\ell' m'}(\Omega'). \end{aligned} \quad (86)$$

That is, compared to Equation (78), there is no special $i = j$ case. Taking the expectation value over realizations of the universe, we follow the same steps as above to evaluate the power spectra of the measured maps in terms of the power spectra of the true maps. The result is

$$\hat{C}_\ell^{G_\alpha g_\beta} \equiv \left\langle \hat{a}_{\ell m}^{G_\alpha} * \hat{a}_{\ell m}^{g_\beta} \right\rangle = \langle B_\ell^g \rangle \left[\overline{C}_\ell^{G_\alpha g_\beta} + \frac{\langle n^{G_\alpha g_\beta} \rangle}{\langle n^{G_\alpha} \rangle \langle n^{g_\beta} \rangle} \right]. \quad (87)$$

Because galaxy localization errors are negligible compared to GW localization errors, we have taken the beam window function of the galaxy localization $B_\ell^g = 1$. We can see that the cross shot noise term is now suppressed by the localization beam, resulting from the fact that GWs and their host galaxies are localized independently. Consistent with intuition, the information that GWs are located in host galaxies becomes diluted with poor localization errors.

Remarkably, we need only to carry the *average* beam window function per shell α

$$\langle B_\ell \rangle_\alpha = \int d\sigma P^\alpha(\sigma) B_\ell(\sigma). \quad (88)$$

If the number of events in the shell is large, B_ℓ can be directly estimated from its empirical distribution as a once-through pre-processing step

$$\langle B_\ell \rangle_\alpha \approx \frac{1}{N^{G_\alpha}} \sum_{i=1}^{N^{G_\alpha}} B_\ell(\sigma_i). \quad (89)$$

A corollary of this is that using the mean localization error $\langle \sigma \rangle$ to compute B_ℓ will overestimate the degree to which small angular scales are suppressed. That is, $B_\ell(\langle \sigma \rangle) < \langle B_\ell(\sigma) \rangle$ if and only if $\sqrt{\ell(\ell+1)} > \langle \sigma \rangle$. This follows from Jensen's inequality. We show this for a set of realistic mock data in Figure 5, which will be described in more detail in Section VII.

In short, Equations (85) and (87) describe how to compute the theoretical expected power spectra corrected for localization errors by multiplying by a beam window function that suppresses small angular scales, which can be estimated via Equation (89) (given a sufficiently large number of observations per bin). $\{\hat{C}_\ell^{\alpha\beta}\}$, the cross-correlation estimators of the noisy GW data, are then an unbiased estimator of these error-corrected theoretical power spectra

$$\hat{C}_\ell^{\alpha\beta} = \left\langle \hat{C}_\ell^{\alpha\beta} \right\rangle \quad (90)$$

Because angular localization errors are effectively suppressing the Gaussian fluctuations at various scales, we can plug these error-corrected theoretical power spectra $\{\hat{C}_\ell^{\alpha\beta}\}$ directly into Equation (47) for the covariance of the $\{\hat{C}_\ell^{\alpha\beta}\}$.

Finally, although we discussed only Gaussian, circular, and homogeneous localization errors, this formalism can

be generalized in principle to any distribution of localization errors. Specifically, the expression for the beam window function in Equation (68) will be different for non-Gaussian distributions. In general, as we discuss further in Appendix B, the beam of a spatially varying (i.e. the localization error depends on Ω) and anisotropic kernel is given by

$$d_{\ell m}^{(i)} = \sum_{\ell', m'} D_{\ell m, \ell' m'} a_{\ell' m'} \quad (91)$$

rather than the simple multiplicative form in Equation (67); the corresponding expressions for the expected cross-correlation power spectra above could be re-derived in this more complicated case. Circular localizations require triangulation from multiple (≥ 3) sensitive detectors, while measurement errors may be spatially varying due to accumulated modulations from Earth's rotation and orbit [95]. This expansion will be left for future work.

B. Incomplete or anisotropic sky coverage

The treatment of incomplete or anisotropic sky coverage has been developed extensively for analyses of both galaxy surveys and the CMB, and thus we only briefly review the results here. For more details, see e.g., [96] and references therein.

Galaxy surveys do not have complete coverage of the sky; at the very least, the galactic plane and other bright sources are masked out. It is also possible that the depth of either the galaxy or GW catalog does not have uniform sensitivity across the sky, in the latter case because of the angular beam pattern of the GW detector network. In the case of angular selection effects, the expected density $\langle n(r, \Omega) \rangle$ depends on not only the distance but also the sky location, and thus a mean density encoding the angular selection effects must be used when computing the overdensity field. The result is a measured overdensity field that has been multiplied by a weights map, $\Delta^\alpha(\Omega) = \Delta^\alpha(\Omega) m^\alpha(\Omega)$. A sky mask would simply be a binary weights map.

This weighted map is no longer isotropic, and thus different ℓ modes are coupled together, making the naive estimator in Equation (46) biased. The expectation value of the naive estimator is related to the true power spectrum via a mode-coupling matrix

$$\left\langle \hat{C}_\ell^{\alpha\beta} \right\rangle = \sum_{\ell'} M_{\ell\ell'} C_{\ell'}^{\alpha\beta}. \quad (92)$$

There are several approaches to deal with the mode-coupling matrix: one could convolve the theory prediction with $M_{\ell\ell'}$, bin together the ℓ 's that are coupled together in bandpowers [96], or use a different estimator (e.g., maximum likelihood [97] or minimum-variance quadratic [83]) to produce an unbiased estimate of the power spectrum in the presence of the weights map.

In practice, if the sky-mask is well-behaved, its fractional sky coverage is not too small, and the underlying power spectrum C_ℓ is smooth with respect to the coupling width, then $M_{\ell\ell'}$ is effectively diagonal or close to diagonal, such that $M_{\ell\ell'} \approx \delta_{\ell\ell'}^{(K)}$, where $f_{\text{sky}}^{\alpha\beta}$ is the overlapping fractional sky coverage of the masks corresponding to both fields

$$f_{\text{sky}}^{\alpha\beta} = \frac{1}{4\pi} \int d\Omega m^\alpha(\Omega) m^\beta(\Omega). \quad (93)$$

In this case, one can use the estimator

$$\hat{C}_\ell^{\alpha\beta} = \sum_{\ell'} M_{\ell\ell'} \tilde{C}_{\ell'}^{\alpha\beta} \approx \frac{1}{f_{\text{sky}}^{\alpha\beta} (2\ell + 1)} \sum_{m=-\ell}^{\ell} \hat{a}_{\ell m}^{\alpha*} \hat{a}_{\ell m}^{\beta} \quad (94)$$

where $\tilde{C}_{\ell'}^{\alpha\beta}$ is the naive estimator given in Equation (46).

The fractional sky coverage also affects how well the power spectra can be measured. On scales smaller than the sky mask, it is often assumed that the number of independent modes is decreased in proportion to the available sky area, which effectively increases the covariance of the angular power spectrum estimators (originally given in Equation (45)) by a factor of $f_{\text{sky}}^{\alpha\beta\mu\nu}$, the fractional sky coverage shared between all four fields [98, 99]. That is,

$$\langle \hat{C}_\ell^{\alpha\beta} \hat{C}_{\ell'}^{\mu\nu} \rangle \approx \frac{\delta_{\ell\ell'}^{(K)}}{f_{\text{sky}}^{\alpha\beta\mu\nu} (2\ell + 1)} \left[\hat{C}_\ell^{\alpha\mu} \hat{C}_\ell^{\beta\nu} + \hat{C}_\ell^{\alpha\nu} \hat{C}_\ell^{\beta\mu} \right]. \quad (95)$$

As with Equation (94), this assumption holds with diagonal or close to diagonal $M_{\ell\ell'}$.

C. Radial localization errors

In Section III B 2, we defined in Equation (31) an effective window function $\phi(r)$ that acts as the radial weighting function when integrating over the 3D power spectrum to produce the theoretical 2D power spectrum in Equation (37). In the presence of radial localization errors, the window function w we use for binning is not in the true distance r but rather in the measured distance \hat{r} , which we must marginalize over [79]:

$$\phi^{X_\alpha}(r) \propto p_{\text{obs}}^X(r) \int d\hat{r} w^{X_\alpha}(\hat{r}) \mathcal{L}^{X_\alpha}(\hat{r}|r) \quad (96)$$

where $p_{\text{obs}}^X(r)$ is the distribution of observable (i.e. with selection effects) tracers X , since the window function is weighted by the number of tracers accessible at each distance r .

For GWs, the measurement error $\mathcal{L}(\hat{d}_L|d_L)$ is not deterministic, varying from event to event depending on the noise realization and source properties. Nonetheless, we can imagine the resulting localization of each GW as arising from some distribution of errors. Generally, the expected localization error will depend on the measured source properties. Nonetheless, motivated by the

idea that the measured strain $h \sim 1/\hat{d}_L$, the distribution of $\Delta \ln \hat{d}_L = \Delta d_L / \hat{d}_L$ evolves slowly across the width of the bin, and thus we can approximate the $\Delta \ln \hat{d}_L$ of the GWs in that bin as being drawn independently from a distribution $p^\alpha(\Delta \ln \hat{d}_L)$. If the number of GWs in each bin is large, then this distribution can be approximated directly, with e.g., a kernel density estimation (KDE) or parameterized fit. The effective window function for each GW bin α (in the high-SNR / gaussian measurement regime) is then

$$\begin{aligned} \phi^{G_\alpha}(d_L) &\propto p_{\text{obs}}^G(d_L) \int d\hat{d}_L w^{G_\alpha}(\hat{d}_L) \\ &\times \int d(\Delta \ln \hat{d}_L) p^\alpha(\Delta \ln \hat{d}_L) \mathcal{N}[\hat{d}_L; d_L, \hat{d}_L \cdot \Delta \ln \hat{d}_L] \end{aligned} \quad (97)$$

up to normalization.

The same idea applies to galaxies. A common model for galaxy redshift errors is a fixed relative redshift error $\Delta \ln z = \Delta z / z$, for example ≈ 0.05 for photometric redshifts and ≈ 0.01 for spectroscopic redshifts [34, 41, 100]. In this case,

$$\phi^{g_\beta}(z) \propto p^{g,\text{obs}}(z) \int d\hat{z} w^{g_\beta}(\hat{z}) \mathcal{N}[\hat{z}; z, z \cdot \Delta \ln z]. \quad (98)$$

for some fixed $\Delta \ln z$.

Note that both Equations (97) and (98) require knowledge of the true radial distribution of the observed tracers $p_{\text{obs}}^X(r)$, despite radial localization errors. We will assume that this can be inferred separately before the cross-correlation analysis, a reasonable assumption for a large number of relatively well-localized observations.

VI. SUMMARY OF FORMALISM

In Section III, we reviewed the standard formalism for dark siren analyses and cross-correlation analyses. In Section IV, we connected these two methods and showed that the Gaussian formalism can encompass dark siren analyses, insofar as Poisson statistics tend to Gaussian with large N . In this framing, the standard galaxy catalog method infers the probability of an observed GW field conditioned on a fixed background galaxy field, which is usually constructed by assuming a uniform distribution of missing galaxies. On the other hand, the cross-correlation method models a joint distribution of the observed GW and galaxy data, conditioning only on the cosmology rather than any specific realization of the universe. We also showed that because we cross-correlate normalized overdensity fields, it uses complementary information to the spectral sirens method. Thus, we are able to write down in Equation (63) a joint population model on the GW and galaxy parameters, which are the GW parameters $\lambda = \{m_1, m_2, d_L\}$ and cross-correlation estimators $\{\tilde{C}_\ell^{[\alpha\beta]}\}$. This population prior includes information from the spectral sirens method, GW-galaxy cross-correlations, and galaxy-galaxy clustering.

In Section V, we discussed the high-SNR limit, in which we can approximate our data as consisting of MAP measurements of the parameters $\hat{\lambda}$ and associated Fisher matrix measurement errors $\Delta\lambda$. In particular, we show how to forward model localization errors into the likelihood on the observed cross-correlation estimators $\{\hat{C}_\ell^{[\alpha\beta]}\}$ rather than doing a Monte-Carlo integration over all possible values of the true parameters. We keep the same Gaussian distribution on the angular power spectrum estimators as in Equation (47):

$$\mathcal{L}\left(\left\{\hat{C}_\ell^{[\alpha\beta]}\right\} \mid \left\{\hat{C}_\ell^{[\alpha\beta]}\right\}\right) = \prod_{\ell=\ell_{\min}}^{\ell_{\max}} \frac{1}{\sqrt{(2\pi)^r \det \Sigma_\ell}} \times \exp\left[-\frac{1}{2} \sum_{\alpha\leq\beta} \sum_{\mu\leq\nu} \sum_{\ell} \Delta\hat{C}_\ell^{\alpha\beta} (\Sigma_\ell)_{\alpha\beta,\mu\nu}^{-1} \Delta\hat{C}_\ell^{\mu\nu}\right]. \quad (99)$$

The error-corrected theoretical expectation for the cross-correlation $\{\hat{C}_\ell^{[\alpha\beta]}\}$ can be computed by integrating the 3D power spectrum via Equation (37) with the error corrected effective window functions in Equations (97) and (98), and multiplying by the appropriate average beam window function per shell in Equations (85) and (87). If the survey sky coverage is anisotropic for either tracer, then one must use an updated expression (Equation (94)) to compute the $\{\hat{C}_\ell^{[\alpha\beta]}\}$ in order for it to be an unbiased estimator of the $\{\hat{C}_\ell^{[\alpha\beta]}\}$, and update the covariance matrix $(\Sigma_\ell)_{\alpha\beta,\mu\nu}$ accordingly (Equation (95)). A flowchart summarizing our approach to the cross-correlation inference formalism can be found in Figure 1.

We can now put everything together and write down a joint hierarchical likelihood given noisy galaxy and GW data. Taking Equation (63) with our error-corrected formulae as our population likelihood, we have

$$\mathcal{L}(\{\mathbf{d}^G\}, \{\mathbf{d}^g\} \mid \Lambda) = \mathcal{L}\left(\left\{\hat{C}_\ell^{[\alpha\beta]}\right\} \mid \{\hat{z}^g, \Delta z^g\}, \{\hat{d}_L, \Delta\lambda\}, \Lambda\right) \quad (100a)$$

$$\times \mathcal{L}(N^G \mid \Lambda) \times \prod_{i=1}^{N^G} \mathcal{L}_i \quad (100b)$$

Equation (100a) is the Gaussian cross-correlation likelihood in Equation (99); the dependence on $\{\hat{z}^g\}$ on $\{\hat{d}_L\}$ enters because these are used to estimate the shot noise per bin $1/\langle n^\alpha \rangle \approx 4\pi/N^\alpha$ (where N^α is the number of tracers observed in bin α), while the galaxy redshift errors $\{\Delta z^g\}$ and GW posterior measurement errors $\{\Delta\lambda\}$, $\lambda \in \{d_L, \Omega, m_1, m_2\}$ are used to estimate the average measurement uncertainties, which are needed to compute the angular beam and effective radial window functions. These, along with the GW and galaxy bias parameters and the 3D matter power spectrum, are sufficient to compute the error-corrected theoretical $\{\hat{C}_\ell^{\alpha\beta}\}$ as well as the

corresponding covariance matrix on the $\{\hat{C}_\ell^{\alpha\beta}\}$.

On the other hand, Equation (100b) is our usual inhomogeneous Poisson likelihood, with the usual product of independent event-level likelihoods

$$\mathcal{L}_i = \int dm_1 dm_2 dd_L p(m_1, m_2, d_L \mid \Lambda) \mathcal{L}\left(\hat{m}_{1,i}, \hat{m}_{2,i}, \hat{d}_{L,i} \mid m_1, m_2, d_L, \Delta\lambda_i, \Lambda\right). \quad (101)$$

Here, we are implicitly including a population prior on the GW d_L but not the z^g ; in principle one could be added here to jointly model the rate evolution of the galaxies. We consider that to be outside the scope of this work.

Note that as written in Equation (100), the data enters both the cross-correlation estimator and the quantities on which it is conditioned (i.e. in $\{\hat{z}^g\}$, $\{\hat{d}_L\}$, and $\{\Delta\lambda\}$), which is technically not allowed as these are not completely independent. A fully self-consistent procedure would be to write down the likelihood on these quantities and marginalize over those, but here we opt not to because of the computational cost. In conditioning on the Poisson-realized number of tracers per bin and realized distribution of measurement errors, rather than the Poisson rate and true distribution of measurement errors per bin, we are missing a *realization variance* contribution that arises from the possible realizations of the tracer population. Thus, this procedure is conservative because we are assuming greater variability than is actually present. As discussed before, we require a large number of events per shell in order for the realization variance contribution to be small.

The final step is to incorporate selection effects. Recall from Section III A that writing down the likelihood with selection effects involves conditioning on the fact that the GW events were detected. Equation (100a), however, is already implicitly conditioned on the fact that the events are detected. The cross-correlation likelihood is a comparison of the observed map to the expected map, where the noisiness of the detections, sampling error (shot noise), and selection effects are already forward-modeled into the mean and covariance of the likelihood function. Radial (as well as angular, as discussed in Section V B) selection effects are accounted for in the fact that overdensity fields are normalized to the expected number density in each shell and pixel. Put another way, the overall normalization (number of tracers per bin) does not enter in the intrinsic clustering patterns of the tracer. Although it affects the expected shot noise, as discussed at the end of Section IV, the shot noise can be directly estimated from the observed number density as long as the number of observations per bin is large, which decouples the cross-correlation from the rate likelihood.

Thus, because incorporating selection effects leaves the likelihood on the cross-correlation unchanged, we only need to impose selection effects on the GW inhomogeneous Poisson likelihood in Equation (100b), which we

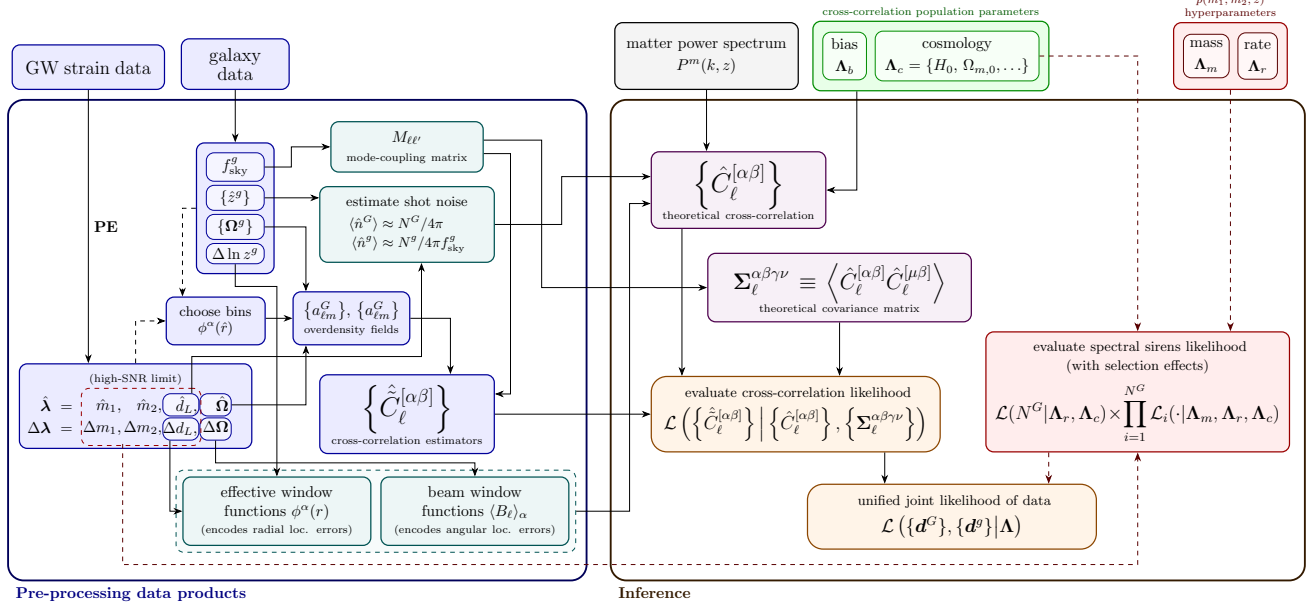


FIG. 1: A flowchart summarizing our cross-correlation formalism. Pre-processing steps for the data (Section V) are shown in the left box, which are used to compute the theoretical cross-correlation and covariance matrix during inference (right box). Boxes are colored roughly as follows: data (blue), estimated noise data products used during inference (teal), theory-level calculations (purple), likelihoods (orange), and the spectral sirens method (red). The cross-correlation and spectral sirens methods are complementary, so they can be done separately and/or combined.

already reviewed in Equation (3). The posterior on the

hyperparameters Λ given the galaxy and GW data under selection effects is therefore given by

$$\mathcal{P}(\Lambda | \{\mathbf{d}^G, D\}, \{\mathbf{d}^g\}) \propto \Pi(\Lambda) e^{-N_{\text{exp}}^G(\Lambda)} N_{\text{tot}}^{N^G} \left[\prod_{i=1}^{N^G} \int d\lambda p(\lambda | \Lambda) \mathcal{L}(\mathbf{d}_i | \lambda, \Lambda) \right] \mathcal{L} \left(\left\{ \hat{C}_\ell^{[\alpha\beta]} \right\} | \{\hat{z}^g\}, \{\hat{d}_L\}, \{\Delta z^g\}, \{\Delta \lambda\}, \Lambda \right) \quad (102)$$

As before, $\{D\}$ denotes the fact that each GW event was detected. The spectral sirens and cross-correlation methods can therefore be carried out as two separate analyses: the joint posterior can be evaluated by using the posterior of one analysis as the prior for the other. The cross-correlation likelihood encodes the additional information not captured by the spectral sirens method, namely angular correlations of overdensities between GWs and galaxies and galaxy–galaxy 2-point correlations.

We will end this discussion with some final caveats on the relationship of the cross-correlation method with the standard galaxy catalog method. We argued in Section IV that the cross-correlation method is an extension of the standard galaxy catalog method—in particular the information from the conditional distribution $p(\mathbf{\Omega} | z, \Lambda)$ —to 2-point statistics. In particular, the GRF formalism reduces in the continuous limit to the standard

galaxy catalog method if one conditions on a fixed known underlying galaxy field.

In practice, one cannot take the continuous limit in a cross-correlation analysis. Because we build measurement errors directly into the theory-level expectation, and because we work in harmonic space rather than real space, the resolution of both the density fields and the theoretical angular power spectrum are truncated at the measurement precision, and therefore one cannot impose exactly the requirement that GWs are hosted in galaxies as the galaxy catalog method does. In fact, much of our formalism relies on the central limit theorem to have many objects per voxel, which (along with the Limber approximation) breaks down if we choose radial bins that are too thin. Another interesting point is that because galaxy clustering can be measured so well, this “host requirement” ends up contributing very little to the con-

straining power of the cross-correlation method. In fact, we show upon implementing this method that it makes no difference to ignore it in our computation altogether. We discuss this at length in Appendix C.

VII. IMPLEMENTATION ON MOCK DATA

To test its validity and constraining power, we implement the cross-correlation framework presented above and test it on a set of mock GW and galaxy catalogs, which we design to emulate next-generation galaxy survey and GW detector networks. In this section, we will describe the details of the mock data generation and numerical implementation.

A. Mock Data Generation

The mock data generation pipeline can be broken down into four steps: (1) generation of a matter density field from a fiducial power spectrum used as a probability distribution to generate a Poisson-sampled galaxy field; (2) galaxy catalog generation by applying selection effects with a magnitude cut and photometric redshift errors; (3) GW catalog generation via injection of BBHs drawn from a fiducial population model into galaxy hosts drawn with rate weighting from the galaxy catalogue, before applying selection effects with an SNR; and (4) construction of the data products needed for the cross-correlation inference, namely the radial binning scheme, estimated localization errors (from simulated Fisher matrix posteriors) and shot noise per bin, and the sky map for each bin constructed from the MAP positions, from which we compute the cross-correlation estimators $\{\hat{C}_\ell^{\alpha\beta}\}$. In all steps of the simulation pipeline, we adopt the flat Planck 2015 cosmology [1] as our fiducial cosmology, which we aim to recover.

1. Density field generation

We use a linear matter power spectrum computed with the Boltzmann code CLASS [101, 102] in our fiducial Planck 2015 cosmology. Because the theory presented in Section III is valid only in the linear regime, we generate a simplified mock density field by drawing from a log-normal field [56, 103, 104], which imposes non-negative densities such that $\delta > -1$. The procedure we follow closely follows that of [56], so we will only summarize it briefly. The matter density field is generated by drawing a GRF with a modified 2-point correlation function (2PCF)

$$\xi'(r) = \ln[1 + \xi(r)] \quad (103)$$

where ξ is the 2PCF of the target power spectrum, while ξ' is the power spectrum from which we draw a GRF

δ' . (The 2PCF is the Fourier pair of the 3D power spectrum; we transform between the two using the package `mcfit` [105]). We generate δ' in Fourier space by drawing a complex field from white noise (enforcing the reality condition $\delta_{\mathbf{k}}^* = \delta_{-\mathbf{k}}$), reweighting it with the power spectrum, and taking the inverse discrete Fourier transform to transform the field back to real space. Then, we compute the field

$$\delta_{\mathbf{r}} = \exp\left(\delta'_{\mathbf{r}} - \frac{\sigma_{\delta'}^2}{2}\right) - 1, \quad (104)$$

where $\sigma_{\delta'}^2$ is the variance of the density field δ' . The field respects $\delta_{\mathbf{r}} > -1$, and one can check that $\delta_{\mathbf{r}}$ has the 2-point statistics of the target power spectrum $\xi(r)$.

Because our goal is to generate a galaxy catalog, we draw a log-normal field with target power spectrum $P^g(k) = (b^g)^2 P^m(k)$ as our galaxy probability density field. Here, $b^g = 1.1$ is our fiducial galaxy linear bias, and $P^m(k)$ is the linear matter power spectrum from CLASS. This field is generated on a cube of size 12 Gpc divided into $2400^3 \sim 10^{10}$ cubic voxels of size 5 Mpc. We are unable to generate a larger volume due to computational constraints; the voxel size is chosen to coincide with scales at which non-linearities become important and our simple linear formalism begins to break down. Therefore, although a log-normal field is a very rough approximation to the true distribution of galaxies on non-linear scales, our mock galaxy density field is realistic on the scales that can be probed by this analysis. Furthermore, modeling non-linearities in the galaxy power spectrum for precision cosmology is an active area of research (see, e.g., [106–109]), and therefore extensions of this analysis to the non-linear regime will be left for future work.

To generate the Poisson-sampled galaxy field, we assume a uniform mean galaxy number density of $\langle n^g \rangle = 2 \cdot 10^{-3} \text{ Mpc}^{-3}$ [110]. We then assign each voxel a galaxy number count by drawing from a Poisson distribution for each voxel. A complete galaxy catalog is then generated by assigning each galaxy a random position within the voxel and a K -band absolute magnitude drawn from a Schechter luminosity function [111] with parameters $M_* = -23.39$, $\alpha = -1.09$, and luminosity cutoff $L > 0.01754 L_*$, following [32, 112]. Since we place the observer at the center of the box, we remove all galaxies outside the radius $\chi_{\text{max}} = 6 \text{ Gpc}$ ($z_{\text{max}} = 2.52$, $d_{L,\text{max}} = 21.1 \text{ Gpc}$) to maintain isotropy.

2. Galaxy catalog

We generate the *observed* galaxy catalog by computing the K -band apparent magnitude with the color and evolution corrections in [112]. To simulate selection effects, we impose an apparent magnitude cut of $m < 26$, which is achievable (not necessarily in the K -band) by next-generation galaxy surveys such as Euclid [90] and LSST [92, 113].

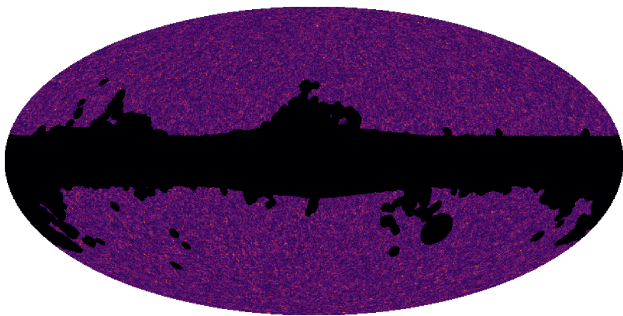


FIG. 2: A slice of the mock galaxy catalog, with measured redshifts $1.17 < \hat{z} < 1.22$. The galaxy sky mask, which we have taken from the WISE x SuperCosmos analysis, is clearly visible.

We also simulate galaxy survey limitations by masking out typical areas of stellar and galactic contamination using the galaxy mask from the WISE x SuperCOSMOS galaxy catalog data release [114], which masks out 32% of the sky. With these selection effects, we have an observed catalog with $\sim 5 \cdot 10^8$ galaxies out to redshift 3. A number counts map of a representative slice of the mock galaxy catalog is shown in Figure 2.

Finally, we assign each galaxy a photometric redshift, assuming Gaussian measurement errors and a relative redshift error of $\sigma_{\ln z} = 0.05$ [34, 41, 100].

3. BBH injections

BBHs are drawn from a fiducial population model consistent with LVK population analyses [115, 116], the full details of which we describe in Appendix D. Each event is assigned a host galaxy drawn from the mock (complete) galaxy catalog, weighted by the redshift-dependent rate in our fiducial model.

To generate the observed catalog, we simulate a detector network of both ET and CE. In particular, we consider 2 L-shaped ET detectors each with 15 km arms offset in orientation by 45° , located in the candidate sites in Sardinia and in the Meuse-Rhine region [117]; we choose this configuration over the triangular configuration as the latter has potentially highly degenerate localization modes [118]. For CE, we consider a 40-km detector in the Idaho candidate site [119, 120].

We use `gwfast` [121] with the `IMRPhenomHM` waveform model [122] to generate approximate SNRs and Fisher-matrix based posteriors. For each event, we:

1. Compute the Fisher matrix at the true BBH parameters
2. Draw a mock MAP measurement from a multivariate Gaussian centered at the true parameters with the inverse Fisher matrix

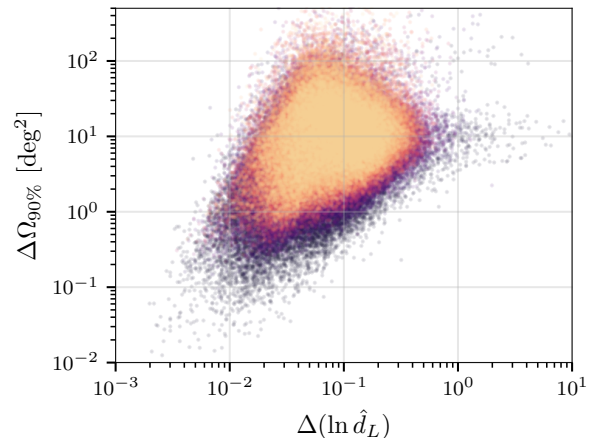


FIG. 3: 90% localization sky area and relative luminosity distance error $\Delta(\ln \hat{d}_L) = \Delta d_L / \hat{d}_L$ of the BBHs in the mock catalog. Colors correspond to the GW radial bins in the top panel of Figure 4, i.e., the observed source distance \hat{d}_L .

3. Compute the SNR and covariance given by the inverse Fisher matrix at the *measured* parameters, imposing a threshold of $\text{SNR} \geq 25$ to count the event as observed

Crucially, our posterior measurements are not centered at the true parameters. Although this procedure does not exactly simulate a true Bayesian parameter estimation of noisy strain data, it is self-consistent if the Fisher matrix does not change significantly between the true and observed parameters, and in this high-SNR regime it is good enough for verifying the validity of our formalism. We verify the self-consistency of this procedure by checking for biases in the recovered posteriors, which we do not see.

The angular sky localizations and the relative luminosity distance errors of the mock BBH catalog are shown in Figure 3. With a local merger rate of $20 \text{ Gpc}^{-3} \text{ yr}^{-1}$ and a 2 year observing run, we have a total of 233499 mock BBHs observed by our 2ET+1CE detector network.

4. Mock maps and data products

To construct the overdensity fields, we first choose a binning scheme based on the radial localization scale of each tracer. For both GW and galaxies, we use tophat window functions in the observed coordinates, i.e., the MAP luminosity distances for the GWs and photometric redshifts for the galaxies. For each tracer, we choose the number of bins by determining the highest number at which more than 75% of the bins have mean redshift errors smaller than the bin half-width. Following [41, 123], the bin edges are chosen such that the bins are equally populated in order to maximize signal to noise.

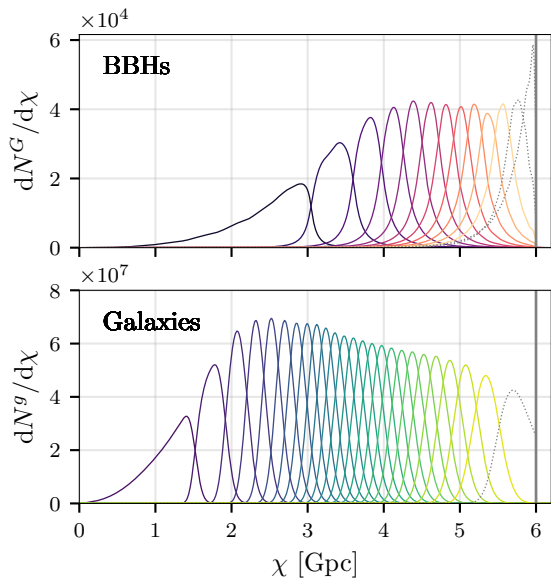


FIG. 4: Galaxy and BBH effective window functions for our equally populated bins evaluated in the fiducial cosmology, normalized to the number count per bin. Dotted lines show bins that were removed due to being too close to the edge of the simulation volume at $\chi_{\max} = 6$ Gpc.

Recall that to compute the effective radial window functions that weight the power spectrum in Equation (37), we need to convolve the tophat window functions with the radial localization errors, and then weight it by the radial distribution of the catalog, as in Equations (96) to (98). In Section V C, we proposed a strategy of empirically fitting the distribution of $P(\Delta \ln \hat{d}_L)$ for each bin. Since we have $\mathcal{O}(10^4)$ BBHs per radial bin, we can do so easily with a Gaussian KDE. We also assume that we are able to obtain an estimate of the true radial distribution of observable tracers *a priori*, a reasonable assumption given $\mathcal{O}(10^9)$ total galaxies and $\mathcal{O}(10^5)$ BBHs. Thus, we fit KDEs to the true galaxy redshifts and BBH luminosity distances to pass into Equation (96).

Figure 4 shows the resulting effective window functions in comoving distance for the BBHs and galaxies, computed from the true cosmology; these window functions are computed on-the-fly during inference to convert between different distances. The overlapping tails are a result of convolving the tophat window functions with the localization error. Because we choose the binning of GWs and galaxies independently, they do not have a 1-to-1 correspondence; the distribution of GWs is visibly skewed towards higher redshifts relative to the galaxies. This is because the sensitive volume of GW detectors is deeper than the galaxy survey, which is true for both current-generation and next-generation GW and galaxy surveys. Also note the hard boundary at $\chi_{\max} = 6$ Gpc; since this artificially squishes the window functions near the bound-

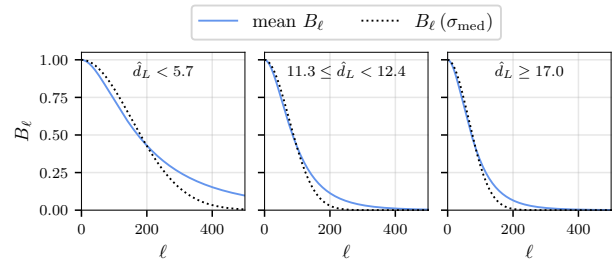


FIG. 5: Beam window functions for the 1st, 6th, and last of our 11 GW bins. The solid blue line shows the average of B_ℓ over all events, while the dotted black line shows B_ℓ computed from the median angular RMS localization error of each bin.

ary, we remove bins that are centered at $\chi > 0.9\chi_{\max}$, which are shown in Figure 4 by dotted lines. In the end, we are left with 11 bins of 18,000 BBHs each, and 24 bins of $2 \cdot 10^7$ galaxies each.

For the BBHs, we account for their localization errors by computing the mean beam window function for each radial bin, as discussed in Section V A. As suggested in Equation (89), we do this by computing $B_\ell(\sigma_i)$ for each event i in the bin with the Gaussian beam window function in Equation (68) and taking the average over the events, where σ is the RMS localization error⁶ of each event. Some resulting computed beams are shown in Figure 5, compared with the result from approximating all events as having the same localization error set equal to the sample median.

Finally, we compute the GW and galaxy overdensity maps and cross-correlations. Number count maps are constructed for each bin with the MAP sky localization of the BBHs and true sky localization of the galaxies (we assume negligible localization error with respect to the pixel size). We use a HEALPix resolution of $n_{\text{side}} = 256$, corresponding to a conservative maximum resolution of $\ell_{\max} \approx 512$, well beyond what can be probed by the GW localizations as seen in Figure 5. Overdensity maps are created by normalizing the number count maps to the mean density. Finally, cross-correlation power spectra $\{\hat{C}_\ell^{\alpha,\beta}\}$ are computed using Equation (46) for $\alpha \geq \beta$, where α, β index the 11 + 24 total GW and galaxy bins; the effect of the galaxy mask is then undone by inverting the mode-coupling matrix, which we compute with NaMaster [96]. We use healpy [124] for all spherical harmonic and angular power spectrum computations.

⁶ Because events are not perfectly circular, this is computed as the geometric average of the square root of the eigenvalues of the $(\theta, \phi / \sin \theta)$ covariance matrix. All of the observed events have near-circular localization ellipses, with a median eccentricity of 0.98.

B. Inference implementation

We infer cosmological parameters $\Lambda_c = (H_0, \Omega_{m,0})$; all other cosmological parameters are fixed at the fiducial Planck 2015 values. We use a simple linear bias $b = b^g = b^G$, assuming that the galaxy and GW biases are the same and do not evolve with redshift, consistent with our assumptions. We also assume that the matter power spectrum is both fixed and known, such that we do not need to re-compute it on the fly during inference for different cosmologies. In a realistic analysis, none of these are a given and we would have further nuisance parameters to model these effects. Nonetheless, the goal of this work is to demonstrate the degree to which this method is precise and unbiased within the assumptions of our simplified mock catalogs, and thus we leave simulating a more sophisticated GW–galaxy cross-correlation to future work.

Finally, we implement the Bayesian inference of the following posterior:

$$\mathcal{P}(\Lambda | \{\mathbf{d}^G\}, \{\mathbf{d}^g\}) \propto \Pi(\Lambda) \mathcal{L} \left(\left\{ \hat{C}_\ell^{[\alpha\beta]} \right\} | \{\mathbf{d}\}, H_0, \Omega_{m,0}, b \right) \quad (105)$$

where the likelihood on the observed angular power spectra $\hat{C}_\ell^{[\alpha\beta]}$ is our usual multivariate Gaussian in Equation (47). Here, $\{\mathbf{d}\}$ includes all the auxiliary data products described in the previous section, including the number density per bin for the shot noise computation, and the localization uncertainties encoded in the beam and radial window functions. These, along with our cosmology and bias parameter, are sufficient to compute the theoretical expected power spectrum and covariance matrix as follows:

1. Using the cosmology, bias parameter, and the GW and galaxy window functions, compute the theoretical angular power spectrum with the Limber approximation in Equation (37)
2. Correct for GW angular localization errors by multiplying by the appropriate beam window functions in Equations (85) and (87)
3. Add the shot noise $\delta_{\alpha\beta}^{(K)} / \langle n^\alpha \rangle$
4. Compute the covariance matrix with Equation (45) from this error-corrected theoretical power spectra
5. Divide all covariance matrix terms that involve a galaxy field by f_{sky} , as described at the end of Section VB

This is repeated at each step of the inference to evaluate the likelihood for each sampling of the cosmology and tracer bias. As discussed at the end of Section VI and at length in Appendix C, we take the cross shot noise between GWs and galaxies to be negligible, which otherwise would be added between steps 1 and 2 above. We

use uniform priors of $H_0 \in [65, 77]$, $\Omega_{m,0} \in [0.25, 0.35]$, and $b \in [0.7, 1.3]$.

We start the analysis at $\ell_{\text{min}} = 20$ and set the cutoff ℓ_{max} of the inference from the GW localization resolution. For each GW bin α , we compute the maximum ℓ such that the beam $\langle B_\ell \rangle_\alpha \geq 1/e$; this goes from $\ell_{\text{max}}^{[1]} = 229$ for the first bin to $\ell_{\text{max}}^{[11]} = 93$ for the last bin. Upon computing the ℓ corresponding to the non-linear scale (i.e., Nyquist frequency) $k_{\text{max}} = 0.1 \text{ Mpc}^{-1}$ at the mid-point distance of each shell, we find $\ell_{\text{max,nl}}$ starting from 262 at the first shell and increasing onwards, and thus the ℓ_{max} set by the localization resolution does not reach non-linear scales. We use $\ell_{\text{max}} = 229$ to analyze all power spectra in the analysis, as higher modes of the cross-correlation are not informative for any GW bin.

Figure 6 shows some theoretical power spectra computed using this framework for the true cosmology. In Figure 6a, we show a grid of error-corrected theoretical $C_\ell^{[\alpha\beta]}$; for each pair of bins (α, β) with $\alpha \geq \beta$, we plot the total SNR across angular modes

$$\text{SNR} = \sqrt{\sum_{\ell=\ell_{\text{min}}}^{\ell_{\text{max}}} \frac{(C_\ell^{\alpha\beta})^2}{\langle (C_\ell^{\alpha\beta})^2 \rangle}}. \quad (106)$$

The top left and bottom right triangles show the GW–GW and galaxy–galaxy auto-power spectra, which have the highest SNR along the diagonal, and smaller but nonzero signals for nearby bins which overlap. The top right rectangle shows the grid of GW–galaxy cross-correlations, in which a band showing the $d_L - z$ relation for the given cosmology is visible. This curve is not diagonal because we have chosen the GW and galaxy bins separately, and thus are not spaced proportionately to each other as seen in Figure 4. One can also see the GW–galaxy cross-correlations are only modestly well-measured, with a total SNR of 30 across all bins together, compared to an SNR of 800 for the galaxy–galaxy auto-power spectra.

To demonstrate this more clearly, we plot in Figure 6b the theoretical power spectra and corresponding error bars for the GW–GW, GW–galaxy, and galaxy–galaxy power spectra in a representative GW and galaxy bin, computed with the true cosmology and bias $b = 1.1$. These three panels correspond to the highlighted pixels in Figure 6a; the GW and galaxy bins are centered at $d_L \approx 8.2 \text{ Gpc}$ and $z \approx 1.2$, respectively, and thus their overlap generates a measurable cross-correlation. We also plot in black the power spectrum estimators computed from our mock data, verifying the goodness of fit of the theoretical prediction. Notice also the scale on the y-axes: C_ℓ^{GG} is large because it is shot noise dominated, while C_ℓ^{Gg} and C_ℓ^{gg} are signal dominated, i.e., $\overline{C}_\ell^{gg} \gg 1/\langle n^g \rangle$ for any galaxy bin. Thus, the GW–GW auto-correlation contributes little to no clustering information for the inference. Furthermore, the largeness of

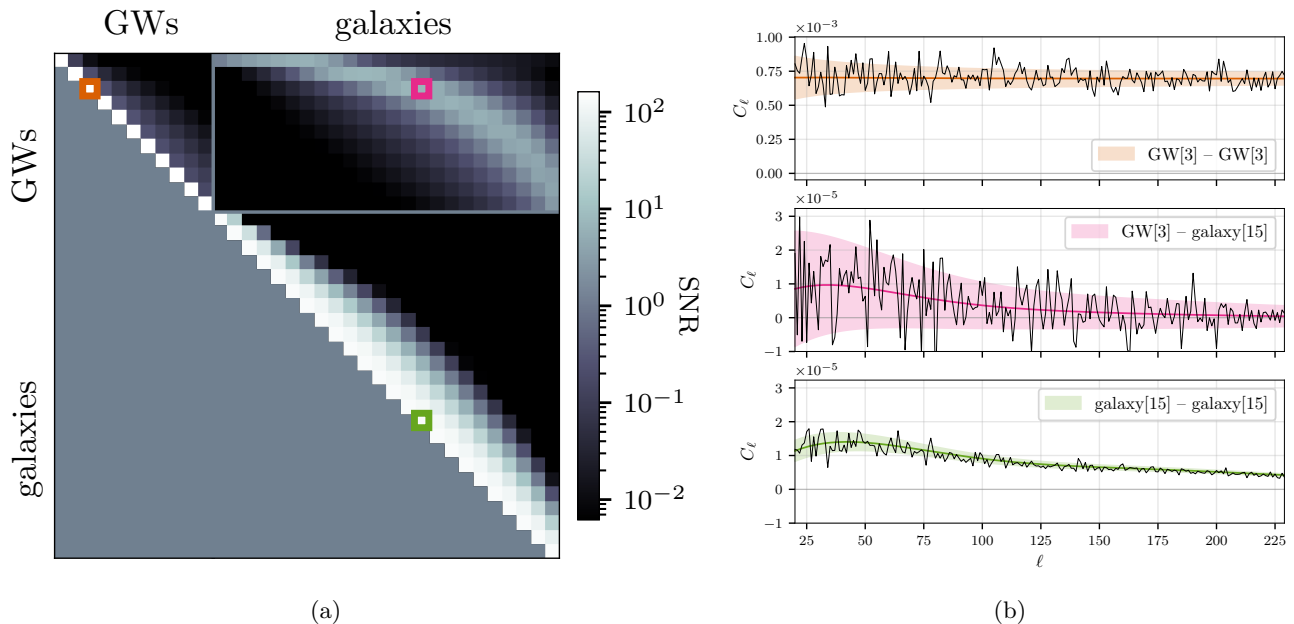


FIG. 6: (a): Theoretical SNR of the cross-correlation signal for each pair of radial bins (α, β) for $\alpha \geq \beta$. Highlighted pixels correspond to the power spectra plotted in (b). (b): From top to bottom, select GW–GW, GW–galaxy, and galaxy–galaxy power spectra; the bottom two panels are plotted on the same scale. The colored curves show the theoretical error-corrected power spectra and 1σ error bars, while the power spectra estimated from our mock data are plotted in black.

the GW shot noise is the main contributor for the large uncertainty in the GW–galaxy cross correlation. The theoretical expectation for C_ℓ^{Gg} and C_ℓ^{gg} are on the same scale, differing by a factor of B_ℓ from the GW localization uncertainty. A plot breaking down the contributions to the total cross-correlation from the shot noise and the signal C_ℓ can be found in Appendix C.

To implement these computations, we use the architecture of `jax_cosmo` [125], a GPU-accelerated and differentiable cosmology library written in `jax`. In particular, we adapt their implementation of the Limber-approximated angular power spectra and computation of covariance matrices, and build upon their architecture of using container objects for the cosmology, bias parameters, and probes such that key `jax` features such as auto-differentiation and `vmap` (a wrapper that can vectorize any operation written in `jax`) are available to them. Because of this, we are able to use Hamiltonian Monte Carlo (HMC) sampling [126–128], which efficiently explores the posterior space using gradient-based methods. For our inference, we use the `NumPyro` [129, 130] implementation of the No-U-Turn Sampler [131], which is a flavor of HMC that adaptively sets the path length.

VIII. RESULTS AND DISCUSSION

In Figure 7, we present the posterior constraints on all of our population parameters — H_0 , $\Omega_{m,0}$, and b .

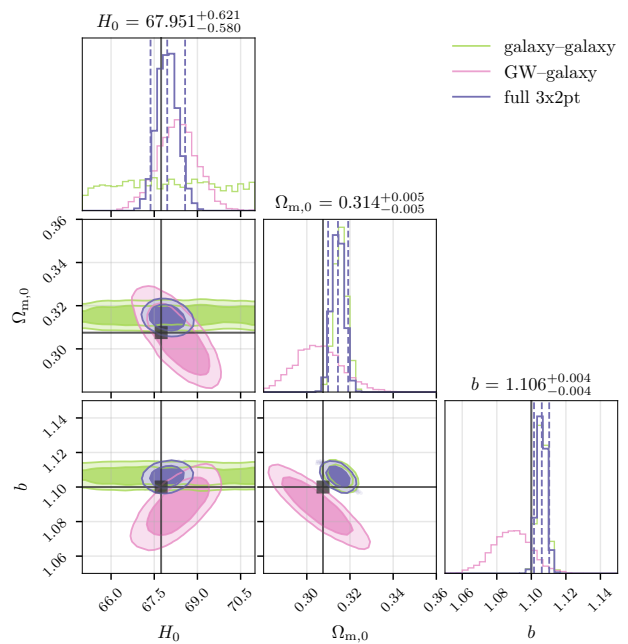


FIG. 7: Corner plot for H_0 (in km/s/Mpc), $\Omega_{m,0}$, and the tracer bias b . We overplot results from an analysis that uses only the galaxy–galaxy correlations, an analysis that uses only the GW–galaxy cross-correlations, and the result from the full 3x2pt analysis.

Contours show the 50% and 90% constraints, while the 1D histograms show the 90% credible intervals.

The results from the full 3x2pt analysis, corresponding to the posterior in Equation (105), are shown in dark purple. We also show the results from an analysis that uses only the galaxy–galaxy (green) or only the GW–galaxy power spectra (pink), i.e., we marginalize over the other power spectra by slicing the covariance matrix in Equation (45). Note that because we marginalize over the galaxy power spectra instead of conditioning on the galaxy data, there is some overlapping information between the pink and green curves. We can see that most of the constraints on H_0 itself come from the GW–galaxy cross-correlation, but adding the galaxy–galaxy correlations tightens the constraint on $\Omega_{m,0}$, thus tightening the constraint on H_0 in the full analysis. This synergy is consistent with the Fisher-matrix based forecast in [41].

In all three analyses, H_0 is recovered correctly and well within the 90% credible intervals. Note also the precision: both the GW–galaxy only and full 3x2pt analysis are able to achieve the percent level precision of modern cosmological experiments. In particular, the GW–galaxy cross-correlation and full 3x2pt analysis measure H_0 to a 1σ precision of 1% and 0.5%, respectively. $\Omega_{m,0}$ is also measured well, with a 1σ precision of 5% and 1%, respectively.

There is a small ($\sim 2\sigma$) bias in $\Omega_{m,0}$, driven by the galaxy–galaxy correlations preferring a higher value of $\Omega_{m,0}$. We show in Appendix E that this bias is removed if we add a first-order correction in $b(k)$, indicating some kind of unmodeled error at small scales. Possible sources of this error include the spectral leakage and non-Gaussianities of the log-normal field discussed earlier, as well as the breakdown of the Limber approximation due to the relatively thin galaxy bin widths. Because there are so many galaxies, and because galaxies have virtually no angular localization errors, the galaxy–galaxy power spectrum is extremely well measured at a total SNR of 800 across all bins, compared to 30 for the GW–galaxy cross power spectrum. Because of this, the measurement precision can often approach or exceed unmodeled systematics. Since the number of independent modes scales linearly with ℓ , small scales in particular contribute more information. Thus, one must have some caution when including information from galaxy–galaxy correlations, a lesson well known in the galaxy survey literature. Therefore, we do not find the bias in $\Omega_{m,0}$ to be too concerning in this work. Crucially, the posteriors on both H_0 and $\Omega_{m,0}$ when we use the GW–galaxy cross-correlation alone are unbiased, making the cross-correlation method a promising avenue for next-generation precision cosmology.

Note that Equation (105) does not include any information from a spectral sirens inference; recall that in the limit of large N^G , the spectral-sirens and cross-correlation likelihoods are decoupled. The goal of this example is to probe the effectiveness of the cross-correlation inference, and a study of the full joint posterior in Equa-

tion (102) is left for future work.

Finally, we would like to highlight the speed of this analysis, which we see as among the primary advantages of this method in the third generation (3G) era of GW detectors. While the dimensionality of our posterior space does not necessarily require HMC, GPU acceleration and `jax`'s XLA (accelerated linear algebra) compiler allows the sampling to be run in less than an hour. Furthermore, we make a series of approximations that eliminates the need for keeping thousands of PE samples per event at inference by binning and compressing the data into a few auxiliary data products. Once this (relatively cheap) upfront computational cost is paid, the inference runtime is roughly constant with the number of GW sources and galaxies. Current methods for analyzing LVK data, involving many products of Monte-Carlo integrals, is known to scale very poorly as our catalog grows and measurement precision improves [132]. Furthermore, current standard galaxy catalog methods are already quite computationally costly, since they involve pre-computing the entire redshift prior for $p^g(z, \mathbf{\Omega})$ to be stored in memory at runtime, which also requires one to fix $\Omega_{m,0}$ [24, 26, 32–34]. The cross-correlation method therefore provides a solution for cheap and accurate GW cosmological inferences in the 3G era.

IX. CONCLUSIONS

We are entering an era in which it is increasingly possible to probe the cosmological properties of the Universe with multiple tracers alongside an ever-increasing catalog of galaxies. Significant upgrades of GW detectors, in particular 3G detectors, would represent a huge leap in the power of multi-tracer cosmology, with tens of thousands of detected BBHs anticipated per year. Despite this, techniques for joint cosmological inference with GWs and galaxies are wide ranging, from the standard galaxy catalog method of statistically assigning each GW a host galaxy to a variety of flavors of 2-point analyses, which are often at odds with standard GW population analysis techniques. In the era of precision cosmology, it is crucial to have a systematic understanding of these dark siren methods and their relationships.

Thus, we have set out in this paper to accomplish the following: 1) provide a pedagogical guide to the cross-correlation method by rigorously deriving the cross-correlation method from first principles (Sections III and IV), including novel results on how to treat GW measurement uncertainties (Section V); and 2) describe the relationship between the cross-correlation method, the standard galaxy catalog method, and the spectral sirens method, and outline a path to a joint inference (Sections IV and VI).

Our primary theoretical results are as follows:

- The primary difference between the cross-correlation and standard galaxy catalog method

is the information we condition upon. The standard formalism for analyzing a set of observed GW sources assumes a fixed distribution of the source parameters ($d_L, \Omega, m_1, m_2, \dots$). In order to use this formalism, the standard galaxy catalog method implicitly conditions upon a known background galaxy distribution, usually by assuming a uniform-in-volume distribution for the unobserved galaxies. On the other hand, if we condition only upon the cosmology, the GWs are a doubly stochastic process: GWs are randomly drawn from a galaxy field which itself is a GRF. To maximize the effectiveness of dark siren analyses with galaxies, one should either marginalize over all possible realizations of the missing galaxies, or more simply perform a joint analysis of the galaxies and GWs as GRFs, which is what the cross-correlation method does.

- The cross-correlation technique is generally thought to impose a weaker requirement than the standard galaxy catalog method, requiring only that the GWs trace the same density field as the galaxies instead of necessarily being hosted in galaxies. We showed that it is possible to impose this requirement exactly in the infinitesimal limit, by showing that the standard galaxy catalog method can be derived from the cross-correlation method under the assumption that the total galaxy field is known. In practice, however, we can only impose the host requirement on the scales that the events are measured, due to the localization errors of the tracers and the discretization of the field into radial bins and pixels. Thus, the constraining power of the cross-correlation method is largely derived from 2-point statistics independent of the constraining power of the standard galaxy catalog method.
- The cross-correlation method acts as a generalized angular distribution at a given radius $p(\{\Omega\}, \{\Omega^g\} | z)$. This is because the cross-correlation power spectra measure correlations between overdensity fields, which are by construction normalized to the rate at each distance. Therefore, they provide exactly complementary information to the spectral sirens method, which have no angular dependence. A corollary of this is that the cross-correlation population likelihood has radial selection effects folded in, and thus selection effects in a joint spectral sirens + cross-correlation analysis are only explicitly manifest in the former.
- Because of prohibitive computational costs of the cross-correlation method with Monte Carlo integration, we propose using an aggressive SNR cut ($\gtrsim 25$) to analytically build localization errors into the theoretical prediction by modeling the likelihood as Gaussian in this limit.

- GW angular localization errors are not the same process as a telescope point spread function and should not be treated as such. We show that if we model each event in a radial bin as being displaced from its true angular sky position by a draw from a homogeneous, isotropic, and Gaussian distribution, then the effective beam window function that multiplies the measured cross-correlation is the expectation value of an ensemble of Gaussian beams corresponding to the localization errors of events in the bin. In this model, contrary to current implementations of the cross-correlation method in the literature, the observed GW overdensity field should be constructed from its maximum likelihood measurement, rather than the posterior draws themselves.
- The cross-correlation formalism relies on many assumptions, requiring at least \sim hundreds of events per bin with high SNR and angular localizations exceeding $\ell \gtrsim 20$ ($\sim 3^\circ$ resolution) to satisfy the central limit theorem for both the shot noise and the likelihood of the power spectrum estimator, as well as to be able to estimate the distribution of localization errors directly from the data. We anticipate that these conditions will be difficult to meet before 3G, and encourage research directions of examining if or when these assumptions can be relaxed. To our knowledge, these caveats have not been addressed in the GW cross-correlation literature, despite the usage of many elements of this formalism that rely on these assumptions.

We also validated our formalism by presenting an implementation on 3G-like data, forecasting its constraining power (Sections VII and VIII). We generated a mock galaxy catalog by drawing from a fiducial 3D matter power spectrum, and generated a mock BBH catalog by computing Fisher matrix posteriors of BBHs drawn from these galaxies, and imposing selection effects for both. We then recovered the fiducial cosmology with a Bayesian inference on the mock data. To our knowledge, this is the first time that the cross-correlation method has been validated in a full Bayesian inference setting with realistic GW localization errors, in which both the measured luminosity distances and angular sky locations are displaced from their true values. With a 2 ET + 1 CE configuration and a 2 year observing run, we find that both the full 3x2pt analysis and an analysis using only the GW–galaxy cross-correlation power spectra achieve percent-level precision in H_0 ; the former also achieves percent-level precision in $\Omega_{m,0}$. It is the GW–galaxy cross-correlation that drives the measurement on H_0 , whereas $\Omega_{m,0}$ is mostly driven by the galaxy–galaxy power spectra.

Furthermore, by leveraging the optimal data compression of the cross-correlation method and a GPU-accelerated implementation, we were able to run the inference in less than an hour. Thus, we demonstrate an avenue for precise and scalable cosmological inferences in the 3G era. Unlike traditional population analysis

techniques, the computational complexity of the cross-correlation method is flat with respect to the number of events.

Although we generated our mock galaxy catalog from a log-normal field, we do not expect the cross-correlation results to be different for a galaxy catalog generated from, e.g., hydrodynamical simulations, because GWs are not well localized enough to probe fully non-linear scales even in 3G. Nonetheless, we acknowledge that this forecast is still relatively simplified. Because the aim of this paper was to focus on the information gained from modeling GWs and galaxies as GRFs, we ignored all effects beyond this model, including non-linearities, gravitational lensing, bias evolution, RSDs and LSDs. We also assumed that the linear matter power spectrum was known, but in general it is sensitive to the cosmology, and thus an analysis in which the 3D power spectrum itself is computed on the fly would be an interesting direction for future research. Furthermore, a more realistic analysis will not be able to assume GWs and galaxies have the same non-evolving bias; GW host galaxies may not cluster the same way as the bright galaxies in our catalog, and therefore in full generality b^G and b^g would have to be inferred separately at each redshift. A more detailed

forecast that includes all of the effects is the most salient next step in advancing our understanding of cosmological inferences with GW–galaxy cross-correlations.

ACKNOWLEDGMENTS

The authors would like to thank Matteo Tagliacruzchi, Haochen Wang, Sylvia Biscoveanu, and James Sunseri for their valuable comments and discussions. This work was made possible by the German-American Fulbright Commission. A.Q.C. is currently supported by the Lowell Wood Endowed Fellowship of the Fannie and John Hertz foundation.

DATA AVAILABILITY

All software used for this work is made available on Github. This includes our branch of `jax_cosmo` [133], which includes significant modifications to implement the specific details of the GW–galaxy cross-correlation outlined in this paper, as well as all scripts and modules for the mock data generation and inference [134].

-
- [1] Planck Collaboration, P. A. R. Ade, N. Aghanim, M. Arnaud, M. Ashdown, J. Aumont, C. Baccigalupi, A. J. Banday, R. B. Barreiro, J. G. Bartlett, N. Bartolo, E. Battaner, R. Battye, K. Benabed, A. Benoît, A. Benoit-Lévy, J.-P. Bernard, M. Bersanelli, P. Bielewicz, J. J. Bock, A. Bonaldi, L. Bonavera, J. R. Bond, J. Borrill, F. R. Bouchet, F. Boulanger, M. Bucher, C. Burigana, R. C. Butler, E. Calabrese, J.-F. Cardoso, A. Catalano, A. Challinor, A. Chambaullu, R.-R. Chary, H. C. Chiang, J. Chluba, P. R. Christensen, S. Church, D. L. Clements, S. Colombi, L. P. L. Colombo, C. Combet, A. Coulais, B. P. Crill, A. Curto, F. Cuttaia, L. Danese, R. D. Davies, R. J. Davis, P. de Bernardis, A. de Rosa, G. de Zotti, J. Delabrouille, F.-X. Désert, E. Di Valentino, C. Dickinson, J. M. Diego, K. Dolag, H. Dole, S. Donzelli, O. Doré, M. Douspis, A. Ducout, J. Dunkley, X. Dupac, G. Efstathiou, F. Elsner, T. A. Enßlin, H. K. Erikson, M. Farhang, J. Fergusson, F. Finelli, O. Forni, M. Frailis, A. A. Fraisse, E. Franceschi, A. Frejsel, S. Galeotta, S. Galli, K. Ganga, C. Gauthier, M. Gerbino, T. Ghosh, M. Giard, Y. Giraud-Héraud, E. Giusarma, E. Gjerløw, J. González-Nuevo, K. M. Górski, S. Gratton, A. Gregorio, A. Gruppuso, J. E. Gudmundsson, J. Hamann, F. K. Hansen, D. Hanson, D. L. Harrison, G. Helou, S. Henrot-Versillé, C. Hernández-Monteagudo, D. Herranz, S. R. Hildebrandt, E. Hivon, M. Hobson, W. A. Holmes, A. Hornstrup, W. Hovest, Z. Huang, K. M. Huffenberger, G. Hurier, A. H. Jaffe, T. R. Jaffe, W. C. Jones, M. Juvela, E. Keihänen, R. Kesitalo, T. S. Kisner, R. Kneissl, J. Knoche, L. Knox, M. Kunz, H. Kurki-Suonio, G. Lagache, A. Lähteenmäki, J.-M. Lamarre, A. Lasenby, M. Lattanzi, C. R. Lawrence, J. P. Leahy, R. Leonardi, J. Lesgourgues, F. Levrier, A. Lewis, M. Liguori, P. B. Lilje, M. Linden-Vørnle, M. López-Cañiego, P. M. Lubin, J. F. Macías-Pérez, G. Maggio, D. Maino, N. Mandolesi, A. Mangilli, A. Marchini, M. Maris, P. G. Martin, M. Martinelli, E. Martínez-González, S. Masi, S. Matarrese, P. McGehee, P. R. Meinhold, A. Melchiorri, J.-B. Melin, L. Mendes, A. Mennella, M. Migliaccio, M. Millea, S. Mitra, M.-A. Miville-Deschênes, A. Moneti, L. Montier, G. Morgante, D. Mortlock, A. Moss, D. Munshi, J. A. Murphy, P. Naselsky, F. Nati, P. Natoli, C. B. Netterfield, H. U. Nørgaard-Nielsen, F. Noviello, D. Novikov, I. Novikov, C. A. Oxborrow, F. Paci, L. Pagano, F. Pajot, R. Paladini, D. Paoletti, B. Partridge, F. Pasian, G. Patanchon, T. J. Pearson, O. Perdereau, L. Perotto, F. Perrotta, V. Pettorino, F. Piacentini, M. Piat, E. Pierpaoli, D. Pietrobon, S. Plaszczynski, E. Pointecouteau, G. Polenta, L. Popa, G. W. Pratt, and G. Prézeau, Planck 2015 results. XIII. Cosmological parameters, *A&A* **594**, A13 (2016), arXiv:1502.01589 [astro-ph.CO].
- [2] Planck Collaboration, N. Aghanim, Y. Akrami, M. Ashdown, J. Aumont, C. Baccigalupi, M. Ballardini, A. J. Banday, R. B. Barreiro, N. Bartolo, S. Basak, R. Battye, K. Benabed, J.-P. Bernard, M. Bersanelli, P. Bielewicz, J. J. Bock, J. R. Bond, J. Borrill, F. R. Bouchet, F. Boulanger, M. Bucher, C. Burigana, R. C. Butler, E. Calabrese, J.-F. Cardoso, J. Carron, A. Challinor, H. C. Chiang, J. Chluba, L. P. L. Colombo, C. Combet, D. Contreras, B. P. Crill, F. Cuttaia, P. de Bernardis, G. de Zotti, J. Delabrouille, J.-M. Delouis, E. Di Valentino, J. M. Diego, O. Doré, M. Douspis, A. Ducout, X. Dupac, S. Dusini, G. Ef-

- stathiou, F. Elsner, T. A. Enßlin, H. K. Eriksen, Y. Fantaye, M. Farhang, J. Fergusson, R. Fernandez-Cobos, F. Finelli, F. Forastieri, M. Frailis, A. A. Fraisse, E. Franceschi, A. Frolov, S. Galeotta, S. Galli, K. Ganga, R. T. Génova-Santos, M. Gerbino, T. Ghosh, J. González-Nuevo, K. M. Górski, S. Gratton, A. Gruppuso, J. E. Gudmundsson, J. Hamann, W. Handley, F. K. Hansen, D. Herranz, S. R. Hildebrandt, E. Hivon, Z. Huang, A. H. Jaffe, W. C. Jones, A. Karakci, E. Keihänen, R. Keskitalo, K. Kiiveri, J. Kim, T. S. Kisner, L. Knox, N. Krachmalnicoff, M. Kunz, H. Kurki-Suonio, G. Lagache, J.-M. Lamarre, A. Lasenby, M. Lattanzi, C. R. Lawrence, M. Le Jeune, P. Lemos, J. Lesgourgues, F. Levrier, A. Lewis, M. Liguori, P. B. Lilje, M. Lilley, V. Lindholm, M. López-Cañego, P. M. Lubin, Y.-Z. Ma, J. F. Macías-Pérez, G. Maggio, D. Maino, N. Mandolesi, A. Mangilli, A. Marcos-Caballero, M. Maris, P. G. Martin, M. Martinelli, E. Martínez-González, S. Matarrese, N. Mauri, J. D. McEwen, P. R. Meinhold, A. Melchiorri, A. Mennella, M. Migliaccio, M. Millea, S. Mitra, M.-A. Miville-Deschênes, D. Molinari, L. Montier, G. Morgante, A. Moss, P. Natoli, H. U. Nørgaard-Nielsen, L. Pagano, D. Paoletti, B. Partridge, G. Patanchon, H. V. Peiris, F. Perrotta, V. Pettorino, F. Piacentini, L. Polastri, G. Polenta, J.-L. Puget, J. P. Rachen, M. Reinecke, M. Remazeilles, A. Renzi, G. Rocha, C. Rosset, G. Roudier, J. A. Rubiño-Martín, B. Ruiz-Granados, L. Salvati, M. Sandri, M. Savelainen, D. Scott, E. P. S. Shellard, C. Sirignano, G. Sirri, L. D. Spencer, R. Sunyaev, A.-S. Suur-Uski, J. A. Tauber, D. Tavagnacco, M. Tenti, L. Toffolatti, M. Tomasi, T. Trombetti, L. Valenziano, J. Valiviita, B. Van Tent, L. Vibert, P. Vielva, F. Villa, N. Vittorio, B. D. Wandelt, I. K. Wehus, M. White, S. D. M. White, A. Zachei, and A. Zonca, Planck 2018 results. VI. Cosmological parameters, *A&A* **641**, A6 (2020), arXiv:1807.06209 [astro-ph.CO].
- [3] A. G. Riess, W. Yuan, L. M. Macri, D. Scolnic, D. Brout, S. Casertano, D. O. Jones, Y. Murakami, G. S. Anand, L. Breuval, T. G. Brink, A. V. Filippenko, S. Hoffmann, S. W. Jha, W. D’arcy Kenworthy, J. Mackenty, B. E. Stahl, and W. Zheng, A Comprehensive Measurement of the Local Value of the Hubble Constant with $1 \text{ km s}^{-1} \text{ Mpc}^{-1}$ Uncertainty from the Hubble Space Telescope and the SH0ES Team, *ApJL* **934**, L7 (2022), arXiv:2112.04510 [astro-ph.CO].
- [4] L. Verde, T. Treu, and A. G. Riess, Tensions between the early and late Universe, *NatAs* **3**, 891 (2019), arXiv:1907.10625 [astro-ph.CO].
- [5] E. Di Valentino, O. Mena, S. Pan, L. Visinelli, W. Yang, A. Melchiorri, D. F. Mota, A. G. Riess, and J. Silk, In the realm of the Hubble tension—a review of solutions, *CQGra* **38**, 153001 (2021), arXiv:2103.01183 [astro-ph.CO].
- [6] B. F. Schutz, Determining the Hubble constant from gravitational wave observations, *Natur* **323**, 310 (1986).
- [7] D. E. Holz and S. A. Hughes, Using Gravitational-Wave Standard Sirens, *ApJ* **629**, 15 (2005), arXiv:astro-ph/0504616 [astro-ph].
- [8] N. Dalal, D. E. Holz, S. A. Hughes, and B. Jain, Short GRB and binary black hole standard sirens as a probe of dark energy, *PhRvD* **74**, 063006 (2006), arXiv:astro-ph/0601275 [astro-ph].
- [9] B. P. Abbott, R. Abbott, T. D. Abbott, F. Acernese, K. Ackley, C. Adams, T. Adams, P. Addesso, R. X. Adhikari, V. B. Adya, C. Affeldt, M. Afrough, B. Agarwal, M. Agathos, K. Agatsuma, N. Aggarwal, O. D. Aguiar, L. Aiello, A. Ain, P. Ajith, B. Allen, G. Allen, A. Allocca, P. A. Altin, A. Amato, A. Ananyeva, S. B. Anderson, W. G. Anderson, S. V. Angelova, S. Antier, S. Appert, K. Arai, M. C. Araya, J. S. Areeda, N. Arnaud, K. G. Arun, S. Ascenzi, G. Ashton, M. Ast, S. M. Aston, P. Astone, D. V. Atallah, P. Aufmuth, C. Aulbert, K. Aultoneal, C. Austin, A. Avila-Alvarez, S. Babak, P. Bacon, M. K. M. Bader, S. Bae, P. T. Baker, F. Baldaccini, G. Ballardín, S. W. Ballmer, S. Banagiri, J. C. Barayoga, S. E. Barclay, B. C. Barish, D. Barker, K. Barkett, F. Barone, B. Barr, L. Barsotti, M. Barsuglia, D. Barta, J. Bartlett, I. Bartos, R. Bassiri, A. Basti, J. C. Batch, M. Bawaj, J. C. Bayley, M. Bazzan, B. Bécsy, C. Beer, M. Bejger, I. Belahcene, A. S. Bell, B. K. Berger, G. Bergmann, J. J. Bero, C. P. L. Berry, D. Bersanetti, A. Bertolini, J. Betzwieser, S. Bhagwat, R. Bhandare, I. A. Bilenko, G. Billingsley, C. R. Billman, J. Birch, R. Birney, O. Birnholtz, S. Biscans, S. Biscoveanu, A. Bisht, M. Bitossi, C. Biwer, M. A. Bizouard, J. K. Blackburn, J. Blackman, C. D. Blair, D. G. Blair, R. M. Blair, S. Bloemen, O. Bock, N. Bode, M. Boer, G. Bogaert, A. Bohe, F. Bondu, E. Bonilla, R. Bonnand, B. A. Boom, R. Bork, V. Boschi, S. Bose, K. Bossie, Y. Bouffanais, A. Bozzi, C. Bradaschia, P. R. Brady, M. Branchesi, J. E. Brau, T. Briant, A. Brillet, M. Brinkmann, V. Brisson, P. Brockill, J. E. Broida, A. F. Brooks, D. A. Brown, D. D. Brown, S. Brunett, C. C. Buchanan, A. Buikema, T. Bulik, H. J. Bulten, A. Buonanno, D. Buskulic, C. Buy, R. L. Byer, M. Cabero, L. Cadonati, G. Cagnoli, C. Cahillane, J. C. Bustillo, T. A. Callister, E. Calloni, J. B. Camp, M. Canepa, P. Canizares, K. C. Cannon, H. Cao, J. Cao, C. D. Capano, E. Capocasa, F. Carbognani, S. Caride, M. F. Carney, J. C. Diaz, C. Casentini, S. Caudill, M. Cavaglià, F. Cavalier, R. Cavalieri, G. Cella, C. B. Cepeda, P. Cerdá-Durán, G. Cerretani, E. Cesarini, S. J. Chamberlin, M. Chan, S. Chao, P. Charlton, E. Chase, E. Chassande-Mottin, D. Chatterjee, K. Chatziioannou, B. D. Cheeseboro, H. Y. Chen, X. Chen, Y. Chen, H.-P. Cheng, H. Chia, A. Chincarini, A. Chiummo, T. Chmiel, H. S. Cho, M. Cho, J. H. Chow, N. Christensen, Q. Chu, A. J. K. Chua, S. Chua, A. K. W. Chung, S. Chung, G. Ciani, and R. Ciolfi, A gravitational-wave standard siren measurement of the Hubble constant, *Natur* **551**, 85 (2017), arXiv:1710.05835 [astro-ph.CO].
- [10] H.-Y. Chen, M. Fishbach, and D. E. Holz, A two per cent Hubble constant measurement from standard sirens within five years, *Natur* **562**, 545 (2018), arXiv:1712.06531 [astro-ph.CO].
- [11] L. S. Finn and D. F. Chernoff, Gravitational Radiation, Inspiral Binaries, and Cosmology, in *American Astronomical Society Meeting Abstracts*, American Astronomical Society Meeting Abstracts, Vol. 183 (1993) p. 67.05.
- [12] S. R. Taylor and J. R. Gair, Cosmology with the lights off: Standard sirens in the Einstein Telescope era, *PhRvD* **86**, 023502 (2012), arXiv:1204.6739 [astro-ph.CO].

- [13] J. M. Ezquiaga and D. E. Holz, Spectral Sirens: Cosmology from the Full Mass Distribution of Compact Binaries, *PhRvL* **129**, 061102 (2022), arXiv:2202.08240 [astro-ph.CO].
- [14] U. Mali and R. Essick, Striking a Chord with Spectral Sirens: Multiple Features in the Compact Binary Population Correlate with H_0 , *ApJ* **980**, 85 (2025), arXiv:2410.07416 [astro-ph.HE].
- [15] S. Mastrogiovanni, K. Leyde, C. Karathanasis, E. Chassande-Mottin, D. A. Steer, J. Gair, A. Ghosh, R. Gray, S. Mukherjee, and S. Rinaldi, On the importance of source population models for gravitational-wave cosmology, *PhRvD* **104**, 062009 (2021), arXiv:2103.14663 [gr-qc].
- [16] M. Mancarella and D. Gerosa, Sampling the full hierarchical population posterior distribution in gravitational-wave astronomy, *PhRvD* **111**, 103012 (2025), arXiv:2502.12156 [gr-qc].
- [17] K. Leyde, S. Mastrogiovanni, D. A. Steer, E. Chassande-Mottin, and C. Karathanasis, Current and future constraints on cosmology and modified gravitational wave friction from binary black holes, *JCAP* **2022** (9), 012, arXiv:2203.11680 [gr-qc].
- [18] S. R. Taylor, J. R. Gair, and I. Mandel, Cosmology using advanced gravitational-wave detectors alone, *PhRvD* **85**, 023535 (2012), arXiv:1108.5161 [gr-qc].
- [19] A. M. Farah, T. A. Callister, J. M. Ezquiaga, M. Zevin, and D. E. Holz, No Need to Know: Toward Astrophysics-free Gravitational-wave Cosmology, *ApJ* **978**, 153 (2025), arXiv:2404.02210 [astro-ph.CO].
- [20] M. Tagliacruzchi, M. Moresco, N. Borghi, and C. Ciapetti, Mind the peak: improving cosmological constraints from GWTC-4.0 spectral sirens using semiparametric mass models, arXiv, arXiv:2601.03347 (2026), arXiv:2601.03347 [astro-ph.CO].
- [21] W. Del Pozzo, Inference of cosmological parameters from gravitational waves: Applications to second generation interferometers, *PhRvD* **86**, 043011 (2012), arXiv:1108.1317 [astro-ph.CO].
- [22] M. Fishbach, R. Gray, I. Magaña Hernandez, H. Qi, A. Sur, F. Acernese, L. Aiello, A. Allocca, M. A. Aloy, A. Amato, S. Antier, M. Arène, N. Arnaud, S. Ascenzi, P. Astone, F. Aubin, S. Babak, P. Bacon, F. Badaracco, M. K. M. Bader, F. Baldaccini, G. Ballardín, F. Barone, M. Barsuglia, D. Barta, A. Basti, M. Bawaj, M. Bazzan, M. Bejger, I. Belahcene, S. Bernuzzi, D. Bersanetti, A. Bertolini, M. Bitossi, M. A. Bizouard, C. D. Blair, S. Bloemen, M. Boer, G. Bogaert, F. Bondu, R. Bondand, B. A. Boom, V. Boschi, Y. Bouffanais, A. Bozzi, C. Bradaschia, P. R. Brady, M. Branchesi, T. Briant, F. Brighenti, A. Brillet, V. Brisson, T. Bulik, H. J. Bulten, D. Buskulic, C. Buy, G. Cagnoli, E. Calloni, M. Canepa, E. Capocasa, F. Carbognani, G. Carullo, J. Casanueva Diaz, C. Casentini, S. Caudill, F. Cavalieri, R. Cavalieri, G. Cella, P. Cerdá-Durán, G. Cerretani, E. Cesarini, O. Chaibi, E. Chassande-Mottin, K. Chatziioannou, H. Y. Chen, A. Chincarini, A. Chiummo, N. Christensen, S. Chua, G. Ciani, R. Ciolfi, F. Cipriano, A. Cirone, F. Cleva, E. Coccia, P.-F. Cohadon, D. Cohen, L. Conti, I. Cordero-Carrión, S. Cortese, M. W. Coughlin, J.-P. Coulon, M. Croquette, E. Cuoco, G. Dálya, S. D'Antonio, L. E. H. Dattier, V. Dattilo, M. Davier, J. Degallaix, M. De Laurentis, S. Deléglise, W. Del Pozzo, M. Denys, R. De Pietri, R. De Rosa, C. De Rossi, R. DeSalvo, T. Dietrich, L. Di Fiore, M. Di Giovanni, T. Di Girolamo, A. Di Lieto, S. Di Pace, I. Di Palma, F. Di Renzo, Z. Doctor, M. Drago, J.-G. Ducoin, M. Eisenmann, R. C. Essick, D. Estevez, V. Fafone, S. Farinon, W. M. Farr, F. Feng, I. Ferrante, F. Ferrini, F. Fidecaro, I. Fiori, D. Fiorucci, R. Flaminio, J. A. Font, J.-D. Fournier, S. Frasca, F. Frasconi, V. Frey, J. R. Gair, L. Gammaitoni, F. Garufi, G. Gemme, E. Genin, A. Gennai, D. George, V. Germain, A. Ghosh, B. Giacomazzo, A. Giazotto, G. Giordano, J. M. Gonzalez Castro, M. Gosselin, R. Gouaty, A. Grado, M. Granata, G. Greco, P. Groot, P. Gruning, G. M. Guidi, Y. Guo, O. Halim, J. Harms, C.-J. Haster, A. Heidmann, H. Heitmann, P. Hello, G. Hemming, M. Hendry, T. Hinderer, D. Hoak, D. Hoffman, D. E. Holz, A. Hreibi, D. Huet, B. Idzkowski, A. Iess, G. Intini, J.-M. Isac, T. Jacqmin, P. Jaranowski, R. J. G. Jonker, S. Katsanevas, E. Katsavounidis, F. Kéfélian, I. Khan, G. Koekoek, S. Koley, I. Kowalska, A. Królak, A. Kutynia, J. Lange, A. Lartaux-Vollard, C. Lazzaro, P. Leaci, N. Letendre, T. G. F. Li, F. Linde, A. Longo, M. Lorenzini, V. Lorette, and G. Losurdo, A Standard Siren Measurement of the Hubble Constant from GW170817 without the Electromagnetic Counterpart, *ApJL* **871**, L13 (2019), arXiv:1807.05667 [astro-ph.CO].
- [23] S. Mastrogiovanni, D. Laghi, R. Gray, G. C. Santoro, A. Ghosh, C. Karathanasis, K. Leyde, D. A. Steer, S. Perriès, and G. Pierra, Joint population and cosmological properties inference with gravitational waves standard sirens and galaxy surveys, *PhRvD* **108**, 042002 (2023), arXiv:2305.10488 [astro-ph.CO].
- [24] R. Gray, F. Beirnaert, C. Karathanasis, B. Revenu, C. Turski, A. Chen, T. Baker, S. Vallejo, A. E. Romano, T. Ghosh, A. Ghosh, K. Leyde, S. Mastrogiovanni, and S. More, Joint cosmological and gravitational-wave population inference using dark sirens and galaxy catalogues, *JCAP* **2023** (12), 023, arXiv:2308.02281 [astro-ph.CO].
- [25] J. R. Gair, A. Ghosh, R. Gray, D. E. Holz, S. Mastrogiovanni, S. Mukherjee, A. Palmese, N. Tamanini, T. Baker, F. Beirnaert, M. Bilicki, H.-Y. Chen, G. Dálya, J. M. Ezquiaga, W. M. Farr, M. Fishbach, J. Garcia-Bellido, T. Ghosh, H.-Y. Huang, C. Karathanasis, K. Leyde, I. Magaña Hernandez, J. Noller, G. Pierra, P. Raffai, A. E. Romano, M. Seglar-Arroyo, D. A. Steer, C. Turski, M. P. Vaccaro, and S. A. Vallejo-Peña, The Hitchhiker's Guide to the Galaxy Catalog Approach for Dark Siren Gravitational-wave Cosmology, *AJ* **166**, 22 (2023), arXiv:2212.08694 [gr-qc].
- [26] R. Gray, I. M. Hernandez, H. Qi, A. Sur, P. R. Brady, H.-Y. Chen, W. M. Farr, M. Fishbach, J. R. Gair, A. Ghosh, D. E. Holz, S. Mastrogiovanni, C. Messenger, D. A. Steer, and J. Veitch, Cosmological inference using gravitational wave standard sirens: A mock data analysis, *PhRvD* **101**, 122001 (2020), arXiv:1908.06050 [gr-qc].
- [27] W. Ballard, A. Palmese, I. M. Hernandez, S. Benzvi, J. Moon, A. J. Ross, G. Rossi, J. Aguilar, S. Ahlen, R. Blum, D. Brooks, T. Claybaugh, A. de la Macorra, A. Dey, P. Doel, J. E. Forero-Romero, S. Gontcho A Gontcho, K. Honscheid, A. Kremin, M. Manera, A. Meisner, R. Miquel, J. Moustakas,

- F. Prada, E. Sanchez, G. Tarlé, Z. Zhou, and DESI Collaboration, A Dark Siren Measurement of the Hubble Constant with the LIGO/Virgo Gravitational Wave Event GW190412 and DESI Galaxies, *RNAAS* **7**, 250 (2023), arXiv:2311.13062 [astro-ph.CO].
- [28] V. Alfradique, C. R. Bom, A. Palmese, G. Teixeira, L. Santana-Silva, A. Drlica-Wagner, A. H. Riley, C. E. Martínez-Vázquez, D. J. Sand, G. S. Stringfellow, G. E. Medina, J. A. Carballo-Bello, Y. Choi, J. Esteves, G. Limberg, B. Mutlu-Pakdil, N. E. D. Noël, A. B. Pace, J. D. Sakowska, and J. F. Wu, A dark siren measurement of the Hubble constant using gravitational wave events from the first three LIGO/Virgo observing runs and DELVE, *MNRAS* **528**, 3249 (2024), arXiv:2310.13695 [astro-ph.CO].
- [29] A. Palmese, C. R. Bom, S. Mucesh, and W. G. Hartley, A Standard Siren Measurement of the Hubble Constant Using Gravitational-wave Events from the First Three LIGO/Virgo Observing Runs and the DESI Legacy Survey, *ApJ* **943**, 56 (2023), arXiv:2111.06445 [astro-ph.CO].
- [30] A. Palmese, J. deVicente, M. E. S. Pereira, J. Annis, W. Hartley, K. Herner, M. Soares-Santos, M. Crocce, D. Huterer, I. Magaña Hernandez, A. Garcia, J. Garcia-Bellido, J. Gschwend, D. E. Holz, R. Kessler, O. Lahav, R. Morgan, C. Nicolaou, C. Conselice, R. J. Foley, M. S. S. Gill, T. M. C. Abbott, M. Agüena, S. Allam, S. Avila, K. Bechtol, E. Bertin, S. Bhargava, D. Brooks, E. Buckley-Geer, D. L. Burke, M. Carrasco Kind, J. Carretero, F. J. Castander, C. Chang, M. Costanzi, L. N. da Costa, T. M. Davis, S. Desai, H. T. Diehl, P. Doel, A. Drlica-Wagner, J. Estrada, S. Everett, A. E. Evrard, E. Fernandez, D. A. Finley, B. Flaugher, P. Fosalba, J. Frieman, E. Gaztanaga, D. W. Gerdes, D. Gruen, R. A. Gruendl, G. Gutierrez, S. R. Hinton, D. L. Hollowood, K. Honscheid, D. J. James, S. Kent, E. Krause, K. Kuehn, H. Lin, M. A. G. Maia, M. March, J. L. Marshall, P. Melchior, F. Menanteau, R. Miquel, R. L. C. Ogando, F. Paz-Chinchón, A. A. Plazas, A. Roodman, M. Sako, E. Sanchez, V. Scarpine, M. Schubnell, S. Serrano, I. Sevilla-Noarbe, J. A. Smith, M. Smith, E. Suchyta, G. Tarle, M. A. Troxel, D. L. Tucker, A. R. Walker, W. Wester, R. D. Wilkinson, J. Zuntz, and DES Collaboration, A Statistical Standard Siren Measurement of the Hubble Constant from the LIGO/Virgo Gravitational Wave Compact Object Merger GW190814 and Dark Energy Survey Galaxies, *ApJL* **900**, L33 (2020), arXiv:2006.14961 [astro-ph.CO].
- [31] M. Soares-Santos, A. Palmese, W. Hartley, J. Annis, J. Garcia-Bellido, O. Lahav, Z. Doctor, M. Fishbach, D. E. Holz, H. Lin, M. E. S. Pereira, A. Garcia, K. Herner, R. Kessler, H. V. Peiris, M. Sako, S. Allam, D. Brout, A. Carnero Rosell, H. Y. Chen, C. Conselice, J. deRose, J. deVicente, H. T. Diehl, M. S. S. Gill, J. Gschwend, I. Sevilla-Noarbe, D. L. Tucker, R. Wechsler, E. Berger, P. S. Cowperthwaite, B. D. Metzger, P. K. G. Williams, T. M. C. Abbott, F. B. Abdalla, S. Avila, K. Bechtol, E. Bertin, D. Brooks, E. Buckley-Geer, D. L. Burke, M. Carrasco Kind, J. Carretero, F. J. Castander, M. Crocce, C. E. Cunha, C. B. D'Andrea, L. N. da Costa, C. Davis, S. Desai, P. Doel, A. Drlica-Wagner, T. F. Eifler, A. E. Evrard, B. Flaugher, P. Fosalba, J. Frieman, E. Gaztanaga, D. W. Gerdes, D. Gruen, R. A. Gruendl, G. Gutierrez, D. L. Hollowood, B. Hoyle, D. J. James, T. Jeltema, K. Kuehn, N. Kuropatkin, T. S. Li, M. Lima, M. A. G. Maia, J. L. Marshall, F. Menanteau, R. Miquel, E. Neilsen, R. L. C. Ogando, A. A. Plazas, A. K. Romer, A. Roodman, E. Sanchez, V. Scarpine, R. Schindler, M. Schubnell, S. Serrano, M. Smith, R. C. Smith, F. Sobreira, E. Suchyta, M. E. C. Swanson, G. Tarle, R. C. Thomas, A. R. Walker, W. Wester, J. Zuntz, DES Collaboration, B. P. Abbott, R. Abbott, T. D. Abbott, S. Abraham, F. Acernese, K. Ackley, C. Adams, R. X. Adhikari, V. B. Adya, C. Affeldt, M. Agathos, K. Agatsuma, N. Aggarwal, O. D. Aguiar, L. Aiello, A. Ain, P. Ajith, G. Allen, A. Allocca, M. A. Aloy, P. A. Altin, A. Amato, A. Ananyeva, S. B. Anderson, W. G. Anderson, S. V. Angelova, S. Appert, K. Arai, M. C. Araya, J. S. Areeda, M. Arène, S. Ascenzi, G. Ashton, S. M. Aston, P. Astone, F. Aubin, P. Aufmuth, K. AultO'Neal, C. Austin, V. Avendano, A. Avila-Alvarez, S. Babak, P. Bacon, F. Badaracco, M. K. M. Bader, S. Bae, P. T. Baker, F. Baldaccini, G. Ballardín, S. W. Ballmer, S. Banagiri, J. C. Barayoga, S. E. Barclay, B. C. Barish, D. Barker, K. Barkett, S. Barnum, F. Barone, B. Barr, L. Barsotti, M. Barsuglia, D. Barta, J. Bartlett, I. Bartos, R. Bassiri, A. Basti, M. Bawaj, J. C. Bayley, M. Bazzan, B. Bécsy, M. Bejger, A. S. Bell, D. Beniwal, G. Bergmann, S. Bernuzzi, J. J. Bero, C. P. L. Berry, D. Bersanetti, A. Bertolini, J. Betzwieser, R. Bhandare, J. Bidler, I. A. Bilenko, S. A. Bilgili, G. Billingsley, J. Birch, R. Birney, O. Birnholtz, S. Biscans, S. Biscoveanu, A. Bisht, M. Bitossi, J. K. Blackburn, C. D. Blair, D. G. Blair, R. M. Blair, S. Bloemen, N. Bode, M. Boer, Y. Boetzel, G. Bogaert, F. Bondu, E. Bonilla, R. Bonnard, and P. Booker, First Measurement of the Hubble Constant from a Dark Standard Siren using the Dark Energy Survey Galaxies and the LIGO/Virgo Binary-Black-hole Merger GW170814, *ApJL* **876**, L7 (2019), arXiv:1901.01540 [astro-ph.CO].
- [32] R. Abbott, H. Abe, F. Acernese, K. Ackley, N. Adhikari, R. X. Adhikari, V. K. Adkins, V. B. Adya, C. Affeldt, D. Agarwal, M. Agathos, K. Agatsuma, N. Aggarwal, O. D. Aguiar, L. Aiello, A. Ain, P. Ajith, T. Akutsu, S. Albanesi, R. A. Alfaidi, A. Allocca, P. A. Altin, A. Amato, C. Anand, S. Anand, A. Ananyeva, S. B. Anderson, W. G. Anderson, M. Ando, T. Andrade, N. Andres, M. Andrés-Carcasona, T. Andrić, S. V. Angelova, S. Ansoldi, J. M. Antelis, S. Antier, T. Apostolatos, E. Z. Appavuravther, S. Appert, S. K. Apple, K. Arai, A. Araya, M. C. Araya, J. S. Areeda, M. Arène, N. Aritomi, N. Arnaud, M. Arogeti, S. M. Aronson, K. G. Arun, H. Asada, Y. Asali, G. Ashton, Y. Aso, M. Assiduo, S. A. de Souza Melo, S. M. Aston, P. Astone, F. Aubin, K. Aultoneal, C. Austin, S. Babak, F. Badaracco, M. K. M. Bader, C. Badger, S. Bae, Y. Bae, A. M. Baer, S. Bagnasco, Y. Bai, J. Baird, R. Bajpai, T. Baka, M. Ball, G. Ballardín, S. W. Ballmer, A. Balsamo, G. Baltus, S. Banagiri, B. Banerjee, D. Bankar, J. C. Barayoga, C. Barbieri, R. Barbieri, B. C. Barish, D. Barker, P. Barneo, F. Barone, B. Barr, L. Barsotti, M. Barsuglia, D. Barta, J. Bartlett, M. A. Barton, I. Bartos, S. Basak, R. Bassiri, A. Basti, M. Bawaj, J. C. Bayley, M. Bazzan, B. R. Becher, B. Bécsy, V. M. Bedakihalé, F. Beirnaert, M. Bejger, I. Belahcene, V. Benedetto, D. Beni-

- wal, M. G. Benjamin, T. F. Bennett, J. D. Bentley, M. Benyaala, S. Bera, M. Berbel, F. Bergamin, B. K. Berger, S. Bernuzzi, C. P. L. Berry, D. Bersanetti, A. Bertolini, J. Betzwieser, D. Beveridge, R. Bhandare, A. V. Bhandari, U. Bhardwaj, R. Bhatt, D. Bhattacharjee, S. Bhaumik, A. Bianchi, I. A. Bilenko, G. Billingsley, M. Bilicki, S. Bini, I. A. Birney, O. Birnholtz, S. Biscans, M. Bisch, S. Biscoveanu, A. Bisht, B. Biswas, M. Bitossi, M.-A. Bizouard, J. K. Blackburn, C. D. Blair, D. G. Blair, R. M. Blair, F. Bobba, N. Bode, M. Boër, G. Bogaert, M. Boldrini, G. N. Bolingbroke, L. D. Bonavena, F. Bondu, E. Bonilla, R. Bonnand, P. Booker, B. A. Boom, R. Bork, V. Boschi, N. Bose, S. Bose, V. Bossilkov, V. Boudart, Y. Bouffanais, A. Bozzi, C. Bradaschia, P. R. Brady, A. Bramley, A. Branch, M. Branchesi, J. E. Brau, M. Breschi, T. Briant, J. H. Briggs, A. Brillet, M. Brinkmann, P. Brockill, A. F. Brooks, J. Brooks, D. D. Brown, S. Brunett, G. Bruno, R. Bruntz, J. Bryant, F. Bucci, T. Bulik, H. J. Bulten, A. Buonanno, K. Burtnyk, R. Buscicchio, D. Buskulic, C. Buy, R. L. Byer, G. S. C. Davies, G. Cabras, R. Cabrita, and L. Cadonati, Constraints on the Cosmic Expansion History from GWTC-3, *ApJ* **949**, 76 (2023), arXiv:2111.03604 [astro-ph.CO].
- [33] The LIGO Scientific Collaboration, the Virgo Collaboration, the KAGRA Collaboration, A. G. Abac, I. Abouelfettouh, F. Acernese, K. Ackley, C. Adamcewicz, S. Adhicary, D. Adhikari, N. Adhikari, R. X. Adhikari, V. K. Adkins, S. Afroz, A. Agapito, D. Agarwal, M. Agathos, N. Aggarwal, S. Aggarwal, O. D. Aguiar, I. L. Ahrend, L. Aiello, A. Ain, P. Ajith, T. Akutsu, S. Albanesi, W. Ali, S. Al-Kershi, C. Alléné, A. Allocca, S. Al-Shammari, P. A. Altin, S. Alvarez-Lopez, W. Amar, O. Amarasinghe, A. Amato, F. Amicucci, C. Amra, A. Ananyeva, S. B. Anderson, W. G. Anderson, M. Andia, M. Ando, M. Andrés-Carcasona, T. Andrić, J. Anglin, S. Ansoldi, J. M. Antelis, S. Antier, M. Aoumi, E. Z. Appavuravther, S. Appert, S. K. Apple, K. Arai, A. Araya, M. C. Araya, M. Arca Sedda, J. S. Areeda, N. Aritomi, F. Armato, S. Armstrong, N. Arnaud, M. Arogeti, S. M. Aronson, K. G. Arun, G. Ashton, Y. Aso, L. Asprea, M. Assiduo, S. Assis de Souza Melo, S. M. Aston, P. Astone, F. Attadio, F. Aubin, K. AultONeal, G. Avallone, E. A. Avila, S. Babak, C. Badger, S. Bae, S. Bagnasco, L. Baiotti, R. Bajpai, T. Baka, A. M. Baker, K. A. Baker, T. Baker, G. Baldi, N. Baldicchi, M. Ball, G. Ballardini, S. W. Ballmer, S. Banagiri, B. Banerjee, D. Bankar, T. M. Baptiste, P. Baral, M. Baratti, J. C. Barayoga, B. C. Barish, D. Barker, N. Barman, P. Barneo, F. Barone, B. Barr, L. Barsotti, M. Barsuglia, D. Barta, A. M. Bartoletti, M. A. Barton, I. Bartos, A. Basalae, R. Bassiri, A. Basti, M. Bawaj, P. Baxi, J. C. Bayley, A. C. Baylor, P. A. Baynard, II, M. Bazzan, V. M. Bedakihalé, F. Beirnaert, M. Bejger, D. Belardinelli, A. S. Bell, D. S. Bellie, L. Bellizzi, W. Benoit, I. Bentara, J. D. Bentley, M. Ben Yaala, S. Bera, F. Bergamin, B. K. Berger, S. Bernuzzi, M. Beroiz, C. P. L. Berry, D. Bersanetti, T. Bertheas, A. Bertolini, J. Betzwieser, D. Beveridge, G. Bevilacqua, N. Bevins, R. Bhandare, R. Bhatt, D. Bhattacharjee, S. Bhattacharyya, S. Bhaumik, V. Biancalana, A. Bianchi, I. A. Bilenko, M. Bilicki, G. Billingsley, A. Binetti, S. Bini, C. Binu, S. Biot, O. Birnholtz, S. Biscoveanu, A. Bisht, M. Bitossi, M. A. Bizouard, S. Blaber, J. K. Blackburn, L. A. Blagg, C. D. Blair, D. G. Blair, N. Bode, N. Boettner, G. Boileau, M. Boldrini, G. N. Bolingbroke, A. Bolliand, L. D. Bonavena, R. Bondarescu, F. Bondu, E. Bonilla, M. S. Bonilla, A. Bonino, R. Bonnand, A. Borchers, S. Borhanian, V. Boschi, S. Bose, V. Bossilkov, Y. Bothra, A. Boudon, L. Bourg, M. Boyle, A. Bozzi, C. Bradaschia, P. R. Brady, A. Branch, M. Branchesi, I. Braun, T. Briant, A. Brillet, M. Brinkmann, and P. Brockill, GWTC-4.0: Constraints on the Cosmic Expansion Rate and Modified Gravitational-wave Propagation, arXiv , arXiv:2509.04348 (2025), arXiv:2509.04348 [astro-ph.CO].
- [34] N. Borghi, M. Mancarella, M. Moresco, M. Tagliacucchi, F. Iacovelli, A. Cimatti, and M. Maggiore, Cosmology and Astrophysics with Standard Sirens and Galaxy Catalogs in View of Future Gravitational Wave Observations, *ApJ* **964**, 191 (2024), arXiv:2312.05302 [astro-ph.CO].
- [35] I. Mandel, W. M. Farr, and J. R. Gair, Extracting distribution parameters from multiple uncertain observations with selection biases, *MNRAS* **486**, 1086 (2019), arXiv:1809.02063 [physics.data-an].
- [36] S. Vitale, D. Gerosa, W. M. Farr, and S. R. Taylor, Inferring the Properties of a Population of Compact Binaries in Presence of Selection Effects, in *Handbook of Gravitational Wave Astronomy*, edited by C. Bambi, S. Katsanevas, and K. D. Kokkotas (2022) p. 45.
- [37] E. Thrane and C. Talbot, An introduction to Bayesian inference in gravitational-wave astronomy: Parameter estimation, model selection, and hierarchical models, *PASA* **36**, e010 (2019), arXiv:1809.02293 [astro-ph.IM].
- [38] M. L. Cross-Parkin, C. Howlett, T. M. Davis, and N. Khetan, Dark sirens and the impact of redshift precision, *PASA* **42**, e149 (2025), arXiv:2502.17747 [astro-ph.CO].
- [39] A. G. Hanselman, A. Vijaykumar, M. Fishbach, and D. E. Holz, Gravitational-wave Dark Siren Cosmology Systematics from Galaxy Weighting, *ApJ* **979**, 9 (2025), arXiv:2405.14818 [astro-ph.CO].
- [40] M. Oguri, Measuring the distance-redshift relation with the cross-correlation of gravitational wave standard sirens and galaxies, *PhRvD* **93**, 083511 (2016), arXiv:1603.02356 [astro-ph.CO].
- [41] A. Pedrotti, M. Mancarella, J. Bel, and D. Gerosa, Cosmology with the angular cross-correlation of gravitational-wave and galaxy catalogs: forecasts for next-generation interferometers and the Euclid survey, arXiv , arXiv:2504.10482 (2025), arXiv:2504.10482 [astro-ph.CO].
- [42] M. Beltrame, M. Bonici, and C. Carbone, Cosmological forecasts from the combination of Stage-IV photometric galaxy surveys and the magnification from forthcoming GW observatories, *JCAP* **2024** (10), 074, arXiv:2403.03859 [astro-ph.CO].
- [43] S. Mukherjee, B. D. Wandelt, S. M. Nissanke, and A. Silvestri, Accurate precision cosmology with redshift unknown gravitational wave sources, *PhRvD* **103**, 043520 (2021), arXiv:2007.02943 [astro-ph.CO].
- [44] C. Cigarrán Díaz and S. Mukherjee, Mapping the cosmic expansion history from LIGO-Virgo-KAGRA in synergy with DESI and SPHEREx, *MNRAS* **511**, 2782 (2022), arXiv:2107.12787 [astro-ph.CO].

- [45] S. Mukherjee, A. Krolewski, B. D. Wandelt, and J. Silk, Cross-correlating Dark Sirens and Galaxies: Constraints on H_0 from GWTC-3 of LIGO–Virgo–KAGRA, *ApJ* **975**, 189 (2024), arXiv:2203.03643 [astro-ph.CO].
- [46] T. Ghosh, S. More, S. Bera, and S. Bose, Bayesian Inference of the Hubble constant from Cross-Correlation of Individual Gravitational Wave Events with Galaxies, in *32nd General Assembly International Union (IAUGA 2024)* (2024) p. 1303, arXiv:2312.16305 [astro-ph.CO].
- [47] T. Namikawa, A. Nishizawa, and A. Taruya, Detecting black-hole binary clustering via the second-generation gravitational-wave detectors, *PhRvD* **94**, 024013 (2016), arXiv:1603.08072 [astro-ph.CO].
- [48] P. Zhang, The large scale structure in the 3D luminosity-distance space and its cosmological applications, arXiv , arXiv:1810.11915 (2018), arXiv:1810.11915 [astro-ph.CO].
- [49] A. Vijaykumar, M. V. S. Sathesh, S. Kumar, P. Ajith, and T. R. Choudhury, Probing the large scale structure using gravitational-wave observations of binary black holes, *PhRvD* **108**, 103017 (2023), arXiv:2005.01111 [astro-ph.CO].
- [50] S. Libanore, M. C. Artale, D. Karagiannis, M. Liguori, N. Bartolo, Y. Bouffanais, N. Giacobbo, M. Mapelli, and S. Matarrese, Gravitational Wave mergers as tracers of Large Scale Structures, *JCAP* **2021** (2), 035, arXiv:2007.06905 [astro-ph.CO].
- [51] S. Kumar, Probing Cosmology with Baryon Acoustic Oscillations Using Gravitational Waves, *ApJ* **959**, 35 (2023), arXiv:2203.04273 [astro-ph.CO].
- [52] A. Dehghani, J. L. Kim, D. S. Hosseini, A. Krolewski, S. Mukherjee, and G. Geshnizjani, The gravitational wave bias parameter from angular power spectra: bridging between galaxies and binary black holes, *JCAP* **2025** (4), 056, arXiv:2411.11965 [astro-ph.GA].
- [53] E. L. Gagnon, D. Anbajagane, J. Prat, C. Chang, and J. Frieman, Cosmological Constraints from Combining Photometric Galaxy Surveys and Gravitational Wave Observatories, *OJAp* **7**, 110 (2024), arXiv:2312.16289 [astro-ph.CO].
- [54] S. Zazzera, J. Fonseca, T. Baker, and C. Clarkson, Gravitational waves and galaxies cross-correlations: a forecast on GW biases for future detectors, *MNRAS* **537**, 1912 (2025), arXiv:2412.01678 [astro-ph.CO].
- [55] J. Ferri, I. L. Tashiro, L. R. Abramo, I. Matos, M. Quartin, and R. Sturani, A robust cosmic standard ruler from the cross-correlations of galaxies and dark sirens, *JCAP* **2025** (4), 008, arXiv:2412.00202 [astro-ph.CO].
- [56] K. Leyde, T. Baker, and W. Enzi, Cosmic cartography: Bayesian reconstruction of the galaxy density informed by large-scale structure, *JCAP* **2024** (12), 013, arXiv:2409.20531 [astro-ph.CO].
- [57] K. Leyde, T. Baker, and W. Enzi, Cosmic cartography. Part II. Completing galaxy catalogs for gravitational-wave cosmology, *JCAP* **2026** (1), 013, arXiv:2507.12171 [astro-ph.CO].
- [58] C. Dalang and T. Baker, The clustering of dark sirens’ invisible host galaxies, *JCAP* **2024** (2), 024, arXiv:2310.08991 [astro-ph.CO].
- [59] C. Dalang, B. Fiorini, and T. Baker, Large scale structure prior knowledge in the dark siren method, *JCAP* **2026** (1), 034, arXiv:2410.03275 [astro-ph.CO].
- [60] A. Begnoni, L. V. Dall’Armi, D. Bertacca, and A. Raccanelli, Gravitational wave luminosity distance-weighted anisotropies, *JCAP* **2024** (10), 087, arXiv:2404.12351 [astro-ph.CO].
- [61] J. Fonseca, S. Zazzera, T. Baker, and C. Clarkson, The observed number counts in luminosity distance space, *JCAP* **2023** (8), 050, arXiv:2304.14253 [astro-ph.CO].
- [62] S. Zazzera, J. Fonseca, T. Baker, and C. Clarkson, Magnification and evolution bias of transient sources: GWs and SNIa, *JCAP* **2024** (5), 095, arXiv:2309.04391 [astro-ph.CO].
- [63] T. Namikawa, Analyzing clustering of astrophysical gravitational-wave sources: luminosity-distance space distortions, *JCAP* **2021** (1), 036, arXiv:2007.04359 [astro-ph.CO].
- [64] A. S. Szalay, T. Matsubara, and S. D. Landy, Redshift-Space Distortions of the Correlation Function in Wide-Angle Galaxy Surveys, *ApJL* **498**, L1 (1998), arXiv:astro-ph/9712007 [astro-ph].
- [65] C. Bonvin and R. Durrer, What galaxy surveys really measure, *PhRvD* **84**, 063505 (2011), arXiv:1105.5280 [astro-ph.CO].
- [66] S. Mastroianni, C. Karathanasis, J. Gair, G. Ashton, S. Rinaldi, H.-Y. Huang, and G. D’Álya, Cosmology with Gravitational Waves: A Review, *AnP* **536**, 2200180 (2024).
- [67] A. Palmese and S. Mastroianni, Gravitational Wave Cosmology, arXiv , arXiv:2502.00239 (2025), arXiv:2502.00239 [astro-ph.CO].
- [68] R. Essick and M. Fishbach, Ensuring Consistency between Noise and Detection in Hierarchical Bayesian Inference, *ApJ* **962**, 169 (2024), arXiv:2310.02017 [gr-qc].
- [69] P. J. E. Peebles, *The Large-Scale Structure of the Universe* (1981).
- [70] S. Dodelson and F. Schmidt, *Modern Cosmology* (2020).
- [71] N. Padmanabhan, D. J. Schlegel, U. Seljak, A. Makarov, N. A. Bahcall, M. R. Blanton, J. Brinkmann, D. J. Eisenstein, D. P. Finkbeiner, J. E. Gunn, D. W. Hogg, Ž. Ivezić, G. R. Knapp, J. Loveday, R. H. Lupton, R. C. Nichol, D. P. Schneider, M. A. Strauss, M. Tegmark, and D. G. York, The clustering of luminous red galaxies in the Sloan Digital Sky Survey imaging data, *MNRAS* **378**, 852 (2007), arXiv:astro-ph/0605302 [astro-ph].
- [72] A. Cooray and R. Sheth, Halo models of large scale structure, *PhR* **372**, 1 (2002), arXiv:astro-ph/0206508 [astro-ph].
- [73] R. E. Smith, J. A. Peacock, A. Jenkins, S. D. M. White, C. S. Frenk, F. R. Pearce, P. A. Thomas, G. Efstathiou, and H. M. P. Couchman, Stable clustering, the halo model and non-linear cosmological power spectra, *MNRAS* **341**, 1311 (2003), arXiv:astro-ph/0207664 [astro-ph].
- [74] R. Takahashi, M. Sato, T. Nishimichi, A. Taruya, and M. Oguri, Revising the Halofit Model for the Non-linear Matter Power Spectrum, *ApJ* **761**, 152 (2012), arXiv:1208.2701 [astro-ph.CO].
- [75] P. J. E. Peebles, Statistical Analysis of Catalogs of Extragalactic Objects. I. Theory, *ApJ* **185**, 413 (1973).
- [76] K. B. Fisher, C. A. Scharf, and O. Lahav, A spherical harmonic approach to redshift distortion and a measurement of $\Omega(0)$ from the 1.2-Jy IRAS Redshift Survey, *MNRAS* **266**, 219 (1994), arXiv:astro-ph/9309027 [astro-ph].
- [77] A. F. Heavens and A. N. Taylor, A spherical harmonic analysis of redshift space, *MNRAS* **275**, 483 (1995), arXiv:astro-ph/9409027 [astro-ph].

- [78] S. Dodelson, V. K. Narayanan, M. Tegmark, R. Scranton, T. Budavári, A. Connolly, I. Csabai, D. Eisenstein, J. A. Frieman, J. E. Gunn, L. Hui, B. Jain, D. Johnston, S. Kent, J. Loveday, R. C. Nichol, L. O’Connell, R. Scoccamarro, R. K. Sheth, A. Stebbins, M. A. Strauss, A. S. Szalay, I. Szapudi, M. S. Vogeley, I. Zehavi, J. Annis, N. A. Bahcall, J. Brinkman, M. Doi, M. Fukugita, G. Hennessy, Ž. Ivezić, G. R. Knapp, P. Kunszt, D. Q. Lamb, B. C. Lee, R. H. Lupton, J. A. Munn, J. Peoples, J. R. Pier, C. Rockosi, D. Schlegel, C. Stoughton, D. L. Tucker, B. Yanny, and D. G. York, The Three-dimensional Power Spectrum from Angular Clustering of Galaxies in Early Sloan Digital Sky Survey Data, *ApJ* **572**, 140 (2002), arXiv:astro-ph/0107421 [astro-ph].
- [79] J. Asorey, M. Crocce, E. Gaztañaga, and A. Lewis, Recovering 3D clustering information with angular correlations, *MNRAS* **427**, 1891 (2012), arXiv:1207.6487 [astro-ph.CO].
- [80] D. N. Limber, The Analysis of Counts of the Extragalactic Nebulae in Terms of a Fluctuating Density Field., *ApJ* **117**, 134 (1953).
- [81] M. LoVerde and N. Afshordi, Extended Limber approximation, *PhRvD* **78**, 123506 (2008), arXiv:0809.5112 [astro-ph].
- [82] P. Simon, How accurate is Limber’s equation?, *A&A* **473**, 711 (2007), arXiv:astro-ph/0609165 [astro-ph].
- [83] M. Tegmark, How to measure CMB power spectra without losing information, *PhRvD* **55**, 5895 (1997), arXiv:astro-ph/9611174 [astro-ph].
- [84] L. R. Abramo, J. V. Dinarte Ferri, I. L. Tashiro, and A. Loureiro, Fisher matrix for the angular power spectrum of multi-tracer galaxy surveys, *JCAP* **2022** (8), 073, arXiv:2204.05057 [astro-ph.CO].
- [85] L. R. Abramo, J. V. D. Ferri, and I. L. Tashiro, Fisher matrix for multiple tracers: the information in the cross-spectra, *JCAP* **2022** (4), 013, arXiv:2112.01812 [astro-ph.CO].
- [86] M. Tegmark, A. N. Taylor, and A. F. Heavens, Karhunen-Loève Eigenvalue Problems in Cosmology: How Should We Tackle Large Data Sets?, *ApJ* **480**, 22 (1997), arXiv:astro-ph/9603021 [astro-ph].
- [87] DESI Collaboration, A. Aghamousa, J. Aguilar, S. Ahlen, S. Alam, L. E. Allen, C. Allende Prieto, J. Annis, S. Bailey, C. Balland, O. Ballester, C. Baltay, L. Beaufore, C. Bebek, T. C. Beers, E. F. Bell, J. L. Bernal, R. Besuner, F. Beutler, C. Blake, H. Bleuler, M. Blomqvist, R. Blum, A. S. Bolton, C. Briceno, D. Brooks, J. R. Brownstein, E. Buckley-Geer, A. Burden, E. Burtin, N. G. Busca, R. N. Cahn, Y.-C. Cai, L. Cardiel-Sas, R. G. Carlberg, P.-H. Carton, R. Casas, F. J. Castander, J. L. Cervantes-Cota, T. M. Claybaugh, M. Close, C. T. Coker, S. Cole, J. Comparat, A. P. Cooper, M. C. Cousinou, M. Crocce, J.-G. Cuby, D. P. Cunningham, T. M. Davis, K. S. Dawson, A. de la Macorra, J. De Vicente, T. Delubac, M. Derwent, A. Dey, G. Dhungana, Z. Ding, P. Doel, Y. T. Duan, A. Ealet, J. Edelman, S. Eftekharzadeh, D. J. Eisenstein, A. Elliott, S. Escoffier, M. Evatt, P. Fagreluis, X. Fan, K. Fanning, A. Farahi, J. Farihi, G. Favole, Y. Feng, E. Fernandez, J. R. Findlay, D. P. Finkbeiner, M. J. Fitzpatrick, B. Flaugher, S. Flenner, A. Font-Ribera, J. E. Forero-Romero, P. Fosalba, C. S. Frenk, M. Fumagalli, B. T. Gaensicke, G. Gallo, J. Garcia-Bellido, E. Gaztanaga, N. Pietro Gentile Fusillo, T. Gerard, I. Gershkovich, T. Giannantonio, D. Gillet, G. Gonzalez-de-Rivera, V. Gonzalez-Perez, S. Gott, O. Graur, G. Gutierrez, J. Guy, S. Habib, H. Heetderks, I. Heetderks, K. Heitmann, W. A. Hellwing, D. A. Herrera, S. Ho, S. Holland, K. Honscheid, E. Huff, T. A. Hutchinson, D. Huterer, H. S. Hwang, J. M. Illa Laguna, Y. Ishikawa, D. Jacobs, N. Jeffrey, P. Jelinsky, E. Jennings, L. Jiang, J. Jimenez, J. Johnson, R. Joyce, E. Jullo, S. Juneau, S. Kama, A. Karcher, S. Karkar, R. Kehoe, N. Kennamer, S. Kent, M. Kilbinger, A. G. Kim, D. Kirkby, T. Kisner, E. Kitaniidis, J.-P. Kneib, S. Kogosov, E. Kovacs, K. Koyama, A. Kremin, R. Kron, L. Kronig, A. Kueter-Young, C. G. Lacey, R. Lafever, O. Lahav, A. Lambert, M. Lampton, M. Landriau, D. Lang, T. R. Lauer, J.-M. Le Goff, L. Le Guillou, A. Le Van Suu, J. H. Lee, S.-J. Lee, D. Leitner, M. Lesser, M. E. Levi, B. L’Huillier, B. Li, M. Liang, H. Lin, E. Linder, S. R. Loebman, Z. Lukic, J. Ma, N. MacCrann, C. Magneville, L. Makarem, M. Manera, C. J. Manser, R. Marshall, P. Martini, R. Massey, T. Matheson, J. McCauley, P. McDonald, I. D. McGreer, A. Meisner, N. Metcalfe, T. N. Miller, R. Miquel, J. Moustakas, A. Myers, M. Naik, J. A. Newman, R. C. Nichol, A. Nicola, L. Nicolati da Costa, J. Nie, G. Niz, P. Norberg, B. Nord, D. Norman, P. Nugent, T. O’Brien, M. Oh, and K. A. G. Olsen, The DESI Experiment Part I: Science, Targeting, and Survey Design, arXiv , arXiv:1611.00036 (2016), arXiv:1611.00036 [astro-ph.IM].
- [88] A. G. Adame, J. Aguilar, S. Ahlen, S. Alam, D. M. Alexander, M. Alvarez, O. Alves, A. Anand, U. Andrade, E. Armengaud, S. Avila, A. Aviles, H. Awan, S. Bailey, C. Baltay, A. Bault, J. Behera, S. Ben-Zvi, F. Beutler, D. Bianchi, C. Blake, R. Blum, S. Brieden, A. Brodzeller, D. Brooks, E. Buckley-Geer, E. Burtin, R. Calderon, R. Canning, A. Carnero Rosell, R. Cereskaite, J. L. Cervantes-Cota, S. Chabanier, E. Chaussidon, J. Chaves-Montero, S. Chen, X. Chen, T. Claybaugh, S. Cole, A. Cuceu, T. M. Davis, K. Dawson, A. de la Macorra, A. de Mattia, N. Deiosso, A. Dey, B. Dey, Z. Ding, P. Doel, J. Edelman, S. Eftekharzadeh, D. J. Eisenstein, A. Elliott, P. Fagreluis, K. Fanning, S. Ferraro, J. Ereza, N. Findlay, B. Flaugher, A. Font-Ribera, D. Forero-Sánchez, J. E. Forero-Romero, C. Garcia-Quintero, L. H. Garrison, E. Gaztañaga, H. Gil-Marín, S. G. A. Gontcho, A. X. Gonzalez-Morales, V. Gonzalez-Perez, C. Gordon, D. Green, D. Gruen, R. Gsponer, G. Gutierrez, J. Guy, B. Hadzhiyska, C. Hahn, M. M. S. Hanif, H. K. Herrera-Alcantar, K. Honscheid, C. Howlett, D. Huterer, V. Iršič, M. Ishak, S. Juneau, N. G. Karaçaylı, R. Kehoe, S. Kent, D. Kirkby, H. Kong, S. E. Kogosov, A. Kremin, A. Krolewski, Y. Lai, T.-W. Lan, M. Landriau, D. Lang, J. Lasker, J. M. Le Goff, L. Le Guillou, A. Leauthaud, M. E. Levi, T. S. Li, K. Lodha, C. Magneville, M. Manera, D. Margala, P. Martini, M. Maus, P. McDonald, L. Medina-Varela, A. Meisner, J. Mena-Fernández, R. Miquel, J. Moon, S. Moore, J. Moustakas, E. Mueller, A. Muñoz-Gutiérrez, A. D. Myers, S. Nadathur, L. Napolitano, R. Neveux, J. A. Newman, N. M. Nguyen, J. Nie, G. Niz, H. E. Noriega, N. Padmanabhan, E. Paillas, N. Palanque-DeLabrouille, J. Pan, S. Penmetsa, W. J. Percival, M. M. Pieri, M. Pinon, C. Poppett, A. Porredon, F. Prada,

- A. Pérez-Fernández, I. Pérez-Ràfols, D. Rabinowitz, A. Raichoor, C. Ramírez-Pérez, S. Ramirez-Solano, M. Rashkovetskyi, C. Ravoux, M. Rezaie, J. Rich, A. Rocher, C. Rockosi, F. Rodríguez-Martínez, N. A. Roe, A. Rosado-Marin, A. J. Ross, G. Rossi, R. Ruggeri, V. Ruhlmann-Kleider, L. Samushia, E. Sanchez, C. Saulder, E. F. Schlafly, D. Schlegel, M. Schubnell, H. Seo, R. Sharples, J. Silber, A. Slosar, A. Smith, D. Sprayberry, T. Tan, G. Tarlé, S. Trusov, R. Vaisakh, D. Valcin, F. Valdes, M. Vargas-Magaña, L. Verde, M. Walther, B. Wang, M. S. Wang, B. A. Weaver, N. Weaverdyck, R. H. Wechsler, D. H. Weinberg, M. White, M. J. Wilson, J. Yu, Y. Yu, S. Yuan, C. Yèche, E. A. Zaborowski, P. Zarrouk, H. Zhang, C. Zhao, R. Zhao, R. Zhou, H. Zou, and The DESI collaboration, DESI 2024 V: Full-Shape galaxy clustering from galaxies and quasars, *JCAP* **2025** (9), 008, arXiv:2411.12021 [astro-ph.CO].
- [89] A. G. Adame, J. Aguilar, S. Ahlen, S. Alam, D. M. Alexander, M. Alvarez, O. Alves, A. Anand, U. Andrade, E. Armengaud, S. Avila, A. Aviles, H. Awan, S. Bailey, C. Baltay, A. Bault, J. Behera, S. Benzvi, F. Beutler, D. Bianchi, C. Blake, R. Blum, S. Brieden, A. Brodzeller, D. Brooks, E. Buckley-Geer, E. Burtin, R. Calderon, R. Canning, A. Carnero Rosell, R. Cereskaite, J. L. Cervantes-Cota, S. Chabanier, E. Chaussidon, J. Chaves-Montero, S. Chen, X. Chen, T. Claybaugh, S. Cole, A. Cuceu, T. M. Davis, K. Dawson, A. de la Macorra, A. de Mattia, N. Deiosso, A. Dey, B. Dey, Z. Ding, P. Doel, J. Edelstein, S. Eftekharzadeh, D. J. Eisenstein, A. Elliott, P. Fagrelus, K. Fanning, S. Ferraro, J. Ereza, N. Findlay, B. Flaugher, A. Font-Ribera, D. Forero-Sánchez, J. E. Forero-Romero, C. Garcia-Quintero, E. Gaztañaga, H. Gil-Marín, S. Gontcho a Gontcho, A. X. Gonzalez-Morales, V. Gonzalez-Perez, C. Gordon, D. Green, D. Gruen, R. Gsponer, G. Gutierrez, J. Guy, B. Hadzhiyska, C. Hahn, M. M. S. Hanif, H. K. Herrera-Alcantar, K. Honscheid, C. Howlett, D. Huterer, V. Iršič, M. Ishak, S. Juneau, N. G. Karaçaylı, R. Kehoe, S. Kent, D. Kirkby, H. Kong, A. Kremin, A. Krolewski, Y. Lai, T.-W. Lan, M. Landriau, D. Lang, J. Lasker, J. M. Le Goff, L. Le Guillou, A. Leauthaud, M. E. Levi, T. S. Li, E. Linder, K. Lodha, C. Magneville, M. Manera, D. Margala, P. Martini, M. Maus, P. McDonald, L. Medina-Varela, A. Meisner, J. Mena-Fernández, R. Miquel, J. Moon, S. Moore, J. Moustakas, E. Mueller, A. Muñoz-Gutiérrez, A. D. Myers, S. Nadathur, L. Napolitano, R. Neveux, J. A. Newman, N. M. Nguyen, J. Nie, G. Niz, H. E. Noriega, N. Padmanabhan, E. Paillas, N. Palanque-Delabrouille, J. Pan, S. Penmetsa, W. J. Percival, M. M. Pieri, M. Pinon, C. Poppett, A. Porredon, F. Prada, A. Pérez-Fernández, I. Pérez-Ràfols, D. Rabinowitz, A. Raichoor, C. Ramírez-Pérez, S. Ramirez-Solano, M. Rashkovetskyi, C. Ravoux, M. Rezaie, J. Rich, A. Rocher, C. Rockosi, N. A. Roe, A. Rosado-Marin, A. J. Ross, G. Rossi, R. Ruggeri, V. Ruhlmann-Kleider, L. Samushia, E. Sanchez, C. Saulder, E. F. Schlafly, D. Schlegel, M. Schubnell, H. Seo, R. Sharples, J. Silber, A. Slosar, A. Smith, D. Sprayberry, J. Swanson, T. Tan, G. Tarlé, S. Trusov, R. Vaisakh, D. Valcin, F. Valdes, M. Vargas-Magaña, L. Verde, M. Walther, B. Wang, M. S. Wang, B. A. Weaver, N. Weaverdyck, R. H. Wechsler, D. H. Weinberg, M. White, M. J. Wilson, J. Yu, Y. Yu, S. Yuan, C. Yèche, E. A. Zaborowski, P. Zarrouk, H. Zhang, C. Zhao, R. Zhao, R. Zhou, H. Zou, and DESI Collaboration, DESI 2024 III: baryon acoustic oscillations from galaxies and quasars, *JCAP* **2025** (4), 012, arXiv:2404.03000 [astro-ph.CO].
- [90] Euclid Collaboration, R. Scaramella, J. Amiaux, Y. Mellier, C. Burigana, C. S. Carvalho, J.-C. Cuilandre, A. Da Silva, A. Derosa, J. Dinis, E. Maiorano, M. Maris, I. Tereno, R. Laureijs, T. Boenke, G. Buenadicha, X. Dupac, L. M. Gaspar Venancio, P. Gómez-Álvarez, J. Hoar, J. Lorenzo Alvarez, G. D. Racca, G. Saavedra-Criado, J. Schwartz, R. Vavrek, M. Schirmer, H. Aussel, R. Azzollini, V. F. Cardone, M. Cropper, A. Ealet, B. Garilli, W. Gillard, B. R. Granett, L. Guzzo, H. Hoekstra, K. Jahnke, T. Kitching, T. Maciaszek, M. Meneghetti, L. Miller, R. Nakajima, S. M. Niemi, F. Pasian, W. J. Percival, S. Pottinger, M. Sauvage, M. Scodreggio, S. Wachter, A. Zaccchi, N. Aghanim, A. Amara, T. Auphan, N. Auricchio, S. Awan, A. Balestra, R. Bender, C. Bodendorf, D. Bonino, E. Branchini, S. Brau-Nogue, M. Brescia, G. P. Candini, V. Capobianco, C. Carbone, R. G. Carlberg, J. Carretero, R. Casas, F. J. Castander, M. Castellano, S. Cavuoti, A. Cimatti, R. Cledassou, G. Congedo, C. J. Conselice, L. Conversi, Y. Copin, L. Corcione, A. Costille, F. Courbin, H. Degaudenzi, M. Douspis, F. Dubath, C. A. J. Duncan, S. Dusini, S. Farrens, S. Ferriol, P. Fosalba, N. Fourmanoit, M. Frailis, E. Franceschi, P. Franzetti, M. Fumana, B. Gillis, C. Giocoli, A. Grazian, F. Grupp, S. V. H. Haugan, W. Holmes, F. Hormuth, P. Hudelot, S. Kermiche, A. Kiessling, M. Kilbinger, R. Kohley, B. Kubik, M. Kümmel, M. Kunz, H. Kurki-Suonio, O. Lahav, S. Ligeri, P. B. Lilje, I. Lloro, O. Mansutti, O. Marggraf, K. Markovic, F. Marulli, R. Massey, S. Maurogordato, M. Melchior, E. Merlin, G. Meylan, J. J. Mohr, M. Moresco, B. Morin, L. Moscardini, E. Munari, R. C. Nichol, C. Padilla, S. Paltani, J. Peacock, K. Pedersen, V. Pettorino, S. Pires, M. Poncet, L. Popa, L. Pozzetti, F. Raison, R. Rebolo, J. Rhodes, H.-W. Rix, M. Roncarelli, E. Rossetti, R. Saglia, P. Schneider, T. Schrabback, A. Secroun, G. Seidel, S. Serrano, C. Sirignano, G. Sirri, J. Skottfelt, L. Stanco, J. L. Starck, P. Tallada-Crespí, D. Tavagnacco, A. N. Taylor, H. I. Teplitz, R. Toledo-Moreo, F. Torradeflot, M. Trifoglio, E. A. Valentijn, L. Valenziano, G. A. Verdoes Kleijn, Y. Wang, N. Welikala, J. Weller, M. Wetzelstein, G. Zamorani, J. Zoubian, S. Andreon, M. Baldi, S. Bardelli, A. Boucaud, S. Camera, D. Di Ferdinando, G. Fabbian, R. Farinelli, S. Galeotta, J. Graciá-Carpio, D. Maino, E. Medinaceli, S. Mei, C. Neisser, G. Polenta, A. Renzi, E. Romelli, C. Rosset, F. Sureau, M. Tenti, T. Vassallo, E. Zucca, C. Baccigalupi, A. Balaguera-Antolínez, P. Battaglia, A. Biviano, S. Borgani, E. Bozzo, R. Cabanac, and A. Cappi, Euclid preparation. I. The Euclid Wide Survey, *A&A* **662**, A112 (2022), arXiv:2108.01201 [astro-ph.CO].
- [91] LSST Science Collaboration, P. A. Abell, J. Allison, S. F. Anderson, J. R. Andrew, J. R. P. Angel, L. Armus, D. Arnett, S. J. Asztalos, T. S. Axelrod, S. Bailey, D. R. Ballantyne, J. R. Bankert, W. A. Barkhouse, J. D. Barr, L. F. Barrientos, A. J. Barth, J. G. Bartlett, A. C. Becker, J. Becla, T. C. Beers, J. P. Bernstein,

- R. Biswas, M. R. Blanton, J. S. Bloom, J. J. Bochanski, P. Boeshaar, K. D. Borne, M. Bradac, W. N. Brandt, C. R. Bridge, M. E. Brown, R. J. Brunner, J. S. Bullock, A. J. Burgasser, J. H. Burge, D. L. Burke, P. A. Cargile, S. Chandrasekharan, G. Chartas, S. R. Chesley, Y.-H. Chu, D. Cinabro, M. W. Claire, C. F. Claver, D. Clowe, A. J. Connolly, K. H. Cook, J. Cooke, A. Cooray, K. R. Covey, C. S. Culliton, R. de Jong, W. H. de Vries, V. P. Debattista, F. Delgado, I. P. Dell’Antonio, S. Dhital, R. Di Stefano, M. Dickinson, B. Dilday, S. G. Djorgovski, G. Dobler, C. Donalek, G. Dubois-Felsmann, J. Durech, A. Eliahdottir, M. Eracleous, L. Eyer, E. E. Falco, X. Fan, C. D. Fassnacht, H. C. Ferguson, Y. R. Fernandez, B. D. Fields, D. Finkbeiner, E. E. Figuerao, D. B. Fox, H. Francke, J. S. Frank, J. Frieman, S. Fromenteau, M. Furqan, G. Galaz, A. Gal-Yam, P. Garnavich, E. Gawiser, J. Geary, P. Gee, R. R. Gibson, K. Gilmore, E. A. Grace, R. F. Green, W. J. Gressler, C. J. Grillmair, S. Habib, J. S. Haggerty, M. Hamuy, A. W. Harris, S. L. Hawley, A. F. Heavens, L. Hebb, T. J. Henry, E. Hileman, E. J. Hilton, K. Hoadley, J. B. Holberg, M. J. Holman, S. B. Howell, L. Infante, Z. Ivezić, S. H. Jacoby, B. Jain, R. Jedicke, M. J. Jee, J. Garrett Jernigan, S. W. Jha, K. V. Johnston, R. L. Jones, M. Juric, M. Kaasalainen, Styliani, Kafka, S. M. Kahn, N. A. Kaib, J. Kalirai, J. Kantor, M. M. Kasliwal, C. R. Keeton, R. Kessler, Z. Knezevic, A. Kowalski, V. L. Krabbendam, K. S. Krughoff, S. Kulkarni, S. Kuhlman, M. Lacy, S. Lepine, M. Liang, A. Lien, P. Lira, K. S. Long, S. Lorenz, J. M. Lotz, R. H. Lupton, J. Lutz, L. M. Macri, A. A. Mahabal, R. Mandelbaum, P. Marshall, M. May, P. M. McGehee, B. T. Meadows, A. Meert, A. Milani, C. J. Miller, M. Miller, D. Mills, D. Minniti, D. Monet, A. S. Mukadam, E. Nakar, D. R. Neill, J. A. Newman, S. Nikolaev, M. Nordby, P. O’Connor, M. Oguri, J. Oliver, S. S. Olivier, J. K. Olsen, K. Olsen, E. W. Olszewski, H. Oluseyi, N. D. Padilla, A. Parker, J. Pepper, J. R. Peterson, C. Petry, P. A. Pinto, J. L. Pizagno, B. Popescu, A. Prsa, V. Radcka, M. J. Raddick, A. Rasmussen, A. Rau, J. Rho, J. E. Rhoads, G. T. Richards, S. T. Ridgway, B. E. Robertson, R. Roskar, A. Saha, A. Sarajedini, E. Scannapieco, T. Schalk, R. Schindler, and S. Schmidt, *LSST Science Book, Version 2.0*, arXiv , arXiv:0912.0201 (2009), arXiv:0912.0201 [astro-ph.IM].
- [92] Ž. Ivezić, S. M. Kahn, J. A. Tyson, B. Abel, E. Acosta, R. Allsman, D. Alonso, Y. AlSayyad, S. F. Anderson, J. Andrew, J. R. P. Angel, G. Z. Angeli, R. Ansari, P. Antilogus, C. Araujo, R. Armstrong, K. T. Arndt, P. Astier, É. Aubourg, N. Auza, T. S. Axelrod, D. J. Bard, J. D. Barr, A. Barrau, J. G. Bartlett, A. E. Bauer, B. J. Bauman, S. Baumont, E. Bechtol, K. Bechtol, A. C. Becker, J. Becla, C. Beldica, S. Bellavia, F. B. Bianco, R. Biswas, G. Blanc, J. Blazek, R. D. Blandford, J. S. Bloom, J. Bogart, T. W. Bond, M. T. Booth, A. W. Borgland, K. Borne, J. F. Bosch, D. Boutigny, C. A. Brackett, A. Bradshaw, W. N. Brandt, M. E. Brown, J. S. Bullock, P. Burchat, D. L. Burke, G. Cagnoli, D. Calabrese, S. Callahan, A. L. Callen, J. L. Carlin, E. L. Carlson, S. Chandrasekharan, G. Charles-Emerson, S. Chesley, E. C. Cheu, H.-F. Chiang, J. Chiang, C. Chirino, D. Chow, D. R. Ciardi, C. F. Claver, J. Cohen-Tanugi, J. J. Cockrum, R. Coles, A. J. Connolly, K. H. Cook, A. Cooray, K. R. Covey, C. Cribbs, W. Cui, R. Cutri, P. N. Daly, S. F. Daniel, F. Daruich, G. Daubard, G. Daus, W. Dawson, F. Delgado, A. Dellapenna, R. de Peyster, M. de Val-Borro, S. W. Digel, P. Doherty, R. Dubois, G. P. Dubois-Felsmann, J. Durech, F. Economou, T. Eifler, M. Eracleous, B. L. Emmons, A. Fausti Neto, H. Ferguson, E. Figuerao, M. Fisher-Levine, W. Focke, M. D. Foss, J. Frank, M. D. Freeman, E. Gangler, E. Gawiser, J. C. Geary, P. Gee, M. Geha, C. J. B. Gessner, R. R. Gibson, D. K. Gilmore, T. Glanzman, W. Glick, T. Goldina, D. A. Goldstein, I. Goodenow, M. L. Graham, W. J. Gressler, P. Gris, L. P. Guy, A. Guyonnet, G. Haller, R. Harris, P. A. Hascall, J. Haupt, F. Hernandez, S. Herrmann, E. Hileman, J. Hoblitt, J. A. Hodgson, C. Hogan, J. D. Howard, D. Huang, M. E. Huffer, P. Ingraham, W. R. Innes, S. H. Jacoby, B. Jain, F. Jammes, M. J. Jee, T. Jenness, G. Jernigan, D. Jevremović, K. Johns, A. S. Johnson, M. W. G. Johnson, R. L. Jones, C. Juramy-Gilles, M. Jurić, J. S. Kalirai, N. J. Kallivayalil, B. Kalmbach, J. P. Kantor, P. Karst, M. M. Kasliwal, H. Kelly, R. Kessler, V. Kinnison, D. Kirkby, L. Knox, I. V. Kotov, V. L. Krabbendam, K. S. Krughoff, P. Kubánek, J. Kuczewski, S. Kulkarni, J. Ku, N. R. Kurita, C. S. Lage, R. Lambert, T. Lange, J. B. Langton, L. Le Guillou, D. Levine, M. Liang, K.-T. Lim, C. J. Lintott, K. E. Long, M. Lopez, P. J. Lotz, R. H. Lupton, N. B. Lust, L. A. MacArthur, A. Mahabal, R. Mandelbaum, T. W. Markiewicz, D. S. Marsh, P. J. Marshall, S. Marshall, M. May, R. McKecher, M. McQueen, J. Meyers, M. Migliore, M. Miller, and D. J. Mills, *LSST: From Science Drivers to Reference Design and Anticipated Data Products*, *ApJ* **873**, 111 (2019), arXiv:0805.2366 [astro-ph].
- [93] M. Vallisneri, Use and abuse of the Fisher information matrix in the assessment of gravitational-wave parameter-estimation prospects, *PhRvD* **77**, 042001 (2008), arXiv:gr-qc/0703086 [gr-qc].
- [94] J. R. Gair, A. Antonelli, and R. Barbieri, A Fisher matrix for gravitational-wave population inference, *MNRAS* **519**, 2736 (2023), arXiv:2205.07893 [gr-qc].
- [95] H.-Y. Chen, R. Essick, S. Vitale, D. E. Holz, and E. Katsavounidis, Observational Selection Effects with Ground-based Gravitational Wave Detectors, *ApJ* **835**, 31 (2017), arXiv:1608.00164 [astro-ph.HE].
- [96] D. Alonso, J. Sanchez, A. Slosar, and LSST Dark Energy Science Collaboration, A unified pseudo- C_ℓ framework, *MNRAS* **484**, 4127 (2019), arXiv:1809.09603 [astro-ph.CO].
- [97] J. R. Bond, A. H. Jaffe, and L. Knox, Estimating the power spectrum of the cosmic microwave background, *PhRvD* **57**, 2117 (1998), arXiv:astro-ph/9708203 [astro-ph].
- [98] E. Hivon, K. M. Górski, C. B. Netterfield, B. P. Crill, S. Prunet, and F. Hansen, MASTER of the Cosmic Microwave Background Anisotropy Power Spectrum: A Fast Method for Statistical Analysis of Large and Complex Cosmic Microwave Background Data Sets, *ApJ* **567**, 2 (2002), arXiv:astro-ph/0105302 [astro-ph].
- [99] A. Cabré, P. Fosalba, E. Gaztañaga, and M. Manera, Error analysis in cross-correlation of sky maps: application to the Integrated Sachs-Wolfe detection, *MNRAS* **381**, 1347 (2007), arXiv:astro-ph/0701393 [astro-ph].
- [100] Euclid Collaboration, F. Lepori, I. Tutusaus, C. Viglione, C. Bonvin, S. Camera, F. J. Cas-

- tander, R. Durrer, P. Fosalba, G. Jelic-Cizmek, M. Kunz, J. Adamek, S. Casas, M. Martinelli, Z. Sakr, D. Sapone, A. Amara, N. Auricchio, C. Bodendorf, D. Bonino, E. Branchini, M. Brescia, J. Brinchmann, V. Capobianco, C. Carbone, J. Carretero, M. Castellano, S. Cavuoti, A. Cimatti, R. Cledassou, G. Congedo, C. J. Conselice, L. Conversi, Y. Copin, L. Corcione, F. Courbin, A. Da Silva, H. Degaudenzi, M. Douspis, F. Dubath, X. Dupac, S. Dusini, A. Ealet, S. Farrens, S. Ferriol, E. Franceschi, M. Fumana, B. Garilli, W. Gillard, B. Gillis, C. Giocoli, A. Grazian, F. Grupp, L. Guzzo, S. V. H. Haugan, W. Holmes, F. Hormuth, P. Hudelot, K. Jahnke, S. Kermiche, A. Kiessling, M. Kilbinger, T. Kitching, M. Kümmel, H. Kurki-Suonio, S. Ligorì, P. B. Lilje, I. Lloro, O. Mansutti, O. Marggraf, K. Markovic, F. Marulli, R. Massey, S. Maurogordato, M. Melchior, M. Meneghetti, E. Merlin, G. Meylan, M. Moresco, L. Moscardini, E. Munari, R. Nakajima, S. M. Niemi, C. Padilla, S. Paltani, F. Pasian, K. Pedersen, W. J. Percival, V. Pettorino, S. Pires, M. Poncet, L. Popa, L. Pozzetti, F. Raison, J. Rhodes, M. Roncarelli, E. Rossetti, R. Saglia, P. Schneider, A. Secroun, G. Seidel, S. Serano, C. Sirignano, G. Sirri, L. Stanco, J.-L. Starck, P. Tallada-Crespí, A. N. Taylor, I. Tereno, R. Toledo-Moreo, F. Torradeflot, E. A. Valentijn, L. Valenziano, Y. Wang, J. Weller, G. Zamorani, J. Zoubian, S. Andreon, S. Bardelli, G. Fabbian, J. Graciá-Carpio, D. Maino, E. Medinaceli, S. Mei, A. Renzi, E. Romelli, F. Sureau, T. Vassallo, A. Zacchei, E. Zucca, C. Baccigalupi, A. Balaguera-Antolínez, F. Bernardeau, A. Biviano, A. Blanchard, M. Bolzonella, S. Borgani, E. Bozzo, C. Burigana, R. Cabanac, A. Cappi, C. S. Carvalho, G. Castignani, C. Colodro-Conde, J. Coupon, H. M. Courtois, J.-G. Cuby, S. Davini, S. de la Torre, D. Di Ferdinando, M. Farina, P. G. Ferreira, F. Finelli, S. Galeotta, K. Ganga, J. Garcia-Bellido, E. Gaztanaga, G. Gozaliasl, I. M. Hook, S. Ilić, B. Joachimi, V. Kansal, E. Keihänen, C. C. Kirkpatrick, V. Lindholm, G. Mainetti, R. Maoli, N. Martinet, M. Maturi, R. B. Metcalf, P. Monaco, G. Morgante, J. Nightingale, A. Nucita, L. Patrizii, V. Popa, D. Potter, G. Riccio, A. G. Sánchez, M. Schirmer, M. Schultheis, V. Scottez, E. Sefusatti, A. Tramacere, J. Valiviita, M. Viel, and H. Hildebrandt, Euclid preparation. XIX. Impact of magnification on photometric galaxy clustering, *A&A* **662**, A93 (2022), arXiv:2110.05435 [astro-ph.CO].
- [101] J. Lesgourgues, The Cosmic Linear Anisotropy Solving System (CLASS) I: Overview, arXiv , arXiv:1104.2932 (2011), arXiv:1104.2932 [astro-ph.IM].
- [102] D. Blas, J. Lesgourgues, and T. Tram, The Cosmic Linear Anisotropy Solving System (CLASS). Part II: Approximation schemes, *JCAP* **2011** (7), 034, arXiv:1104.2933 [astro-ph.CO].
- [103] P. Coles and B. Jones, A lognormal model for the cosmological mass distribution., *MNRAS* **248**, 1 (1991).
- [104] A. Agrawal, R. Makiya, C.-T. Chiang, D. Jeong, S. Saito, and E. Komatsu, Generating log-normal mock catalog of galaxies in redshift space, *JCAP* **2017** (10), 003, arXiv:1706.09195 [astro-ph.CO].
- [105] Y. Li, mcfits: Multiplicatively Convolutional Fast Integral Transforms, Astrophysics Source Code Library, record ascl:1906.017 (2019), ascl:1906.017.
- [106] A. Amon and G. Efstathiou, A non-linear solution to the S_8 tension?, *MNRAS* **516**, 5355 (2022), arXiv:2206.11794 [astro-ph.CO].
- [107] H. A. Winther, S. Casas, M. Baldi, K. Koyama, B. Li, L. Lombriser, and G.-B. Zhao, Emulators for the non-linear matter power spectrum beyond Λ CDM, *PhRvD* **100**, 123540 (2019), arXiv:1903.08798 [astro-ph.CO].
- [108] M. P. van Daalen, J. Schaye, C. M. Booth, and C. Dalla Vecchia, The effects of galaxy formation on the matter power spectrum: a challenge for precision cosmology, *MNRAS* **415**, 3649 (2011), arXiv:1104.1174 [astro-ph.CO].
- [109] N. E. Chisari, A. J. Mead, S. Joudaki, P. G. Ferreira, A. Schneider, J. Mohr, T. Tröster, D. Alonso, I. G. McCarthy, S. Martin-Alvarez, J. Devriendt, A. Slyz, and M. P. van Daalen, Modelling baryonic feedback for survey cosmology, *OJAp* **2**, 4 (2019), arXiv:1905.06082 [astro-ph.CO].
- [110] P. Torrey, S. Wellons, F. Machado, B. Griffen, D. Nelson, V. Rodriguez-Gomez, R. McKinnon, A. Pillepich, C.-P. Ma, M. Vogelsberger, V. Springel, and L. Hernquist, An analysis of the evolving comoving number density of galaxies in hydrodynamical simulations, *MNRAS* **454**, 2770 (2015), arXiv:1507.01942 [astro-ph.GA].
- [111] P. Schechter, An analytic expression for the luminosity function for galaxies., *ApJ* **203**, 297 (1976).
- [112] C. S. Kochanek, M. A. Pahre, E. E. Falco, J. P. Huchra, J. Mader, T. H. Jarrett, T. Chester, R. Cutri, and S. E. Schneider, The K-Band Galaxy Luminosity Function, *ApJ* **560**, 566 (2001), arXiv:astro-ph/0011456 [astro-ph].
- [113] J. F. Crenshaw, B. Leistedt, M. L. Graham, C. Payne, A. J. Connolly, E. Gawiser, T. Karim, A. I. Malz, J. A. Newman, M. Ricci, and The LSST Dark Energy Science Collaboration, Quantifying the Impact of LSST u-band Survey Strategy on Photometric Redshift Estimation and the Detection of Lyman-break Galaxies, *ApJS* **281**, 54 (2025), arXiv:2503.06016 [astro-ph.CO].
- [114] M. Bilicki, J. A. Peacock, T. H. Jarrett, M. E. Cluver, N. Maddox, M. J. I. Brown, E. N. Taylor, N. C. Hambly, A. Solarz, B. W. Holwerda, I. Baldry, J. Loveday, A. Moffett, A. M. Hopkins, S. P. Driver, M. Alpaslan, and J. Bland-Hawthorn, WISE \times SuperCOSMOS Photometric Redshift Catalog: 20 Million Galaxies over $3/\pi$ Steradians, *ApJS* **225**, 5 (2016), arXiv:1607.01182 [astro-ph.CO].
- [115] R. Abbott, T. D. Abbott, F. Acernese, K. Ackley, C. Adams, N. Adhikari, R. X. Adhikari, V. B. Adya, C. Affeldt, D. Agarwal, M. Agathos, K. Agatsuma, N. Aggarwal, O. D. Aguiar, L. Aiello, A. Ain, P. Ajith, T. Akutsu, P. F. de Alarcón, S. Akcay, S. Albanesi, A. Allocca, P. A. Altin, A. Amato, C. Anand, S. Anand, A. Ananyeva, S. B. Anderson, W. G. Anderson, M. Ando, T. Andrade, N. Andres, T. Andrić, S. V. Angelova, S. Ansoldi, J. M. Antelis, S. Antier, F. Antonini, S. Appert, K. Arai, K. Arai, Y. Arai, S. Araki, A. Araya, M. C. Araya, J. S. Areeda, M. Arène, N. Armitani, N. Arnaud, M. Arogeti, S. M. Aronson, K. G. Arun, H. Asada, Y. Asali, G. Ashton, Y. Aso, M. Assisduo, S. M. Aston, P. Astone, F. Aubin, C. Austin, S. Babak, F. Badaracco, M. K. M. Bader, C. Badger, S. Bae, Y. Bae, A. M. Baer, S. Bagnasco, Y. Bai, L. Baiotti, J. Baird, R. Bajpai, M. Ball, G. Ballardin, S. W. Ballmer, A. Balsamo, G. Baltus, S. Banagiri,

- D. Bankar, J. C. Barayoga, C. Barbieri, B. C. Barish, D. Barker, P. Barneo, F. Barone, B. Barr, L. Barsotti, M. Barsuglia, D. Barta, J. Bartlett, M. A. Barton, I. Bartos, R. Bassiri, A. Basti, M. Bawaj, J. C. Bayley, A. C. Baylor, M. Bazzan, B. Bécsy, V. M. Bedakihale, M. Bejger, I. Belahcene, V. Benedetto, D. Beniwal, T. F. Bennett, J. D. Bentley, M. Benyaala, F. Bergamin, B. K. Berger, S. Bernuzzi, C. P. L. Berry, D. Bersanetti, A. Bertolini, J. Betzwieser, D. Beveridge, R. Bhandare, U. Bhardwaj, D. Bhattacharjee, S. Bhaumik, I. A. Bilenko, G. Billingsley, S. Bini, R. Birney, O. Birnholtz, S. Biscans, M. Bisch, S. Biscoveanu, A. Bisht, B. Biswas, M. Bitossi, M.-A. Bizouard, J. K. Blackburn, C. D. Blair, D. G. Blair, R. M. Blair, F. Bobba, N. Bode, M. Boer, G. Bogaert, M. Boldrini, L. D. Bonavena, F. Bondu, E. Bonilla, R. Bonnand, P. Booker, B. A. Boom, R. Bork, V. Boschi, N. Bose, S. Bose, V. Bossilkov, V. Boudart, Y. Bouffanais, A. Bozzi, C. Bradaschia, P. R. Brady, A. Bramley, A. Branch, M. Branchesi, J. Brandt, J. E. Brau, M. Breschi, T. Briant, J. H. Briggs, A. Brillet, M. Brinkmann, P. Brockill, A. F. Brooks, J. Brooks, D. D. Brown, S. Brunett, G. Bruno, R. Bruntz, J. Bryant, T. Bulik, H. J. Bulten, A. Buonanno, R. Busicchio, D. Buskalic, C. Buy, R. L. Byer, L. Cadonati, G. Cagnoli, C. Cahillane, J. C. Bustillo, J. D. Callaghan, T. A. Callister, E. Calloni, J. Cameron, J. B. Camp, M. Canepa, S. Canevarolo, M. Cannavacciolo, K. C. Cannon, H. Cao, Z. Cao, E. Capocasa, E. Capote, and G. Carapella, Population of Merging Compact Binaries Inferred Using Gravitational Waves through GWTC-3, *PhRvX* **13**, 011048 (2023), arXiv:2111.03634 [astro-ph.HE].
- [116] The LIGO Scientific Collaboration, the Virgo Collaboration, the KAGRA Collaboration, A. G. Abac, I. Abouelfettouh, F. Acernese, K. Ackley, C. Adamcewicz, S. Adhicary, D. Adhikari, N. Adhikari, R. X. Adhikari, V. K. Adkins, S. Afroz, D. Agarwal, M. Agathos, M. Aghaei Abchouyeh, O. D. Aguiar, S. Ahmadzadeh, L. Aiello, A. Ain, P. Ajith, T. Akutsu, S. Albanesi, R. A. Alford, A. Al-Jodah, C. Alléné, A. Allocca, S. Al-Shammari, P. A. Altin, S. Alvarez-Lopez, O. Amaras-inghe, A. Amato, C. Amra, A. Ananyeva, S. B. Anderson, W. G. Anderson, M. Andia, M. Ando, T. Andrade, M. Andrés-Caracsona, T. Andrić, J. Anglin, S. Ansoldi, J. M. Antelis, S. Antier, M. Aoumi, E. Z. Appavuravther, S. Appert, S. K. Apple, K. Arai, A. Araya, M. C. Araya, M. Arca Sedda, J. S. Areeda, L. Argianas, N. Aritomi, F. Armato, S. Armstrong, N. Arnaud, M. Arogeti, S. M. Aronson, K. G. Arun, G. Ashton, Y. Aso, M. Assiduo, S. Assis de Souza Melo, S. M. Aston, P. Astone, F. Attadio, F. Aubin, K. AultONeal, G. Avallone, S. Babak, F. Badaracco, C. Badger, S. Bae, S. Bagnasco, E. Bagui, L. Baiotti, R. Bajpai, T. Baka, T. Baker, M. Ball, G. Ballardín, S. W. Ballmer, S. Banagiri, B. Banerjee, D. Bankar, T. M. Baptiste, P. Baral, J. C. Barayoga, B. C. Barish, D. Barker, N. Barman, P. Barneo, F. Barone, B. Barr, L. Barsotti, M. Barsuglia, D. Barta, A. M. Bartoletti, M. A. Barton, I. Bartos, S. Basak, A. Basalaev, R. Bassiri, A. Basti, D. E. Bates, M. Bawaj, P. Baxi, J. C. Bayley, A. C. Baylor, P. A. Baynard, II, M. Bazzan, V. M. Bedakihale, F. Beirnaert, M. Bejger, D. Belardinelli, A. S. Bell, D. S. Bellie, L. Bellizzi, D. Beltran-Martinez, W. Benoit, I. Bentara, J. D. Bentley, M. Ben Yaala, S. Bera, F. Bergamin, B. K. Berger, S. Bernuzzi, M. Beroiz, C. P. L. Berry, D. Bersanetti, A. Bertolini, J. Betzwieser, D. Beveridge, G. Bevilacqua, N. Bevins, R. Bhandare, R. Bhatt, D. Bhattacharjee, S. Bhaumik, S. Bhowmick, V. Biancalana, A. Bianchi, I. A. Bilenko, G. Billingsley, A. Binetti, S. Bini, C. Binu, O. Birnholtz, S. Biscoveanu, A. Bisht, M. Bitossi, M. A. Bizouard, S. Blaber, J. K. Blackburn, L. A. Blagg, C. D. Blair, D. G. Blair, F. Bobba, N. Bode, G. Boileau, M. Boldrini, G. N. Bolingbroke, A. Bolliand, L. D. Bonavena, R. Bondarescu, F. Bondu, E. Bonilla, M. S. Bonilla, A. Bonino, R. Bonnand, P. Booker, A. Borchers, S. Borhanian, V. Boschi, S. Bose, V. Bossilkov, A. Boudon, A. Bozzi, C. Bradaschia, P. R. Brady, A. Branch, M. Branchesi, I. Braun, T. Briant, A. Brillet, M. Brinkmann, P. Brockill, E. Brockmueller, A. F. Brooks, B. C. Brown, D. D. Brown, M. L. Brozzetti, S. Brunett, G. Bruno, R. Bruntz, and J. Bryant, GWTC-4.0: Population Properties of Merging Compact Binaries, arXiv , arXiv:2508.18083 (2025), arXiv:2508.18083 [astro-ph.HE].
- [117] M. Branchesi, M. Maggiore, D. Alonso, C. Badger, B. Banerjee, F. Beirnaert, E. Belgacem, S. Bhagwat, G. Boileau, S. Borhanian, D. D. Brown, M. Leong Chan, G. Cusin, S. L. Danilishin, J. Degallaix, V. De Luca, A. Dhani, T. Dietrich, U. Dupletsa, S. Foffa, G. Franciolini, A. Freise, G. Gemme, B. Goncharov, A. Ghosh, F. Gulminelli, I. Gupta, P. Kumar Gupta, J. Harms, N. Hazra, S. Hild, T. Hinderer, I. Siong Heng, F. Iacovelli, J. Janquart, K. Janssens, A. C. Jenkins, C. Kalaghatgi, X. Korovesi, T. G. F. Li, Y. Li, E. Loffredo, E. Maggio, M. Mancarella, M. Mapelli, K. Martinovic, A. Maselli, P. Meyers, A. L. Miller, C. Mondal, N. Muttoni, H. Narola, M. Oertel, G. Oganesyan, C. Pacilio, C. Palomba, P. Pani, A. Pasqualetti, A. Perego, C. Péroigois, M. Pieroni, O. J. Piccinni, A. Puecher, P. Puppo, A. Ricciardone, A. Riotto, S. Ronchini, M. Sakellariadou, A. Samajdar, F. Santoliquido, B. S. Sathyaprakash, J. Steinlechner, S. Steinlechner, A. Utina, C. Van Den Broeck, and T. Zhang, Science with the Einstein Telescope: a comparison of different designs, *JCAP* **2023** (7), 068, arXiv:2303.15923 [gr-qc].
- [118] F. Santoliquido, J. Tissino, U. Dupletsa, M. Branchesi, J. Harms, M. Arca Sedda, M. Dax, A. Kofler, S. R. Green, N. Gupte, I. M. Romero-Shaw, and E. Berti, Fast and accurate parameter estimation of high-redshift sources with the Einstein Telescope, *PhRvD* **112**, 103015 (2025), arXiv:2504.21087 [astro-ph.HE].
- [119] M. Evans, R. X. Adhikari, C. Afle, S. W. Ballmer, S. Biscoveanu, S. Borhanian, D. A. Brown, Y. Chen, R. Eisenstein, A. Gruson, A. Gupta, E. D. Hall, R. Huxford, B. Kamai, R. Kashyap, J. S. Kissel, K. Kuns, P. Landry, A. Lenon, G. Lovelace, L. McCuller, K. K. Y. Ng, A. H. Nitz, J. Read, B. S. Sathyaprakash, D. H. Shoemaker, B. J. J. Slagmolen, J. R. Smith, V. Srivastava, L. Sun, S. Vitale, and R. Weiss, A Horizon Study for Cosmic Explorer: Science, Observatories, and Community, arXiv , arXiv:2109.09882 (2021), arXiv:2109.09882 [astro-ph.IM].
- [120] K. Kuns, P. Fulda, L. Barsotti, and M. Evans, Cosmic Explorer Strain and Displacement Sensitivity, <https://dcc.cosmicexplorer.org/CE-T2000017/>

- public (2024).
- [121] F. Iacovelli, M. Mancarella, S. Foffa, and M. Maggiore, GWFASST: A Fisher Information Matrix Python Code for Third-generation Gravitational-wave Detectors, *ApJS* **263**, 2 (2022), arXiv:2207.06910 [astro-ph.IM].
- [122] L. London, S. Khan, E. Fauchon-Jones, C. García, M. Hannam, S. Husa, X. Jiménez-Forteza, C. Kalaghatgi, F. Ohme, and F. Pannarale, First Higher-Multipole Model of Gravitational Waves from Spinning and Coalescing Black-Hole Binaries, *PhRvL* **120**, 161102 (2018), arXiv:1708.00404 [gr-qc].
- [123] Euclid Collaboration, A. Pocino, I. Tutusaus, F. J. Castander, P. Fosalba, M. Crocce, A. Porredon, S. Camera, V. Cardone, S. Casas, T. Kitching, F. Lacasa, M. Martinelli, A. Pourtsidou, Z. Sakr, S. Andreon, N. Auricchio, C. Baccigalupi, A. Balaguera-Antolínez, M. Baldi, A. Balestra, S. Bardelli, R. Bender, A. Biviano, C. Bodendorf, D. Bonino, A. Boucaud, E. Bozzo, E. Branchini, M. Brescia, J. Brinchmann, C. Burigana, R. Cabanac, V. Capobianco, A. Cappi, C. S. Carvalho, M. Castellano, G. Castignani, S. Cavuoti, A. Cimatti, R. Cledassou, C. Colodro-Conde, G. Congedo, C. J. Conselice, L. Conversi, Y. Copin, L. Corcione, A. Costille, J. Coupon, H. M. Courtois, M. Cropper, J.-G. Cuby, A. Da Silva, S. de la Torre, D. Di Ferdinando, F. Dubath, C. Duncan, X. Dupac, S. Dusini, S. Farrens, P. G. Ferreira, I. Ferrero, F. Finelli, S. Fotopoulou, M. Frailis, E. Franceschi, S. Galeotta, B. Garilli, W. Gillard, B. Gillis, C. Giocoli, G. Gozaliasl, J. Graciá-Carpio, F. Grupp, L. Guzzo, W. Holmes, F. Hormuth, K. Jahnke, E. Keihanen, S. Kermiche, A. Kiessling, C. C. Kirkpatrick, M. Kunz, H. Kurki-Suonio, S. Ligori, P. B. Lilje, I. Lloro, D. Maino, E. Maiorano, O. Mansutti, O. Marggraf, N. Martinet, F. Marulli, R. Massey, S. Maurogordato, E. Medinaceli, S. Mei, M. Meneghetti, R. Benton Metcalf, G. Meylan, M. Moresco, B. Morin, L. Moscardini, E. Munari, R. Nakajima, C. Neisser, R. C. Nichol, S. Niemi, J. Nightingale, C. Padilla, S. Paltani, F. Pasian, L. Patrizzii, K. Pedersen, W. J. Percival, V. Pettorino, S. Pires, G. Polenta, M. Poncet, L. Popa, D. Potter, L. Pozzetti, F. Raison, A. Renzi, J. Rhodes, G. Riccio, E. Romelli, M. Roncarelli, E. Rossetti, R. Saglia, A. G. Sánchez, D. Sapone, R. Scaramella, P. Schneider, V. Scottetz, A. Secroun, G. Seidel, S. Serrano, C. Sirignano, G. Sirri, L. Stanco, F. Sureau, A. N. Taylor, M. Tenti, I. Tereno, R. Teyssier, R. Toledo-Moreo, A. Tramacere, E. A. Valentijn, L. Valenziano, J. Valiviita, T. Vassallo, M. Viel, Y. Wang, N. Welikala, L. Whittaker, A. Zacchei, G. Zamorani, J. Zoubian, and E. Zucca, Euclid preparation. XII. Optimizing the photometric sample of the Euclid survey for galaxy clustering and galaxy-galaxy lensing analyses, *A&A* **655**, A44 (2021), arXiv:2104.05698 [astro-ph.CO].
- [124] A. Zonca, L. Singer, D. Lenz, M. Reinecke, C. Rosset, E. Hivon, and K. Gorski, healpy: equal area pixelization and spherical harmonics transforms for data on the sphere in Python, *JOSS* **4**, 1298 (2019).
- [125] J.-E. Campagne, F. Lanusse, J. Zuntz, A. Boucaud, S. Casas, M. Karamanis, D. Kirkby, D. Lanzieri, A. Peel, and Y. Li, JAX-COSMO: An End-to-End Differentiable and GPU Accelerated Cosmology Library, *OJAp* **6**, 15 (2023), arXiv:2302.05163 [astro-ph.CO].
- [126] S. Duane, A. D. Kennedy, B. J. Pendleton, and D. Roweth, Hybrid Monte Carlo, *PhLB* **195**, 216 (1987).
- [127] R. Neal, MCMC Using Hamiltonian Dynamics, in *Handbook of Markov Chain Monte Carlo* (2011) pp. 113–162.
- [128] M. Betancourt, A Conceptual Introduction to Hamiltonian Monte Carlo, arXiv , arXiv:1701.02434 (2017), arXiv:1701.02434 [stat.ME].
- [129] D. Phan, N. Pradhan, and M. Jankowiak, Composable Effects for Flexible and Accelerated Probabilistic Programming in NumPyro, arXiv , arXiv:1912.11554 (2019), arXiv:1912.11554 [stat.ML].
- [130] D. Phan, N. Pradhan, M. Jankowiak, E. Bingham, J. P. Chen, F. Obermeyer, T. Karaletsos, R. Singh, P. Szerlip, P. Horsfall, and N. D. Goodman, NumPyro: Probabilistic programming with NumPy, *Astrophysics Source Code Library*, record ascl:2505.005 (2025), ascl:2505.005.
- [131] M. D. Hoffman and A. Gelman, The No-U-Turn Sampler: Adaptively Setting Path Lengths in Hamiltonian Monte Carlo, arXiv , arXiv:1111.4246 (2011), arXiv:1111.4246 [stat.CO].
- [132] C. Talbot and J. Golomb, Growing pains: understanding the impact of likelihood uncertainty on hierarchical Bayesian inference for gravitational-wave astronomy, *MNRAS* **526**, 3495 (2023), arXiv:2304.06138 [astro-ph.IM].
- [133] A. Q. Cheng and Differentiable Universe Initiative, https://github.com/aqcheng/jax_cosmo.
- [134] A. Q. Cheng, https://github.com/aqcheng/gw_xcosmo.
- [135] M. Raffei-Ravandi, K. M. Smith, and K. W. Masui, Characterizing fast radio bursts through statistical cross-correlations, *PhRvD* **102**, 023528 (2020), arXiv:1912.09520 [astro-ph.CO].
- [136] P. Madau and M. Dickinson, Cosmic Star-Formation History, *ARA&A* **52**, 415 (2014), arXiv:1403.0007 [astro-ph.CO].
- [137] T. Callister, M. Fishbach, D. E. Holz, and W. M. Farr, Shouts and Murmurs: Combining Individual Gravitational-wave Sources with the Stochastic Background to Measure the History of Binary Black Hole Mergers, *ApJL* **896**, L32 (2020), arXiv:2003.12152 [astro-ph.HE].
- [138] C. Talbot and E. Thrane, Measuring the Binary Black Hole Mass Spectrum with an Astrophysically Motivated Parameterization, *ApJ* **856**, 173 (2018), arXiv:1801.02699 [astro-ph.HE].
- [139] S. Ho, A. Cuesta, H.-J. Seo, R. de Putter, A. J. Ross, M. White, N. Padmanabhan, S. Saito, D. J. Schlegel, E. Schlafly, U. Seljak, C. Hernández-Monteagudo, A. G. Sánchez, W. J. Percival, M. Blanton, R. Skibba, D. Schneider, B. Reid, O. Mena, M. Viel, D. J. Eisenstein, F. Prada, B. A. Weaver, N. Bahcall, D. Bizyaev, H. Brewinton, J. Brinkman, L. Nicolaci da Costa, J. R. Gott, E. Malanushenko, V. Malanushenko, B. Nichol, D. Oravetz, K. Pan, N. Palanque-DeLabrouille, N. P. Ross, A. Simmons, F. de Simoni, S. Snedden, and C. Yeche, Clustering of Sloan Digital Sky Survey III Photometric Luminous Galaxies: The Measurement, Systematics, and Cosmological Implications, *ApJ* **761**, 14 (2012), arXiv:1201.2137 [astro-ph.CO].

Appendix A: Recovering the standard galaxy catalog method from a GRF

In this section, we check explicitly that we can recover the standard galaxy catalog population prior under the change of variables from event-level parameters $\{\mathbf{r}\}$ to an overdensity field $\{a_{\ell m}\}$ described in Section IV B 3. That is, we show that the spatial distribution $p(\mathbf{\Omega}|z)$ constructed from the observed galaxies in the standard galaxy catalog method can be recovered from a Gaussian distribution on the GW overdensity field.

Recall that the standard galaxy catalog method conditions on the *total* galaxy field as a fixed distribution. Therefore, we are interested in the population prior of a GW field on some thin shell⁷ at redshift \bar{z} , conditioned on the GW redshifts $\{z\}$ and total galaxy field

$$p(\mathbf{a}^G[\bar{z}]|\{z\}, \{z^{g,\text{tot}}\}, \mathbf{a}^{g,\text{tot}}[\bar{z}], \mathbf{\Lambda}) = \prod_{\ell,m} p(a_{\ell m}^G[\bar{z}]|n^G[\bar{z}], n^{g,\text{tot}}[\bar{z}], a_{\ell m}^{g,\text{tot}}[\bar{z}], \mathbf{\Lambda}) \quad (\text{A1})$$

where \mathbf{a} refers to the vector of $a_{\ell m}$ over (ℓ, m) , taking advantage of the separation of harmonic modes. We model the GW field as a Poisson realization of the total galaxy field

$$a_{\ell m}^G[\bar{z}] = a_{\ell m}^{g,\text{tot}}[\bar{z}] + s_\ell^G[\bar{z}] \quad (\text{A2})$$

where $s_\ell^G[\bar{z}] = 1/\langle n^G[\bar{z}] \rangle$ is the shot noise of this shell.

The conditional distribution of a multivariate Gaussian is also a multivariate Gaussian, with a modified mean and variance. To compute what those are, we need the quantities

$$\begin{aligned} C_\ell^{Gg,\text{tot}}[\bar{z}] &= \langle a_{\ell m}^G[\bar{z}]^* a_{\ell m}^{g,\text{tot}}[\bar{z}] \rangle \\ &= \langle (a_{\ell m}^{g,\text{tot}}[\bar{z}] + s_\ell^G[\bar{z}])^* a_{\ell m}^{g,\text{tot}}[\bar{z}] \rangle \\ &= \bar{C}_\ell^{gg}[\bar{z}] + \frac{1}{\langle n^{g,\text{tot}}[\bar{z}] \rangle} \end{aligned} \quad (\text{A3})$$

and (via a similar calculation)

$$C_\ell^{GG}[\bar{z}] = \bar{C}_\ell^{gg}[\bar{z}] + \frac{1}{\langle n^G[\bar{z}] \rangle} \quad (\text{A4})$$

Equation (A3) was derived modeling GWs as a Poisson point process of the total galaxy field. Equation (A3) is what we ought to expect; GWs have the same clustering patterns as the galaxies they are drawn from, and we can recognize the cross shot noise term in the last line (as in Equation (38)). Equation (A4) is also what we expect from a Poisson point process which traces the galaxies. Note that here, $\bar{C}_\ell^{gg} = \bar{C}_\ell^{Gg} = \bar{C}_\ell^{GG}$ because

we have assumed that GWs are uniformly drawn from the galaxies, and that observed and unobserved galaxies do not cluster differently. A more flexible model is easily accommodated by modeling a luminosity-dependent galaxy bias along with selection effects, or more simply by allowing GWs and galaxies to have separate biases.

Using Equations (A3) and (A4), the distribution of the GW overdensity field conditioned on the observed galaxy overdensity field is

$$p(a_{\ell m}^G[\bar{z}]|n^G[\bar{z}], n^{g,\text{tot}}[\bar{z}], a_{\ell m}^{g,\text{tot}}[\bar{z}], \mathbf{\Lambda}) = \mathcal{N}[a_{\ell m}^G[\bar{z}]; \mu_{\ell m}, \Sigma_{\ell m}] \quad (\text{A5a})$$

$$\mu_{\ell m} = a_{\ell m}^{g,\text{tot}}[\bar{z}] \quad (\text{A5b})$$

$$\Sigma_{\ell m} = \frac{1}{\langle n^G[\bar{z}] \rangle} \quad (\text{A5c})$$

Notice that the variance of the GW field is now a scale-independent shot noise; we've showed explicitly that conditioning on a fixed background of galaxies removes 2-point correlations, as we discussed above! Transforming Equation (A5) to real space, one can show that the probability of a GW being found in a given infinitesimal shell \bar{z} and pixel $\bar{\mathbf{\Omega}}$ is given by

$$\begin{aligned} p[N^G(\bar{z}, \bar{\mathbf{\Omega}}) = 1] &= \langle n^G[\bar{z}] \rangle [1 + \Delta^{g,\text{tot}}(\bar{\mathbf{\Omega}}|\bar{z})] \delta\mathbf{\Omega} \\ &= \frac{dN^G}{dz} \Big|_{\bar{z}} \frac{1}{4\pi} [1 + \Delta^{g,\text{tot}}(\bar{\mathbf{\Omega}}|\bar{z})] \delta z \delta\mathbf{\Omega} \end{aligned} \quad (\text{A6})$$

where δz and $\delta\mathbf{\Omega}$ are the shell width and pixel size, respectively. Taking the infinitesimal limit gives us the continuous GW spatial probability distribution of the standard galaxy catalog method, i.e., Equation (9). One can substitute in the expression for $\Delta^{g,\text{tot}}$ in Equation (56) and take $\Delta^{g,\text{miss}} = 0$, for example, for the ‘‘homogeneous completion’’ implementation of the galaxy catalog method. Thus, a spatial population prior informed by the galaxies $p(z, \mathbf{\Omega}|\mathbf{\Lambda}, \{\mathbf{d}^g\})$ to be evaluated on an event-by-event basis, as in standard dark siren methods, can be recovered from the Gaussian population prior on the GW fields, if we make some heuristic assumption about the missing galaxies to treat the total underlying galaxy field as known.

As discussed in the main text, the correct thing to do would be to condition only on the observed galaxies $a_{\ell m}^g$, rather than the entire galaxy field $a_{\ell m}^{g,\text{tot}}$. To derive this, we need to compute $C_\ell^{Gg}[\bar{z}]$, which can be derived as follows:

$$\begin{aligned} C_\ell^{Gg}[\bar{z}] &= \langle a_{\ell m}^G[\bar{z}]^* a_{\ell m}^g[\bar{z}] \rangle = \langle (\bar{a}_{\ell m}^G[\bar{z}] + s_\ell^G[\bar{z}])^* a_{\ell m}^g[\bar{z}] \rangle \\ &= p(D^g|\bar{z}) \left(\bar{C}_\ell^{gg}[\bar{z}] + \frac{1}{n^g} \right) + (1 - p(D^g|\bar{z})) \bar{C}_\ell^{gg}[\bar{z}] \\ &= \bar{C}_\ell^{gg}[\bar{z}] + \frac{p(D^g|\bar{z})}{n^g[\bar{z}]} \end{aligned} \quad (\text{A7})$$

⁷ Here, we are ignoring for simplicity the coupling between shells via radial modes, but the same result can be shown in that case.

This follows from Equation (56); the second term in the last line can be identified as the cross shot noise (as in Equation (38))

Using Equations (A4) and (A7), the distribution of the GW field conditioned only on the observed galaxies is

$$\mathcal{L}(a_{\ell m}^G | \mathbf{\Lambda}, n^G, n^g, a_{\ell m}^g) = \mathcal{N}[a_{\ell m}^G; \mu_{\ell m}, \Sigma_{\ell m}] \quad (\text{A8a})$$

$$\mu_{\ell m} = \frac{\overline{C}_\ell^{gg} + \frac{p(D^g|z, \mathbf{\Lambda})}{n^g}}{\overline{C}_\ell^{gg} + \frac{1}{n^g}} a_{\ell m}^g \quad (\text{A8b})$$

$$\Sigma_{\ell m} = \overline{C}_\ell^{gg} + \frac{1}{n^G} - \frac{\left[\overline{C}_\ell^{gg} + \frac{p(D^g|z, \mathbf{\Lambda})}{n^g} \right]^2}{\overline{C}_\ell^{gg} + \frac{1}{n^g}}. \quad (\text{A8c})$$

With the usual assumption that $N^g \gg N^G$, this reduces to Equation (A5) only in the case of galaxy catalog completeness, i.e., $p(D^g|z, \mathbf{\Lambda}) = 1$. If all possible host galaxies are known, then 2-point correlations do not provide any new information for the possible GW host locations.

Appendix B: Beam window functions

In this section, we derive the kernel for a Gaussian and isotropic localization error of an individual event. While this is a well known result in the context of, e.g., CMB cosmology [70], we find it useful to derive this explicitly for the GW measurement process, in which we model the MAP sky localization as randomly displaced from its true position.

For a given realization of the universe, the probability density map under noise of the MAP position of some observed GW i is given by $p^{(i)}(\mathbf{\Omega})$, which we model as an isotropic Gaussian of width σ_i centered at its true location $\mathbf{\Omega}_i$.

By the orthonormality of the spherical harmonics, $p^{(i)}(\mathbf{\Omega})$ admits a multipole expansion

$$p(\mathbf{\Omega} | \mathbf{\Omega}_i) = \sum_{\ell, m} \sum_{\ell', m'} D_{\ell m, \ell' m'} Y_{\ell m}(\mathbf{\Omega}) Y_{\ell' m'}^*(\mathbf{\Omega}_i). \quad (\text{B1})$$

Let $d_{\ell m}^{(i)}$ be the SHT of $p^{(i)}(\mathbf{\Omega})$. The true map of this event and its spherical transform are given by

$$\rho_i(\mathbf{\Omega}) = \delta^{(D)}(\mathbf{\Omega} - \mathbf{\Omega}_i) \quad (\text{B2})$$

$$a_{\ell m}^{(i)} = Y_{\ell m}^*(\mathbf{\Omega}_i) \quad (\text{B3})$$

and thus $p^{(i)}(\mathbf{\Omega})$ is written in harmonic space as

$$d_{\ell m}^{(i)} = \sum_{\ell', m'} D_{\ell m, \ell' m'} a_{\ell' m'}. \quad (\text{B4})$$

This expression simplifies if $p(\mathbf{\Omega} | \mathbf{\Omega}_i)$ is isotropic and spatially invariant, i.e., it can be written as a function of $\cos \theta = \mathbf{\Omega} \cdot \mathbf{\Omega}_i$. We can do this by expanding $P(\cos \theta)$ in

the complete basis of the Legendre polynomials $\mathcal{P}_\ell(\cos \theta)$

$$\begin{aligned} P(\cos \theta) &= \sum_{\ell} B_\ell \frac{2\ell + 1}{4\pi} \mathcal{P}_\ell(\cos \theta) \\ &= \sum_{\ell, m} B_\ell Y_{\ell m}(\mathbf{\Omega}) Y_{\ell m}^*(\mathbf{\Omega}_i) \end{aligned} \quad (\text{B5})$$

which implies the result in Equation (67)

$$d_{\ell m}^{(i)} = B_\ell a_{\ell m}. \quad (\text{B6})$$

Thus, B_ℓ serves to suppress features in the map on the scale of the localization error corresponding to the convolution; localization errors negligible with respect to the resolution of ℓ_{\max} have $B_\ell = 1$, as is the case for galaxies. One can solve for the B_ℓ corresponding to any localization error $P(\mathbf{\Omega} | \mathbf{\Omega}')$ by inverting Equation (B5):

$$B_\ell = \frac{4\pi}{2\ell + 1} \int d \cos \theta P(\cos \theta) \mathcal{P}_\ell(\cos \theta). \quad (\text{B7})$$

In particular, a Gaussian and isotropic localization error with width σ

$$P(\cos \theta) \propto \exp \left[-\frac{(\cos \theta - 1)^2}{2\sigma} \right] \quad (\text{B8})$$

has a corresponding expansion

$$B_\ell(\sigma) = \exp \left[-\frac{1}{2} \ell(\ell + 1) \sigma^2 \right] \quad (\text{B9})$$

which yields the expression in Equation (68). Although we limit ourselves to isotropic and Gaussian localization errors in Section V A, our formalism can be extended to more general localization errors using Equation (B4).

Appendix C: Cross shot noise

The fundamental assumption of the standard galaxy catalog method is that GW sources are hosted in galaxies. In the cross-correlation method, this is encoded in the cross shot noise: the $1/n^{g, \text{tot}}$ shot noise term in Equation (A3), for example, is a direct result from assuming that the GWs are drawn from the galaxies as a doubly stochastic process. Nonetheless, we claimed in the main text that in practice, the cross shot noise does not actually contribute much to the cosmological constraints relative to the information gained from 2-point correlations, due to the binning of the data, a large number of galaxies per bin, and low galaxy completeness. In this section, we make this claim more concrete, as well as show for reference how one could in theory compute the expected cross shot noise for full consistency with the standard galaxy catalog method.

From Section III, the cross shot noise between the GW bin α and galaxy bin β is

$$s_\ell^{G_\alpha G_\beta} = \frac{\langle n^{G_\alpha} n^{G_\beta} \rangle}{\langle n^{G_\alpha} \rangle \langle n^{G_\beta} \rangle}. \quad (\text{C1})$$

$\langle n^{G_\alpha} n^{g_\beta} \rangle$ is the Poisson rate of coincidence, which encodes how often a GWs in bin α has a host galaxy in bin β . For two bins that are perfectly coincident, $\langle n^{G_\alpha} n^{g_\beta} \rangle = p(D^g|z_\beta)$, the fraction of GW host galaxies observed in the catalog, and thus the shot noise is something like $p(D^g|z_\beta)/n^g(z_\beta)$. This is already quite small if we have a large number of galaxies in each bin or if the galaxy catalog has low completeness, both of which we expect to be true. The cross shot noise is even smaller with arbitrary GW and galaxy bins, which can be computed as

$$\langle n^{G_\alpha} n^{g_\beta} \rangle = \langle n^{G_\alpha} \rangle \int dz p(D^g|z) \phi^{G_\alpha}(z) p^g(\beta|z) \quad (\text{C2})$$

where $p^g(\beta|z)$ is the probability that a detected host galaxy at redshift z is found in bin β , and $p(D^g|z)$ is again the host galaxy detection probability at redshift z , which can be computed following the standard galaxy catalog literature [24, 26, 34] by integrating the luminosity function up to the k-corrected threshold magnitude.

For tophat radial bins, the probability $p^g(\beta|z)$ of a galaxy in the catalog with true redshift z to be found in with $\hat{z} \in [\hat{z}_{\min}^\beta, \hat{z}_{\max}^\beta]$ is

$$p^g(\beta|z) = \int_{\hat{z}_{\min}^\beta}^{\hat{z}_{\max}^\beta} d\hat{z} \mathcal{L}(\hat{z}|z). \quad (\text{C3})$$

Thus, the GW–galaxy cross shot noise is given by

$$s_\ell^{G_\alpha g_\beta} = \frac{1}{\langle n^{g_\beta} \rangle} \int dz f_{\text{obs}}^g(z) \phi^{G_\alpha}(z) \int_{\hat{z}_{\min}^\beta}^{\hat{z}_{\max}^\beta} d\hat{z} \mathcal{L}(\hat{z}|z). \quad (\text{C4})$$

We can use this to compute the cross shot noise and compare it to the biased matter power spectrum in our mock universe in Section VII. This is shown in Figure 8, which plots the kernel-smoothed power spectrum of the probability density fields (i.e., the 2-point correlations that we can measure, suppressed at small scales by GW angular localization errors) as well as the shot noise for the same power spectra that we showed in Figure 6. In particular, we can see that the GW–galaxy cross-correlation in the middle panel is signal-dominated by a factor of ~ 100 . Furthermore, even though the signal is suppressed by the beam window function at large ℓ (it drops much faster with ℓ than the galaxy–galaxy power spectrum), the cross shot noise also drops by the same factor, as we showed in Equation (87).

With the large error bars in the cross-correlation (as seen in Figure 6), which are driven by the large shot noise of the GW field, the cross shot noise ends up with negligible impact on the inference. We have repeated our inference in Section VII including the computation of the cross shot noise outlined above and found no discernible differences in inference results. Thus, the constraints on H_0 presented in this paper arise purely from 2-point correlations as two tracers tracing the same Gaussian matter density field.

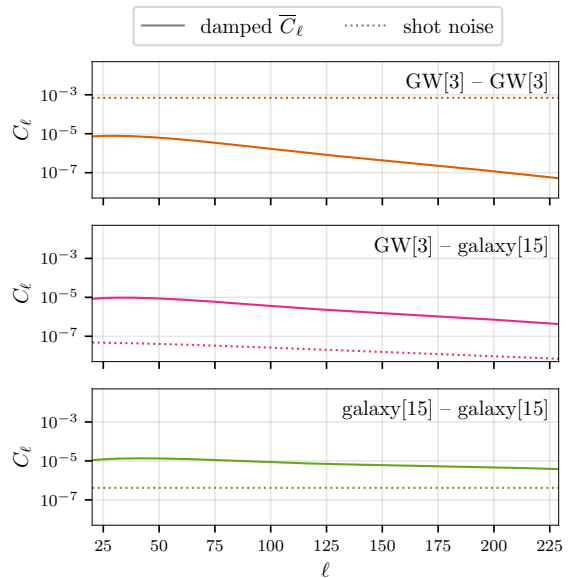


FIG. 8: Kernel-smoothed power spectrum of the probability density fields ($\overline{C}_\ell^{\alpha\beta}$) vs the shot noise for a GW–GW, GW–galaxy, and galaxy–galaxy power spectrum (top to bottom). We show the same GW and galaxy radial bins as in Figure 6.

The physical explanation of why this is the case is that the identification of a GW host galaxy is difficult, for the standard reasons why the galaxy catalog method is often not informative: galaxy catalogs are large and incomplete, and GW localization errors are large. This is also made worse in the cross-correlation method because we discretize the data and build measurement errors into the theory prediction, such that the GW host requirement can only be imposed up to a certain scale, which is a weaker requirement than the standard galaxy catalog method. Thus, the information on cosmological parameters from matching a GW to a host galaxy is negligible compared to that of the high-SNR measurements of galaxy and GW clustering. It is for these reasons that most multi-tracer applications ignore the cross shot noise altogether, even if the tracers can be coincident (e.g., [135]).

Appendix D: BBH population model

In this section, we describe the details of the BBH population model and the implementation of their injection into galaxies. The true values of the population model parameters can be found in Table II; recall that we use the Planck 2015 values for H_0 and $\Omega_{m,0}$ as our fiducial cosmology. We will use $\mathbf{\Lambda}_c$, $\mathbf{\Lambda}_r$, and $\mathbf{\Lambda}_m$ to abbreviate the cosmological, rate, and mass population parameters, respectively.

We use a Madau-Dickinson redshift model [136, 137]

	Parameter	Value
$\mathbf{\Lambda}_r$ [Gpc ⁻³ yr ⁻¹]	\mathcal{R}_0	20
	γ	2.7
	κ	3.0
	z_p	2.0
$\mathbf{\Lambda}_m$ [M_\odot]	α	3.4
	μ_p	34
	σ_p	3.6
	λ_p	0.04
	δ_m	4.8
	m_{\min}	5.1
	m_{\max}	87
	β	1.1

TABLE II: True values of the BBH rate ($\mathbf{\Lambda}_r$) and mass ($\mathbf{\Lambda}_m$) population model parameters used to generate the mock catalog.

to model the rate evolution of the BBHs

$$\mathcal{R}(z|\mathbf{\Lambda}_r) = \mathcal{C}(\gamma, \kappa, z_p) \frac{\mathcal{R}_0(1+z)^\gamma}{1 + \left(\frac{1+z}{1+z_p}\right)^{\gamma+\kappa}} \quad (\text{D1})$$

where $\mathcal{R}(z)$ is the source-frame rate per comoving volume at redshift z ; the normalization constant $\mathcal{C}(\gamma, \kappa, z_p) = 1 + (1+z_p)^{-\gamma-\kappa}$ ensures that \mathcal{R}_0 corresponds to the present-day merger rate. Then, for a given redshift chunk of galaxies between z_{\min} and z_{\max} , the total number of expected mergers during a detector-frame observing length of T_{obs} is

$$N_{\text{exp}}(\mathbf{\Lambda}_r, \mathbf{\Lambda}_c, z_{\min}, z_{\max}) = T_{\text{obs}} \int_{z_{\min}}^{z_{\max}} dz \frac{\mathcal{R}(z|\mathbf{\Lambda}_r) dV_c}{1+z} (\mathbf{\Lambda}_c) \quad (\text{D2})$$

$$S(m_1 | m_{\min}, \delta_m) = \begin{cases} 0 & m_1 < m_{\min} \\ \left[1 + \exp\left(\frac{\delta_m}{m - m_{\min}} + \frac{\delta_m}{m_1 - m_{\min} - \delta_m}\right)\right]^{-1} & m_{\min} \leq m_1 < m_1 + \delta_m \\ 0 & m_1 \geq m_1 + \delta_m \end{cases} \quad (\text{D5})$$

is a Planck taper window to smooth the distribution at minimum mass.

To model the mass ratio distribution, we use a truncated power law with exponent β

$$p(q|m_1, \beta, m_{\max}) = p_{\text{PL}}\left(q \middle| \beta, \frac{m_1}{m_{\max}}, 1\right). \quad (\text{D6})$$

The observed SNRs, posterior measurements, etc. are then computed as described in Section VII A 3.

where the factor of $1+z$ is from the conversion of the source frame to the detector frame. We use an observing time of $T_{\text{obs}} = 2$ years.

Thus, we divide the entire underlying set of galaxies into chunks in redshift. For each chunk i , we draw the number of galaxies in the chunk N^i from a Poisson distribution with expectation N_{exp}^i using Equation (D2). Then, we inject N^i BBHs into randomly drawn galaxies in the chunk weighted by their redshift as in Equation (D1). Finally, for each of the N_i BBHs, we draw the primary mass and mass ratio (m_1, q) via rejection sampling, and draw the aligned spins from a uniform distribution $\chi_{1,z}, \chi_{2,z} \in [-1, 1]$. These parameters, along with uniformly drawn extrinsic parameters (inclination angle, polarization angle, GPS time of arrival, coalescence phase), are sufficient to pass into **gwfast** for non-precessing waveforms (including **IMRPhenomHM**) as mock BBHs. This procedure is repeated for all chunks.

We now describe the mass population model. We model the primary mass distribution as a mixture model of a power law and a Gaussian distribution with a low-mass smoothing function [138]

$$\begin{aligned} \pi(m_1|\mathbf{\Lambda}_m) & \propto [(1-\lambda_p) p_{\text{PL}}(m_1 | -\alpha, m_{\min}, m_{\max}) \\ & + \lambda_p \mathcal{N}[m_1; \mu_p, \sigma_p]] \times S(m_1 | m_{\min}, \delta_m) \end{aligned} \quad (\text{D3})$$

where

$$p_{\text{PL}}(m_1 | -\alpha, m_{\min}, m_{\max}) = \begin{cases} \frac{m_1^{-\alpha}}{m_{\max}^{1-\alpha} - m_{\min}^{1-\alpha}} & m_{\min} < m_1 < m_{\max} \\ 0 & \text{otherwise} \end{cases} \quad (\text{D4})$$

is a truncated power law between m_{\min} and m_{\max} with exponent $-\alpha$, μ_p and σ_p are the mean and width of the Gaussian \mathcal{N} , λ_p is the mixing fraction of the peak, and

Appendix E: Quasi-linear corrections to the power spectrum

In Equation (27), we wrote down a simple series expansion for $b(k)$. This is a common technique to model and marginalize over unknown deviations from the linear power spectrum at quasi-linear scales (e.g., [139]). A first order correction would be

$$b(k, z) = b + a \left(\frac{k}{0.1 \text{ Mpc}^{-1}} \right). \quad (\text{E1})$$

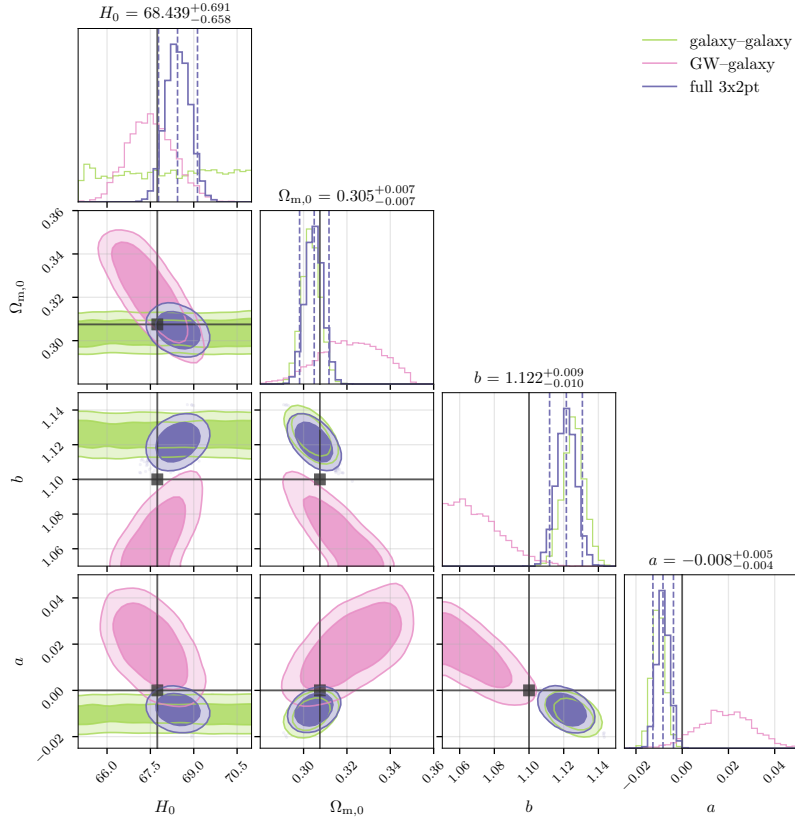


FIG. 9: Corner plot for an analysis that includes a first-order correction for non-linear scales, resulting in an unbiased measurement of $\Omega_{m,0}$ from galaxy-galaxy clustering compared to the result in the main text, Figure 7.

Figure 9 shows the same corner plot as in Figure 7, but with this added first-order correction parameter a ; we used a uniform prior of $a \in [-0.2, 0.2]$. Compared to the results in Figure 7, we find that adding the nuisance parameter is sufficient to account for unmodeled systematics, removing the bias in $\Omega_{m,0}$ from the galaxy-galaxy analysis. Note that the true values of the nuisance pa-

rameters $a = 0$ and $b = 1.1$ are not recovered exactly correctly, but for our purposes they are nuisance parameters that we marginalize over to encode uncertainty in the shape of the power spectrum. Inferring the shape of the power spectrum requires a more careful analysis that would, for example, include higher-order terms in the Limber approximation.